Dynamic modelling and comparison of wind turbine blade installation methods

Bob Kerkhofs

TU Delft

TWD

Dynamic modelling and comparison of wind turbine blade installation methods

by

Bob Kerkhofs

Thesis committee:

Chair:	Prof. Dr. A. Metrikine
Supervisor TU Delft:	Dr. Ir. B. Ummels
Supervisor TWD:	Ir. M. Rozemeijer
Place:	Faculty of Civil Engineering, Delft
Project Duration:	February, 2023 - June, 2024
Student number:	4560124

Faculty of Civil Engineering · Delft University of Technology

Preface

I'm excited to share that an amazing chapter is coming to an end. Reflecting on a journey of a year, I feel a deep sense of pride in my accomplishments and the challenges I've conquered. What seemed like a project without an end became a period in which I was able to move borders.

I want to extend my heartfelt thanks to everyone who played a significant role in supporting my research efforts. Additionally, I am grateful to the institutions that made it possible for me to undertake such an informative and enjoyable project. Achieving the standard required to present a graduation thesis would not have been feasible without the resources and support provided by TU Delft and TWD. Specifically, I would like to express my appreciation to:

Bart Ummels, for his endless support as my daily supervisor from TU Delft. With your enthusiasm, expertise and general support my life was a lot better in the last steps of my academic career. Without your support the light at the end of the tunnel would have been vanished sometimes. In my future career I hope to take your enthusiasm and drive with me.

Martijn Rozemeijer, for guiding me throughout my journey as my daily supervisor from TWD. I am happy with your sharpness on the subject and pulling me back when I was lost in my enthusiasm or ignorance of hard subjects. Working together to late in the evening in the office is something I really appreciated.

Andrei Metrikine, for motivating me to tackle the complexities of my research and to state some bold results. Yet, your expertise opened my eyes to the vast depths of knowledge still to be explored and aspired to.

Bas van Wuijckhuijse of TWD, for his help and expertise during the process. Your enthusiasm in innovative installation methods kickstarted my research.

Jelmer Mulder for helping me making some nice pictures and a cool 3D print. Niels Bakx for his help when my python model didn't yet work. Volken-Jan Koelewijn, Piet Bastiaanse and Cyril Girardeaux for their expertise in lifing operations. Cadeler with especially Marijn Dijk and Quintin Meissonier on sharing their experience with offshore installations.

My colleagues at TWD, my family and my roommates for their support when I was struggling with my thesis. Being able to not talk about my thesis and express my hard feelings was really essential to get over that finish line.

Bob Kerkhofs
Rotterdam, June 2024

Abstract

In recent decades, the global push for sustainable energy has grown, with offshore wind turbines emerging as a successful solution. This has led to the rapid growth of the offshore wind farm industry. As more wind farms are built, the demand for offshore installation vessels has increased significantly. It's crucial for contractors to complete wind turbine installations safely, reliably, and fast. As turbines continue to increase in size, they require higher lifts of larger blades, complicating the installation process due to component movement.

One of the most critical stages in turbine installation is aligning the rotor blade with the hub. Blades can be attached to the hub from various sides. The most used method involves horizontal blade installation, but also diagonal and vertical installation has been done. To achieve alignment with the hub, the blades are lifted using yokes and their position is controlled using taglines. Taglines connected to the crane boom, slewing platform, or both are used. Taglines can operate in constant tension or speed-dependent tension modes. The question arises, how do different blade installation methodologies perform and compare.

The objective of this research was to model and quantitatively compare the performance of various blade installation configurations. Performance is measured by how well the blade root stays within a 0.2 meter envelope under different wind conditions to allow the final mating of blade and hub. The first step was to study the parameters affecting turbine blade alignment simulation, focusing on wind as the main environmental factor causing blade movement. This led to a detailed examination of the essential parameters to accurately model turbine blades.

A 6 degrees-of-freedom dynamic simulation model of a 15 MW wind turbine blade suspended from an installation crane was developed, focusing on the blade's dynamic behavior during alignment with the hub. The model simulates the aerodynamic forces on the blade and its motions under different scenarios, considering environmental factors like wind velocity and turbulence intensity, but excluding movement of the jack-up vessel, vessel crane, and hub. The model allows for simulating many combinations of blade position, tagline configuration, and tagline operation mode, comparing the performance of different installation techniques during various wind conditions.

From the results, it is most likely that the way of attacking the hub by the turbine blade (side or bottom) is of high importance. From the results it appears that horizontal installation is most reliable. The model indicates that a tagline system that adjusts the pull force based on the speed of the blade's movement as the most effective and the tagline configuration was of less importance. The results demonstrated that a higher steepness of the slope (ratio between tagline force and pay-out speed) of the damping tugger improves the damping of the blade and is most favourable for offshore turbine blade installation. The model indicated that the horizontal-horizontal installation method was the most effective. The results showed that it was most feasible to install the blades at wind speeds up to 8 m/s. For higher wind speeds, installations could still proceed if there was lower turbulence intensity.

It is recommended to extend the model to include vessel, crane, and hub motions. Another recommendation is to validate the simplified blade model with detailed (confidential) blade data. Finally, using a more detailed model to explore tools and control strategies to minimize blade root motions is recommended to improve workability.

Contents

Nomenclature

List of Abbreviations

AOA	Angle of attack
AR	Aspect Ratio
BEM	Blade element Momentum
CFD	Computational Fluid Dynamics
CO2	Carbon Dioxide
COG	Centre Of Gravity
GW	gigawatts
IPCC	Intergovernmental Panel on Climate Change
MW	megawatts
NECP	National Energy and Climate Plan
ODE	Ordinary Differential Equation
RAO	Response Amplitude Operator
TI	Turbulence Intensity
WSE	Wind Shear Exponent

List of Symbols

α	WSE
α_i	incoming wind speed angle
μ	dynamic viscosity
μ	rotation of blade around its longitudinal axis
ω	angular velocity
ρ	density
τ	shear stress
A	cross sectional area
a	axial induction factor
AOA_i	twist angle of blade section i
B	damping
C_d	drag coefficient
C_l	lift coefficient
c_t	thrust coefficient
D	pitch angle
d	airfoil length
D_{hub}	Hub diameter
deg	degree
E	elastic modulus
g	gravitational acceleration
I	second moment of area
L	length of pendulum
m	mass
N_{Re}	Reynolds Number
P	Pressure
r	radius rotor
T_C	estimated maximum coningency time
T_r	operational reference period
T_{pop}	planned operational period
u	wind speed
V	wind speed
z	height
z_0	height, wind speed = 0 m/s
z_{ref}	reference height

List of Figures

List of Tables

1

Introduction

1.1. Background

The Paris Agreement [1] represents a legally binding international treaty pertaining to climate change. It was adopted during the 21st United Nations Climate Change Conference (COP21) held in Paris, France, on December 12, 2015, with participation from 196 Parties. Subsequently, the agreement came into force on the 4th of November, 2016. The primary objective of this agreement is to constrain the escalation of the global average temperature to levels substantially below 2°C in comparison to pre-industrial benchmarks. Additionally, it calls for concerted efforts to confine the temperature increase to merely 1.5°C above pre-industrial levels.

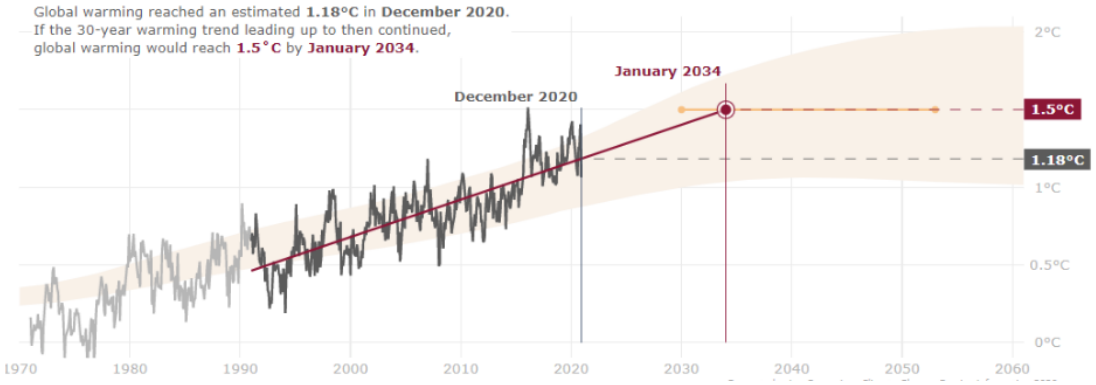

Figure 1.1: Global Temperature Trend [2]

Nevertheless, recent years have seen global leaders emphasizing the urgency of limiting global warming to 1.5°C by the conclusion of this century. This shift in focus stems from assessments provided by the United Nations Intergovernmental Panel on Climate Change (IPCC), which underscore the substantial risks associated with surpassing the 1.5°C threshold. Such risks encompass heightened occurrences of severe droughts, heatwaves, and intensified precipitation patterns.

To achieve the objective of restricting global warming to 1.5°C, it is imperative that greenhouse gas emissions reach their peak, at the latest, by 2025 and subsequently experience a 43% reduction by 2030. The Paris Agreement stands as a landmark milestone within the multilateral framework for addressing climate change. Notably, it represents the inaugural instance in which a legally binding accord unites nations worldwide in the shared mission to combat climate change and adapt to its consequences.

In its endeavor to address climate change, the Dutch government has articulated its intention to diminish greenhouse gas emissions emanating from the Netherlands by 49% by the year 2030

[3], as contrasted with the levels recorded in 1990. Additionally, the government aims to achieve a substantial reduction of 95% by 2050. These objectives have been codified in the Climate Act, enacted on May 28, 2019. The strategic framework for realizing these climate objectives is delineated in the Climate Plan [4], the National Energy and Climate Plan (NECP) [5] , and the National Climate Agreement [6], encompassing a comprehensive array of policies and measures tailored to attaining these climate-related targets.

1.2. Offshore Wind Projects

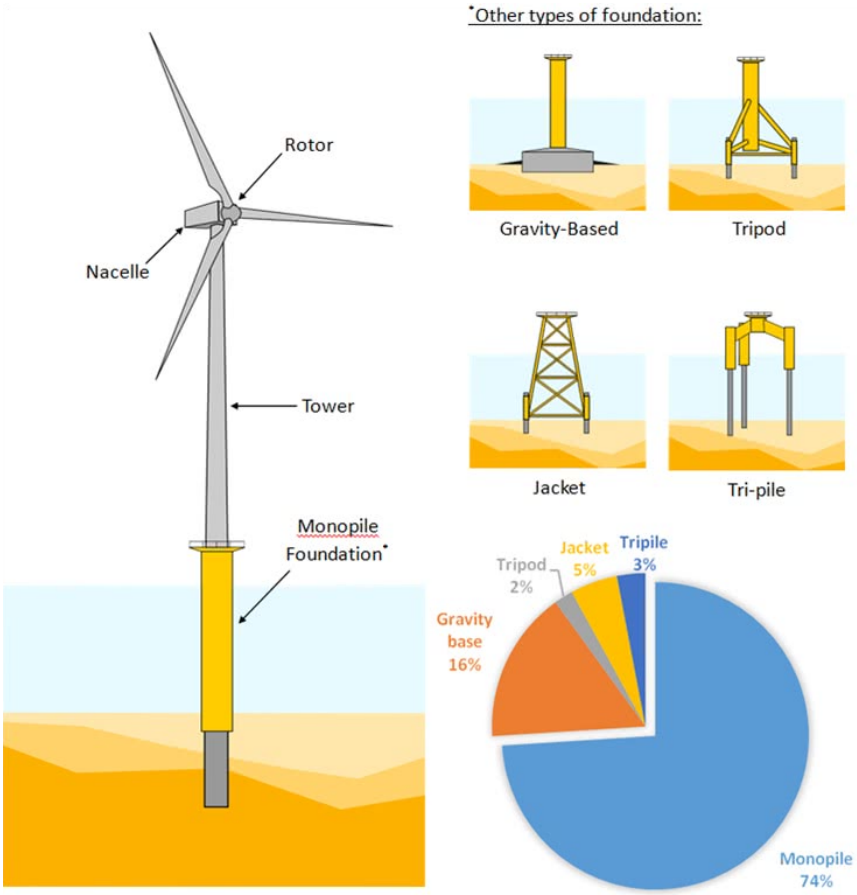

Figure 1.2: Turbine Components and Foundations[7]

Understanding the components of offshore wind turbines is crucial. While offshore turbines resemble their onshore counterparts, they differ in their foundations – offshore turbines stand on offshore foundations, while onshore turbines stand on onshore foundations. Both types consist of a rotor, nacelle, and tower (as depicted in Figure 1.2). However, offshore towers aren't anchored to the ground; instead, they're fixed to foundations tailored to the sea depth and site-specific conditions. In the North Sea along the Dutch coast, monopiles are prevalent for fixed foundations. As illustrated on the right side of Figure 1.2, monopiles are most commonly used foundations.

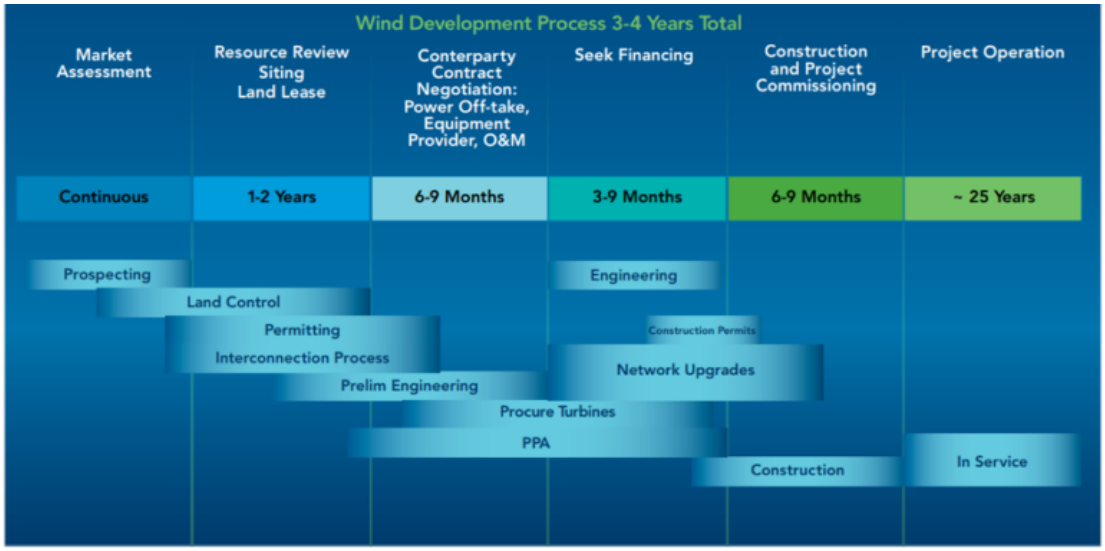

Figure 1.3: Installation Timeline [8]

In Figure 1.3, a project development timeline is shown. Constantly governments are looking for areas where wind farms can be built. Afterwards there will be made a site visit where bottom research is done, with this information it is possible to decide which foundation suits best at the location being investigated. Thereafter there will be counter-party contract negotiation about the power take-off, equipment, provider and operations & maintenance. Subsequently financing of the project should be guaranteed, where after the construction of the wind farm can be started.

As multiple ventures are working together to construct a wind farm, it is important to keep the price of the projects as low as possible. While turbine prices and the cost of the electrical infrastructure and foundations are almost fixed it is important to be innovative during the turbine installation process. As can be seen in Figure 1.4 the logistics and installation count for about 20% of the cost for wind farms. With this known it is possible to make impact in the overall turbine wind farm cost if turbine blade installation is more safe and quick.

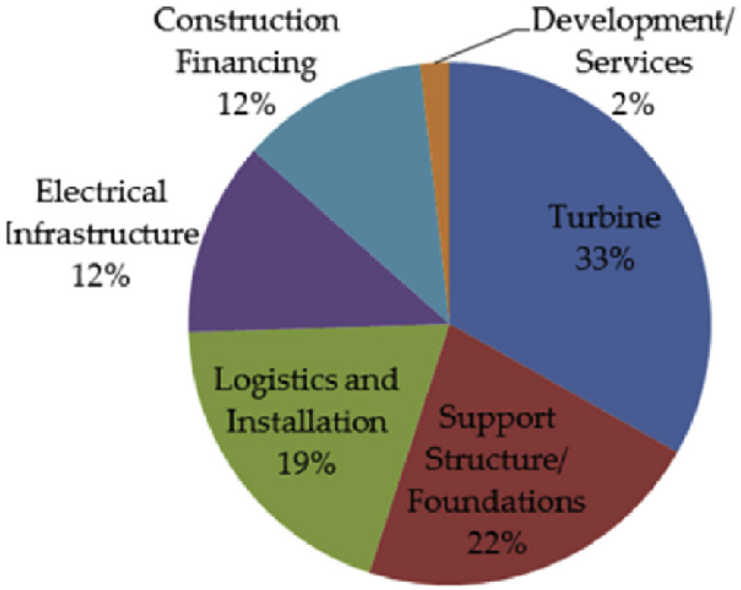

Figure 1.4: Offshore Wind Farm Plant Capital Cost Breakdown [9]

1.3. Offshore Wind in the Netherlands

Offshore wind energy stands as a fundamental pillar within the Netherlands' climate policy landscape. Its expansion is deemed essential for the nation to achieve its climate target, which entails a 55% reduction in CO2 emissions by 2030 [10]. To meet this challenge, the Dutch Government took significant steps in 2022 by revising its offshore wind capacity goal, elevating it from the initial 11 gigawatts (GW) to an ambitious 21 GW by the period spanning 2030 to 2031. Figure 1.5 shows the outlined cumulative offshore energy production. Achieving this heightened target implies that offshore wind farms will contribute approximately 16% of the Netherlands' total energy needs, equivalent to about 75% of the current electricity consumption.

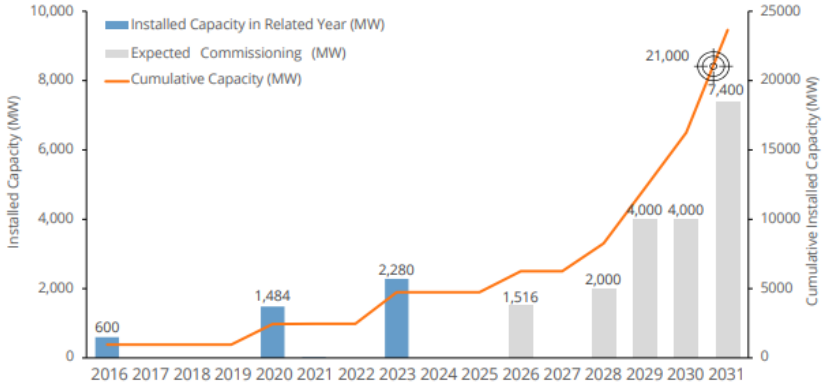

Figure 1.5: Cumulative and Expected Yearly Installed Capacity of Offshore Wind in the Netherlands from 2016 to 2031 [11]

However, it's important to recognize that the nation's electricity consumption is expected to grow in the coming years, necessitating further expansion of offshore wind energy post-2030. Forecasts based on prospective scenarios for energy systems, encompassing supply and demand dynamics, along with insights from the North Sea Energy Outlook (Noordzee Energie Outlook [12]), collectively indicate a need for cumulative offshore wind capacity ranging between 38 and 72 GW by 2050 to meet the evolving energy requirements and environmental objectives.

1.4. Wind Turbines

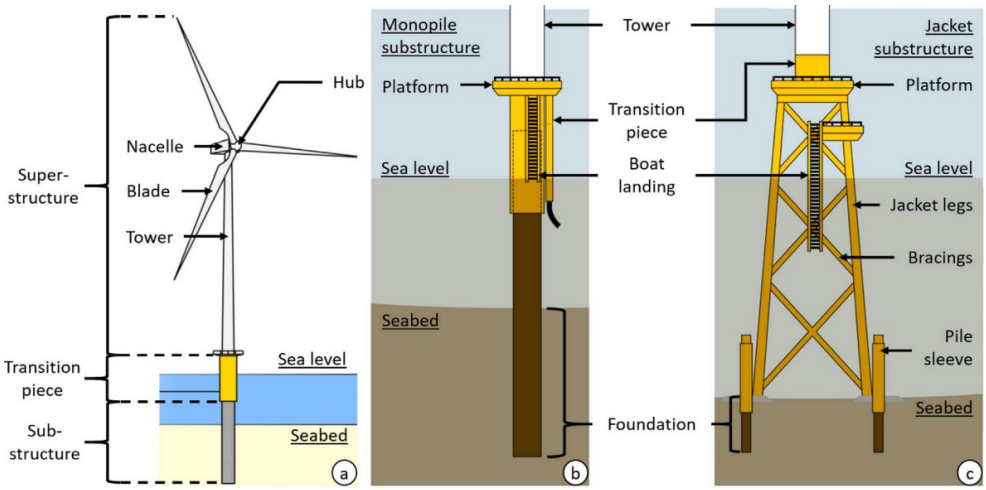

Figure 1.6: Turbine Components [13]

1.4.1. Support Structure

The support structure, is the structure which is able to to withstand enormous forces. These forces created by wind, waves, currents and gravity are putting big loads and moments on this support structure. The support structure consists of a tower, transition piece and a sub structure. The sub structure can be of different forms, as can be seen in figure 1.6. Both of these foundations are bottom fixed. Next to these bottom fixed foundations nowadays there are also floating substructures [14]. The foundation of a location depends on the characteristics of the sea depth and the seabed structure. Mostly Monopiles are used at lower sea depths with a sandy soil.

1.4.2. Nacelle

On top the support structure rests the nacelle, a large enclosure housing essential components such as the main bearing, gearbox, and generator.

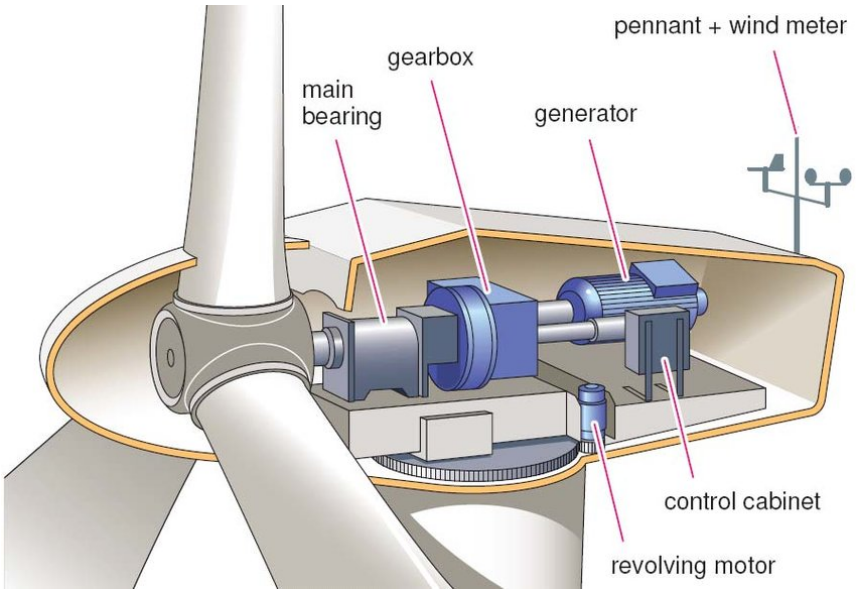

Figure 1.7: Turbine Nacelle [13]

Pennant and Anemometer

Installed on top the nacelle are the pennant and anemometer. The pennant aids in wind direction detection, enabling the turbine to align itself accordingly. The anemometer measures wind speed, facilitating adjustment of blade pitch for optimal performance.

Generator

Housed within the nacelle, the wind turbine generator converts kinetic energy from the wind into electrical energy through electromagnetic induction, contributing to renewable power generation.

Gearbox

The gearbox within the nacelle increases the rotational speed of the wind-driven rotor to an optimal level for efficient power generation. It accomplishes this by transmitting torque from the slower-moving rotor shaft to the faster-moving generator shaft.

Main Bearing

The main bearing within the nacelle supports the rotor's weight and enables its rotation. It plays a critical role in transferring mechanical loads and ensuring smooth, efficient operation of the turbine's components.

1.4.3. Hub

The hub, which is connected to a wind turbine's nacelle serves as the central connection point for the rotor blades, effectively transferring the aerodynamic forces generated by the wind to the rotor shaft. It securely holds the blades in place while allowing them to pitch or rotate to optimize their angle of attack for efficient energy capture. Additionally, the hub facilitates the transmission of mechanical energy from the blades to the rotor shaft, enabling the rotation necessary for electricity generation by the turbine's generator. Overall, the hub plays a critical role in the structural integrity and performance of the wind turbine system and installation.

1.4.4. Blades

Blades in a wind turbine's nacelle are the primary components responsible for capturing kinetic energy from the wind and converting it into rotational motion. Their aerodynamic design allows them to efficiently harness wind energy, with airfoil shapes generating lift as the wind passes over them. The blades are connected to the hub, which transfers the captured energy to the rotor shaft. Through their rotation, the blades drive the rotor shaft, which in turn spins the generator to produce electricity. Thus, the blades are fundamental elements in the process of converting wind power into usable electrical energy in a wind turbine system.

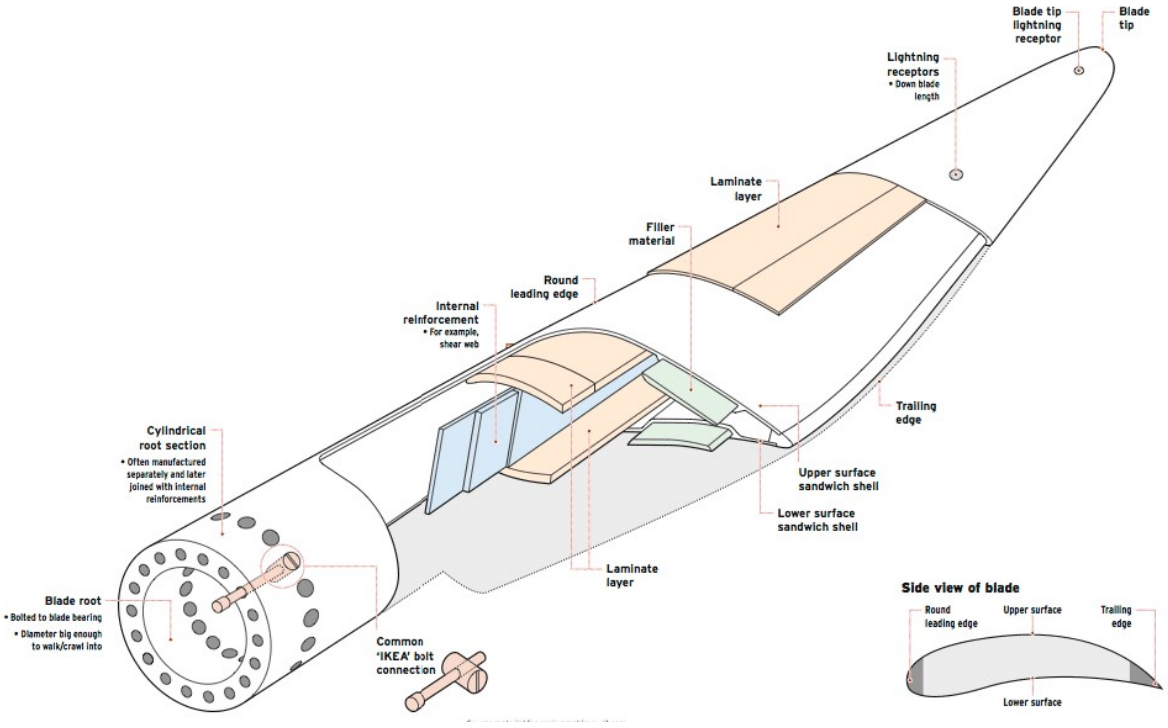

Figure 1.8: Turbine Blade [15]

Figure 1.8 provides an insightful look at a turbine blade and its construction process. Turbine blades are engineered with precision to be durable, lightweight, and aerodynamic, ensuring optimal performance. Table 1.1 details the dimensions of turbine blades. Blade data isn't widely available due to companies don't want to give away their knowledge, therefore the Technical University of Denmark engineered a turbine blade which could be used for research [16]. It's important to recognize that turbine blades can vary significantly between manufacturers and turbine types, each employing distinct construction methods tailored to their specific needs and objectives. .

Slicing the blade in half reveals a sectional view, as shown in the bottom-right of Figure 1.8. This side-view outlines what's known as an airfoil. The dimensions and profile of this airfoil are crucial for determining the characteristics of the turbine blade.

During this thesis the 15MW reference turbine blade [16] will be used. This blade is 117 meters long with a root diameter of 5.2 meter, with a chord of 5.77 meter. The Mass of the blade is almost 65 tons and is designed to obtain a power coefficient of 0.489. All other info of the turbine blade can be found in Table 1.1 and appendix B.

Description	Value	Units
Blade length	117	m
Root Diameter	5.2	m
Root cylinder length	2.34	m
Max chord	5.77	m
Max chord spanwise position	27.2	m
Tip prebend	4	m
Precone	4	deg
Blade Mass	65.250	kg
Blade Center of Mass	26.8	m
Design tip-speed ratio	9.00	-
First flapwise natural frequency	0.555	Hz
First edgewise natural frequency	0.642	Hz
Design Cp	0.489	-
Design Ct	0.799	-
Annual energy production	77.4	GWh

Table 1.1: Blade Properties [16]

1.5. Problem Definition

The installation of wind turbine blades presents a significant challenge in the renewable energy sector. Key challenges stem from the size and weight of the blades, the need for precise positioning to harness wind effectively, and the impact of variable weather conditions on the installation of wind turbines, in particular the rotor blades. The utilization of diverse blade orientations and tag control strategies complicates and objective comparison.

A primary objective of the offshore wind industry is to streamline the installation of wind turbine blades, making it faster and more cost-effective, also for even larger blades. Achieving this goal necessitates a comprehensive comparison of various installation methods and the associated control systems (tagline systems). Presently, a comprehensive assessment of these methods and tools is lacking, hindering efforts to determine optimal approaches for different scenarios. Developing such a tool could significantly enhance the ability to safely install blades in adverse weather conditions, such as higher wind speeds and turbulence levels.

1.6. Research Objective and Question

Based on the results of the literature review and the problem definition above, the aim of this research is:

to develop a dynamic simulation model that allows an objective comparison of the performance of various rotor blade installation methods.

With this objective the following main research question is established.

How can various blade installation methods for wind turbines be modelled dynamically?

To answer the main research question, the following sub-questions have been defined:

1. How can a wind turbine rotor blade during installation be modeled aerodynamically?
2. How do environmental factors influence the choice of blade installation methods in offshore applications?
3. What is the interaction between the blade installation method and the dynamic behaviour of the blade?
4. What is the relative performance of the blade installation methods investigated?
5. How can the model be used to assess the installation of future-sized wind turbine blades?

1.7. Approach

This thesis specifically investigates the installation of individual turbine blades under offshore conditions. Previous studies have revealed that wind represents the primary constraint during the turbine blade installation phase. Consequently, this phase's critical aspect lies in the mating process between the turbine blade and the turbine hub. As a result, other stages of the installation process are not within the scope of this thesis. Furthermore, vessel and crane motions are not considered in this research.

To conduct this study, initial research is conducted on pure aerodynamics, followed by an examination of the turbine blade itself. Finally, the motions of the turbine blade are analyzed to provide a comprehensive understanding of the installation process under offshore conditions.

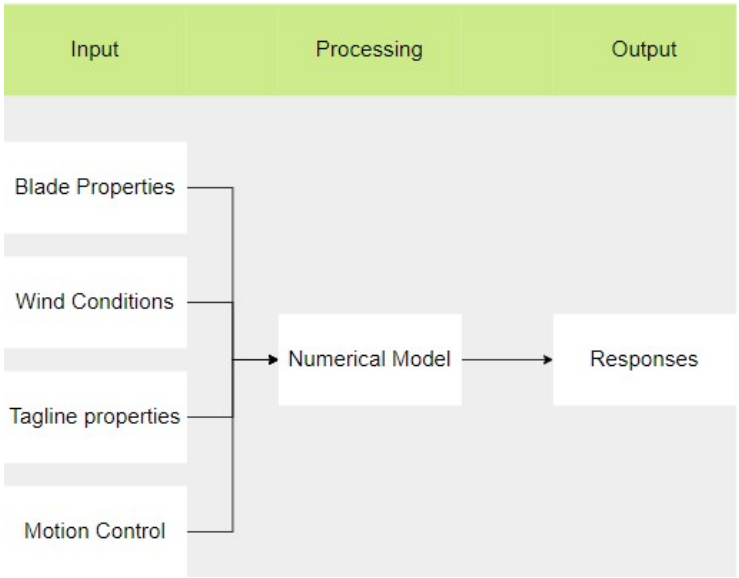

Figure 1.9: Research Approach

A numerical computational model is developed to characterize the impact of wind on single-blade installations. Assumptions are outlined to delineate the model's constraints, which are based on rigid body dynamics. The model incorporates three distinct approaches to simulate the behavior of taglines, which govern the blade's motion. Wind-induced loads acting on the blade are simulated using an artificial wind field, with simulations conducted across various wind field characteristics, including mean wind velocity and turbulence intensity. Throughout these simulations, the system's responses to aerodynamic loading are monitored, tracking the motion of the blade root center and the wind-induced loads on the blade.

Following data processing from these simulations, insights into the feasibility of specific wind conditions are derived. Upon model validation, a reference load case involving a 15MW turbine blade is examined to facilitate comparative analysis. Time domain simulations are executed to emulate real offshore conditions, generating results that can be assessed against predefined operational criteria. Subsequently, the findings are interpreted, offering valuable insights into the feasibility of single-blade installation under specific environmental conditions and utilizing particular installation methods.

2

Wind Turbine and Installation Equipment

In the following chapter, an in-depth exploration of the turbine blade's dimensions and physical characteristics will be conducted. Following this, information about the equipment employed in the installation process of these turbine blades will be provided. Lastly, a brief overview of the installation boundary conditions and the necessary weather window for turbine blade installations will be presented.

2.1. Vessels

Figure 2.1: Voltaire, Jan de Nul [13]

For turbine blade installation, different vessels can be used. Often a jack-up vessel is used for turbine installation. In Figure 2.1, one of the vessels used by Jan de Nul can be seen. A jack-up vessel is known by its legs. These legs can be lowered to the seabed to lift the vessel out of the water. As Figure 2.1 shows, these vessels have big leg encircling cranes, which they use for installation of the turbines. Next to that the vessel is used for accommodation for the employees and deck space is used for storage of equipment and turbine components.

Crane vessels can be used for turbine blade installation. These ships don't have legs to lift the ship out of the water, Figure 2.2. These vessels mostly work with dynamic positioning (DP) systems. This system automatically keeps the vessel at the right position, this can be compared with the cruise control of a normal car. These ships are less used for blade installation operations while they are mostly used for heavy lifting operations and are even more expensive.

Unless vessel and crane motions are not covered in this thesis it is of importance to know how these vessel work and what their seizes are. With this knowledge it is convenient to know

Figure 2.2: Les Alizes, Jan de Nul (Left) and Sleipnir, Heerema (Right)

that those vessels are subjected to enormous forces such as wind, waves and currents. While those motions are out of the scope of this thesis, it can not be neglected in the analysis of the response, especially when a firm conclusion needs to be drawn out of the simulation.

2.2. Wind Turbine Blade Installation

As mentioned before, the blade is connected to the rotor and the rotor to the hub. In Figure 2.3 the connection is shown. Pins are connected to the blade which will be bolted to the rotor. To make installation more easy one or multiple pins are a bit longer than others. This pin, is also called the guide pin and with this pin it is more easy to align the blade to the hub.

Figure 2.3: Offshore Wind Turbine Blade-Rotor Connection

As depicted in Figure 2.4, various installation methods exist for constructing offshore wind turbines. Section 1.2 discusses the capital costs of wind farms, it can be reduced through innovative installation methods. This drives offshore contractors to continuously explore new installation techniques or seek enhancements to existing ones. While Figure 2.4 illustrates the most prevalent methods, future innovations may yield additional ways to install turbines. Currently, method 2 stands as the most commonly employed installation approach. Ultimately, the turbine installation contractor must weigh several factors when selecting a method, including the transportation of turbine components, the installation process itself, and the availability of equipment.

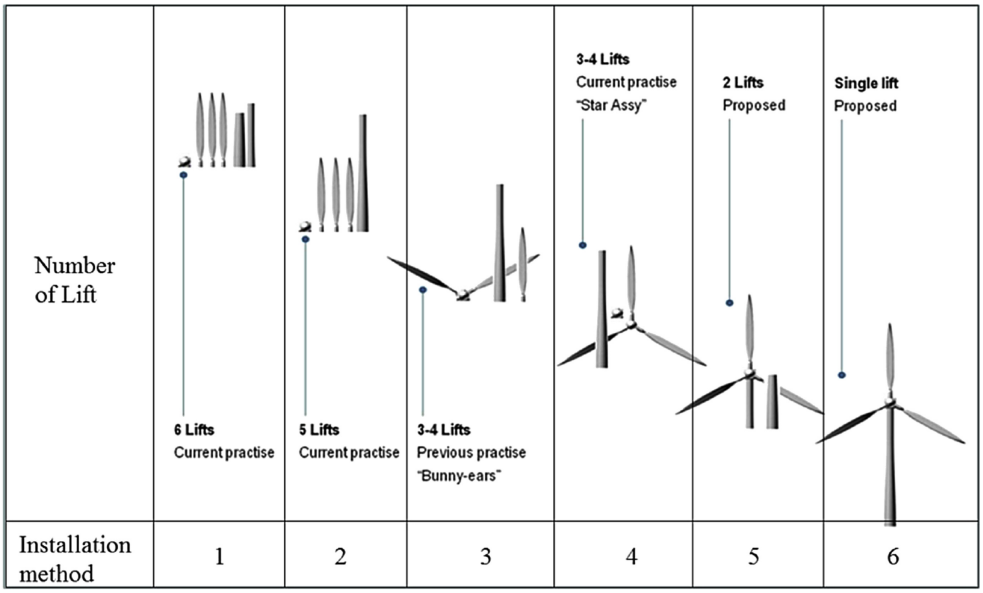

Figure 2.4: Offshore Wind Turbine Installation Method [9]

2.2.1. Installation Equipment

In the process of lifting turbine blades, various lifting gears, known as yokes, can be utilized. This section aims to elucidate several types of yokes commonly employed in blade installations. Typically, installation companies assess the suitability of different equipment for their specific installation methods. It is essential to note that not all equipment is universally applicable for every blade. For instance, the same blade yoke cannot be employed for both a 5MW blade and a 20MW blade due to differences in size and weight. Therefore, careful consideration and selection of the appropriate yoke are paramount to ensure the safe and efficient installation of turbine blades.

CY-Yoke

Figure 2.5: CY-Yoke, Enable [17]

The CY-Yoke enables the vertical installation of turbine blades (blade chord length perpendicular to the sea surface) . Once the blade is attached to the hub, the tires on the bottom side of the yoke disengage, allowing the installation tool to return to the vessel for the installation of another blade.

One advantage of this yoke is its minimal lift force on the blade, as the lift coefficient approaches zero. Additionally, detaching the yoke is straightforward, requiring only vertical lifting, as the lift

coefficient remains nearly zero. However, a downside of the CY-Yoke is its susceptibility to wind, given its high drag force.

C-Yoke

Figure 2.6: C-Yoke, Enable [17]

The C-yoke, a steel construction resembling the letter ”C,” streamlines the handling of individual blades during installation or disassembly. Engineered for rapid on-site assembly, it boasts a sleek design. Equipped with an integrated tilt function, the C-yoke can pivot up to 30 degrees. During operation, it positions the blade horizontally, orienting the up-/downwind side upwards.

The advantages of the C-yoke include its relatively low drag force on the blade, enhancing its resilience against wind compared to the CY-Yoke. However, a drawback is its sensitivity to small changes in the angle of attack, which can significantly affect the lift forces acting on the blade. Additionally, detaching the yoke from the blade presents challenges, particularly in executing a horizontal motion with the crane without making contact with the blade.

Blade Dragon

Figure 2.7: Blade Dragon, Liftra [18]

The Blade Dragon offers the flexibility to install blades at various angles relative to the hub. This tool allows contractors to select the direction from which they approach the hub to install

the blade. One advantage of this tool is the ability to choose the installation angle at the blade's location, providing adaptability to different scenarios.

However, it's worth noting that when the blade is installed in a standing position, there will be a variation in wind speed across the blade, as will be elaborated in Section 3.1.2. It's essential to account for these significant differences in wind speed, as they could potentially affect the installation process.

In conclusion, a comparison between these yokes is presented in the table below.

	CY-Yoke	C-Yoke	Blade Dragon
Vertical installation	Not possible	Not Possible	Possible
Horizontal installation	Possible	Possible	Possible
Drag Force	High	Low	Based on position
Sensibility Lift	Low	High	Based on position
Flexible hub approach	No	No	Yes

Table 2.1: Blade Yoke Comparison

2.3. Blade Positions

This thesis is about a comparison of the performance of various blade installation methods. Four different positions are considered and shown in following section.

2.3.1. Horizontal-Horizontal (HH)

Figure 2.8: Horizontal-Horizontal Installation

Figure 2.8 illustrates the positioning of the blade, representing one of the widely adopted methods for turbine blade installation. In this method, the blade is lifted at its center of gravity (COG). By lifting the blade in this manner, the pitch moment caused by its weight is eliminated, as the weight is evenly distributed on both sides.

Additionally, laying the blade flat ensures a low drag component in the direction of the wind. Consequently, this leads to smaller accelerations, indicating that taglines require less force to maintain the blade's position.

2.3.2. Horizontal-Vertical (HV)

Figure 2.9: Horizontal-Vertical Installation

In the horizontal-vertical installation method, the blade is rotated 90 degrees around its longitudinal length. Figure 2.9 illustrates the blade's position in this configuration. In this orientation, the chord line of the blade is perpendicular to the sea surface, maximizing the blade's surface area exposed to the incoming wind.

Due to the angle of attack being 90 degrees, high loads can be expected, while lift forces perpendicular to the wind streamline are nearly zero. As a result, robust taglines are required to maintain stability, and there is minimal need to control lift-induced moments. This method offers distinct advantages in terms of wind exposure and load distribution during installation.

2.3.3. Vertical-Horizontal (VH)

Figure 2.10: Vertical-Horizontal Installation

In the vertical-horizontal installation method, the blade is attached to the hub from the bottom. While the blades chord line is positioned in the direction of the wind , this results in low drag due to the blade's small angle of attack.

While the blade is now oriented vertically, there remains a variation in wind speed along its length. The power law explains this phenomenon, elaboration about this will be given in Section 3.1.2. Consequently, it can be anticipated that the forces acting on the blade are generally lower compared to when the entire blade is at higher altitudes.

As depicted on the right side of Figure 2.10, the blade is not perfectly perpendicular to the sea surface but has a slight angle. This deviation is necessary to account for tower clearance. For instance, with a 15 MW reference turbine, this angle is typically around 10 degrees. This is due to the offset the blade need to make due to the tower clearance.

2.3.4. Vertical-Vertical (VV)

Figure 2.11: Vertical-Vertical Installation

In the Vertical-vertical installation method, the blade is connected to the bottom of the hub, similar to the Vertical-horizontal installation. This setup maximizes the blade area, resulting in higher loads. Unlike the horizontal-vertical installation, where wind speed varies with the height of the blade section, in the Vertical-vertical installation, the blade maintains a consistent vertical orientation throughout.

	HH	HV	VH	VV
Drag force	Low	High	Low	High
Lift force	Sensible	Low	Sensible	Low
Approximation hub	Side	Side	Bottom	Bottom

Table 2.2: Blade Positions

2.4. Lifting Cables

The turbine blade is lifted using several hoist cables attached to the top of the crane boom. These cables lift the blade to the hub height. This lifting process involves multiple cables connected to a main hoist block. Each cable comprises one or more layers of wire spirally wound around a core. This core can be made of one or more steel wires (known as a steel core) or fibers (known as a rope core). The arrangement of these layers significantly influences the technical characteristics of the cable assembly [19].

Multilayer stranded cables typically employ low-twist or twist-free designs. The construction of multiple strand layers enables the creation of cables with minimal torque, as the torsional forces within the different layers counteract each other [20].

Figure 2.12: Offshore Leg Encircling Crane [21]

Figure 2.12 displays the crane boom top, featuring hoist cables connected to a hook block. This hook block serves as the link between the main hoist cables and the equipment used for lifting the blade. A close-up image of the hook block is provided in Appendix D. In this block, all cables are interconnected, ensuring robust lifting capabilities. Within the block, a thrust bearing is positioned to facilitate free rotation of the main hook around its axis. Through a private discussion with an offshore specialist, it was revealed that the lifting cables do not provide rotational stiffness; instead, the thrust bearing primarily offers damping, typically ranging from 3 to 6% [20][22]. To counteract moments in the lifting equipment, taglines are employed.

The design of the hook block, the quantity of lifting cables, the characteristics of the hook, and various other components can vary significantly across different vessels. Each offshore crane is meticulously engineered to suit its unique operational requirements. Despite these variations, the fundamental principles remain consistent, allowing for uniform functionality across different crane systems. One notable assumption applicable to nearly all cranes is the absence of rotational stiffness in the lifting mechanism.

2.5. Taglines

The subsequent section of this thesis will provide an in-depth examination of various methods used to control horizontal motions associated with turbine blade installations. Before delving into motion control, it is imperative to comprehend the concept of taglines.

Taglines are robust ropes or cables specifically engineered to withstand the dynamic forces encountered during offshore installation operations [23]. Constructed from durable materials such as synthetic fibers or steel, these lines exhibit exceptional tensile strength. They are securely attached to key points on the yokes, typically at designated lifting or attachment points. This connection is meticulously designed to evenly distribute loads across the blade structure, ensuring

effective guidance and control of blade movement during installation.

Throughout the installation process, taglines serve as a guiding force, facilitating precise navigation of turbine blades from the installation vessel to their final destination. Operators utilize controlled tension and release of taglines to manipulate the orientation and alignment of the blades, compensating for environmental factors such as wind, waves, and vessel motions. This level of control is essential for avoiding collisions, minimizing installation time, and safeguarding both personnel and equipment.

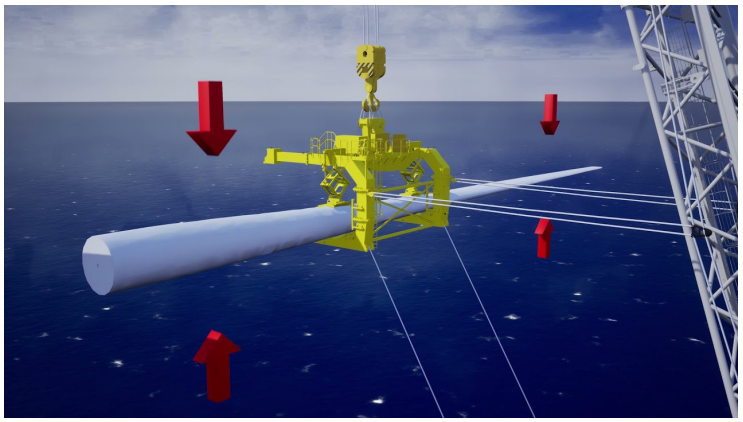

Figure 2.13: Blade Lifting Operation

The operation of taglines involves winches, and there are diverse configurations for attachment points on the components, along with multiple methods to control the winches for the taglines. For example, in Figure 2.13, taglines are utilized to regulate the movements of a lifted blade, with connection points located on the crane boom. To prevent slack lines, pre-tension is applied to the taglines.

Figure 2.14: Offshore Winches [24]

Offshore winches, as shown in Figure 2.14, are essential pieces of equipment in the maritime and offshore industry. These robust devices are specifically engineered to handle heavy loads and function effectively in the demanding conditions of open water environments. Offshore winches serve a crucial role in various offshore activities, including lifting and lowering equipment,

deploying and retrieving subsea assets, and assisting with anchor handling operations on ships and oil rigs. Their sturdy construction and advanced technology make them reliable tools for ensuring safety and efficiency in offshore operations, rendering them indispensable assets for offshore oil and gas exploration, wind farm installation, and marine construction projects.

The winches on each vessel are often customized to meet the specific requirements and functions of that particular vessel. This customization is necessary because different vessels serve diverse purposes, ranging from cargo transport to offshore drilling or marine research. Factors such as load capacity, line speed, and the type of operations conducted dictate the design and specifications of the winches [25]. Vessels used for offshore oil drilling may have heavy-duty winches capable of handling large loads of drilling equipment, while research vessels may feature winches designed for delicate and precise handling of scientific instruments. Therefore, the unique characteristics of each vessel's winches ensure they are tailored to perform their designated tasks effectively and safely in their respective maritime applications.

Typically, the winches are positioned on the deck, and from there, the taglines run through the slewing platform or craneboom to the sheave and are then attached to the load through specific points. The sheave is fixed at a particular height on the slewing platform, or somewhere at the crane boom. This location is determined for which the operation can be controlled best.

2.6. Tagline Positions

The comparison doesn't just focus on blade positions; it also takes into account the tagline configuration. Taglines are positioned at various points relative to the vessel, resulting in different force directions in these configurations. In the following section the tagline positions will be shown.

2.6.1. Slewing Platform (SP)

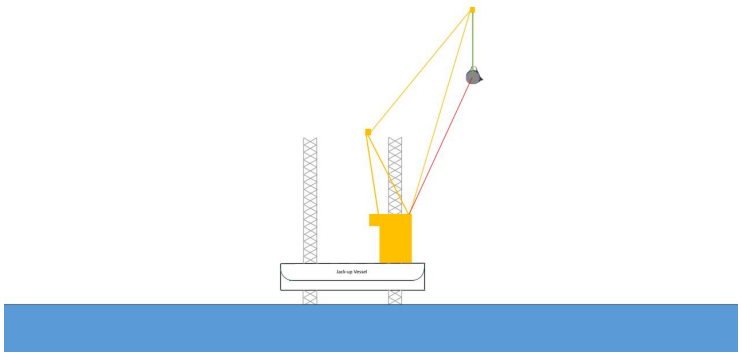

Figure 2.15: Slewing Platform Configuration

When the tagline cables are connected to the slewing platform, the taglines are able to restore horizontal and vertical forces. The ratio (vertical:horizontal) of the force is dependent on the position of the blade. If this ratio is low the restoring coefficient of the pendulum will be higher.

2.6.2. Crane Boom (CB)

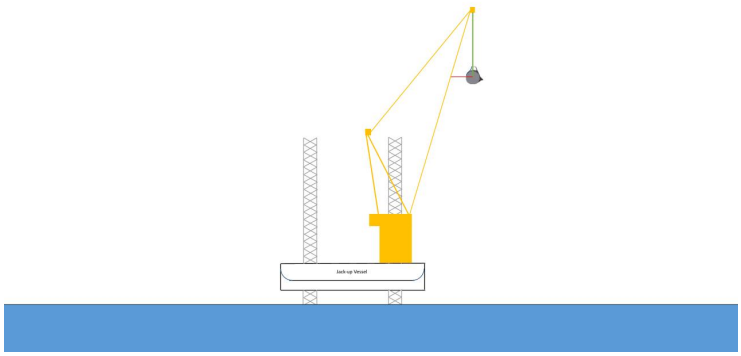

Figure 2.16: Crane Boom Configuration

Taglines connected to the craneboom are able to change in positions. These taglines follow the height of the blade. In the simulation is assumed that this works perfectly. In practice, there will always be delay, but addressing this falls outside the scope of this thesis. With the craneboom tagline system the taglines are only able to restore horizontal forces.

2.6.3. Combined Tagline Configuration (CS)

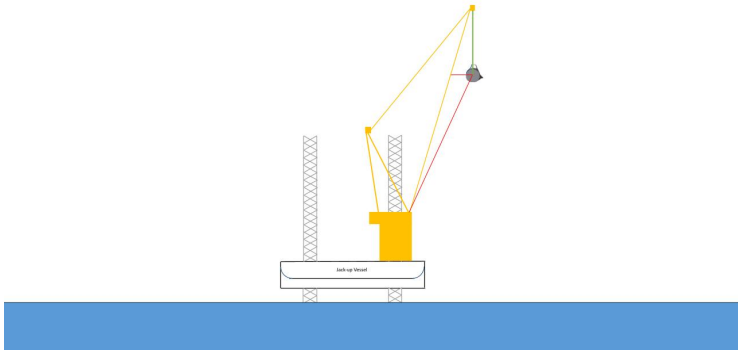

Figure 2.17: Combined Configuration

In this configuration both tagline systems are combined. This configuration is therefore able to restore horizontal and vertical motions.

	SP	CB	CS
Horizontal force	Yes	Yes	Yes
Vertical force	Yes	No	Yes
Location dependent	No	Yes	Yes

Table 2.3: Tagline Positions

2.7. Tagline Operation Modes

Winches offer three operating modes; constant tension, brake mode or damping tuggers. In the simulation all three modes are simulated and compared. In the subsequent section those modes will be elaborated and therefor no delay is in the tagline forces.

2.7.1. Constant Tension Tuggers (CF)

Recognizing the risks associated with breaking tugger lines in offshore operations, tugger winches are often operated in constant tension mode [26]. If the winch's pay-in and pay-out velocity is sufficiently high to keep pace with the load, it endeavors to maintain a consistent tension on the lines.

$$F = Constant \tag{2.1}$$

Consequently, the impact of dynamics on the system remains minimal. However, due to the inherent imperfections in winch operation, tension fluctuations around the constant tension magnitude occur, resulting in dissipation that dampens the motion of the load. Therefore, constant tension tuggers are deemed effective in controlling motions. In this thesis is assumed that the tension is perfectly constant.

2.7.2. Brake Mode (SF)

In the fixed tuggers mode, the winch is engaged with the brake, resulting in the tugger line remaining stationary at a fixed length. The desired pretension is set on the winch and maintained throughout the operation. In essence, the tugger lines function as a spring, where the spring stiffness aligns with the tugger line stiffness.

$$F = \begin{cases} 0 & \text{for } L_0 < L_{tagline} \\ -k * (L_{tagline} - L_0) & \text{for } L_0 > L_{tagline} \end{cases} \tag{2.2}$$

However, this setup introduces substantial loads in the tugger lines. If these loads surpass the applied pretension, the tugger lines may slack, leading to abrupt loads, posing hazardous situations, and potentially causing line failure.

2.7.3. Damping Tuggers (DF)

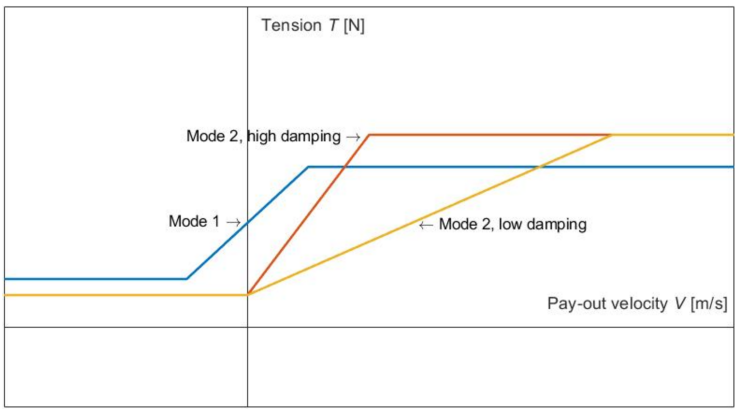

Figure 2.18: Tension of Tagline with a Damping Winch [27]

To mitigate the swinging motion of a load, damping is essential. The damping tugger winch, developed by Meskers and Van Dijk [28], operates as a modified version of the constant tension winch. When the load moves away from the crane boom, the winch increases tension to pull the

load back into position. Conversely, if the load moves toward the crane boom, the winch reduces tension.

$$F = \begin{cases} F_{min} & \text{for } v < v_{min} \\ F_{min} + \text{slope} \cdot v & \text{for } v_{min} \leq v \leq v_{max} \\ F_{max} & \text{for } v > v_{max} \end{cases} \tag{2.3}$$

While maintaining tension to prevent line slack, the decrease in tension facilitates the load's return to the desired position. Consequently, this mode allows for higher load displacements during lifting to hub height, with considerably lower tugger line forces. Damping winches can operate in different modes, as depicted in Figure 2.18, accommodating various requirements and physical limitations. For this thesis mode 2 is simulated.

	CF	SF	DF
Force	Constant	Linear (only pull)	speed dependent

Table 2.4: Tagline Operation Modes

2.8. Installation Boundary Conditions

The alignment phase is starting when the blade is raised to hub height. This concluding stage of a single-blade lift operation is normal anticipated to happen within a maximum duration of 30 minutes [29].

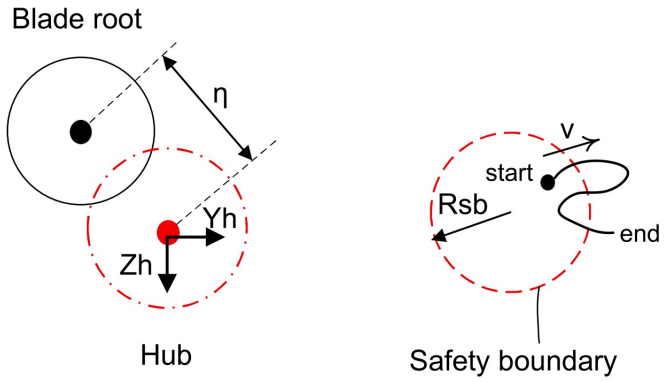

Figure 2.19: Relative Position of the Blade Root and the Hub

The parameter η represents temporal variation in the distance between the blade and hub centers. In practical terms, there exists a circular safety boundary with a radius of R_{sb}. Manual alignment of the center axes can be performed when η is less than R_{sb}. Figure 2.19 illustrates the outcrossing process of η beyond the safety boundary. For a given time span, the outcrossing number can be counted, and the outcrossing rate denotes the frequency of such occurrences. A lower outcrossing rate indicates a higher success rate of alignment. The outcrossing rate, v, is a function of η . In this context, the critical outcrossing rate, $_cr$, is defined as the permissible outcrossing rate for a specified R_{sb}. Empirical selection of $_{cr}$ is often based on knowledge of the installation facilities.

It is assumed that the final installation stage lasts a maximum of 30 minutes, and a successful alignment requires fewer than 10 outcrossings beyond the safety boundary within this time

frame ($_{cr} = 5.5{\times}10^3 Hz$). These specific values were chosen after consultation with a consultant experienced in single-blade installations [30]. The distance η to be able to correctly allign the blade and hub is in this thesis set to 0.2 meters.

2.9. Weather Window

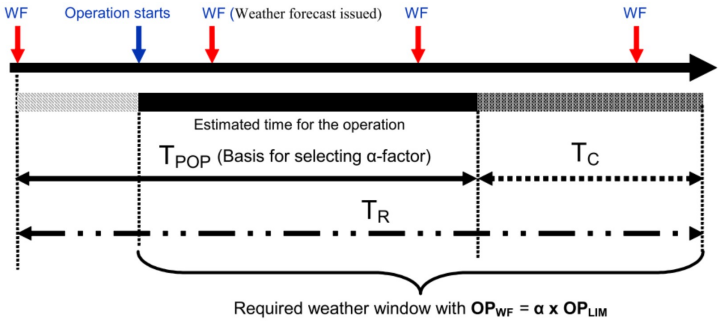

Figure 2.20: Operation Time

Considerations for uncertainties in weather forecasting are crucial in offshore lift operations. Offshore operations can be categorized as either weather-restricted or unrestricted, with the process to determine the necessary weather window outlined in Appendix G. Blade lift operations fall under the category of weather-restricted operations, necessitating the establishment of a required weather window. The duration of one blade installation is defined by an operation reference period (T_r):

$$T_r = T_{pop} + T_c \tag{2.4}$$

where:

$$T_r = \text{operation reference period}$$
$$T_{pop} = \text{planned operation period}$$
$$T_c = \text{estimated maximum coningency time}$$

Blade lift operations are repetitive offshore activities with a scheduled planned operation time T_{pop} is normally accepted. Contingency time is incorporated to account for uncertainties in the scheduled operation time. In the case of repetitive operations, a standard contingency time (T_C) of 50% of T_{pop} is typically allocated.

The next step involves defining the operational limiting criteria OP_{LIM} for the lift installation. This criterion is typically set by the turbine supplier and is dependent on the installation tools. To incorporate uncertainty in both forecasting and monitoring of environmental conditions, the forecasted operational criteria is defined as:

$$OP_{wf} = \alpha_{wf} * OP_{LIM} \tag{2.5}$$

For an operational limiting wind speed of 10m/s, an alpha factor of 0.80 is specified in DNVGL-ST-N001 [31]. With this α_{wf} factor it is possible to calculate the OP_{wf} for a wind speed of 10m/s, this becomes 8 m/s. At the start of the operation the wind speed during the estimated maximum coningency time can't exceed 8 m/s.

From this section can be concluded that three parameters are important to fulfill blade installation. These three key parameters all have to be considered in the engineering phase. So firstly the contractor together with the turbine manufacturer have to discuss which blade lifting tool suits best for the installation process. Then the boundary conditions of the installation should be reviewed and in the end the correct weather window should be established. Within this thesis a time period of 30 minutes is considered for the alignment phase.

3

Aerodynamic Loads

The next chapter will explore the origin of aerodynamic forces, beginning with an explanation of how wind is generated. Following this, will be demonstrated how wind loads on a blade can be calculated.

3.1. Wind

3.1.1. Nature of Wind

As our research centers around wind, it's crucial to thoroughly understand how wind is created and behaves in offshore environments. The sun plays a pivotal role in this process, as temperature differences lead to the emergence of wind.

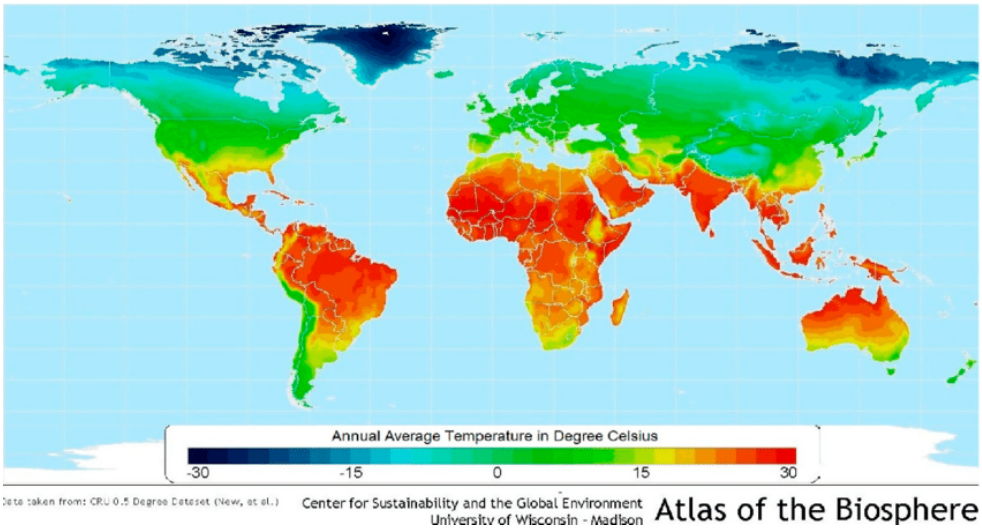

Figure 3.1: Annual Temperature [32]

Figure 3.1 depicts the average surface temperature of the Earth. Notably, temperatures vary, with higher values found near the equator and lower values near the poles. These temperature differences play a significant role in driving global atmospheric circulation.

Examining the Earth's atmospheric dynamics laterally reveals the formation of circulation cells, which are caused by temperature variations across the planet's surface. Near the equator, warm air rises, displacing cooler air at higher altitudes. This creates either northward or southward movement. As this warm air interacts with cooler air from polar regions, it descends back to the Earth's surface, completing the circulation cycle. Similar circulation patterns, but in reverse, occur

near the polar regions. Cold air from the North Pole descends and moves southward, merging with air currents from the south, which then ascend. This atmospheric structure forms three circulation cells between each pole and the equator.

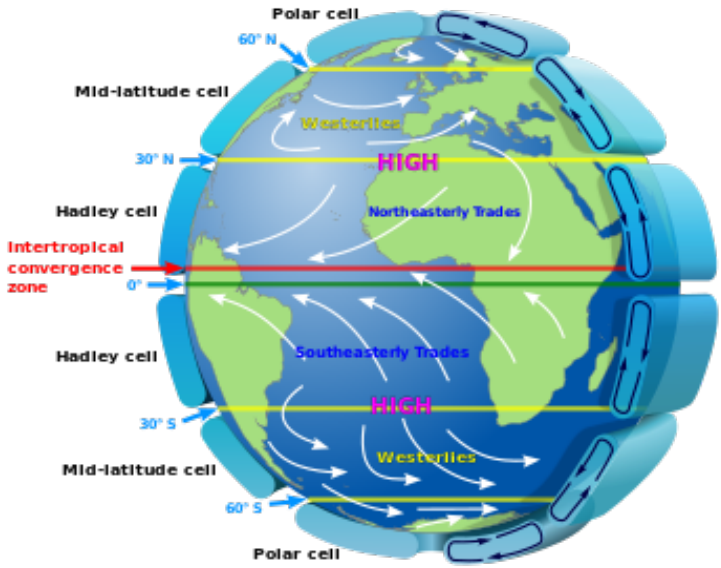

Figure 3.2: Global Atmospheric Circulation [33]

Within these circulation cells, ascending air leads to the formation of areas with low atmospheric pressure, while descending air creates zones with high pressure. Importantly, the size of these circulation cells significantly influences the occurrence of low-pressure systems in the northwestern European region. This distinct distribution of high and low-pressure areas along specific latitudes is evident on the provided map. The Mediterranean region experiences a high-pressure system, while Scandinavia corresponds to a low-pressure area. The map depicts isobars, which represent lines of equal pressure, shown as white lines, outlining the direction of prevailing winds.

At first glance, one might expect winds to move directly from high-pressure to low-pressure areas. However, upon closer inspection, it becomes clear that the Earth's rotation causes deviations from this direct path, leading the winds to follow the contours of the isobars. The placement of low-pressure regions in northern latitudes and high-pressure regions in southern latitudes results in prevailing westerly wind patterns over the northwestern European region.

3.1.2. Power Law

Locally, the Earth's surface friction shapes the atmospheric boundary layer, a vertical wind profile transitioning from zero at ground level to higher speeds above. Figure 3.3 shows the different profiles above some landscapes. The boundary layer's form is influenced by surface roughness, determined by features like houses and trees. Two types of wind profile laws [34] are often used for the vertical extrapolation of wind speeds $u(z)$ in the atmospheric surface-layer. The first law is the logarithmic profile:

$$u(z) = u(z_{ref}) \frac{ln(\frac{z}{z_0})}{ln(\frac{z_{ref}}{z_0})} \tag{3.1}$$

The second formula is the power law:

$$u(z) = u(z_{ref})(\frac{z}{z_{ref}})^{\alpha} \tag{3.2}$$

From a practical standpoint, the 1/7th power law [35], α is $1/7$, has been widely employed in the wind energy community to estimate wind speed. However, numerous scholarly inquiries have illuminated that using the 1/7th power law without qualification can sometimes lead to misleading results due to the complex and fluctuating nature of wind shear phenomena.

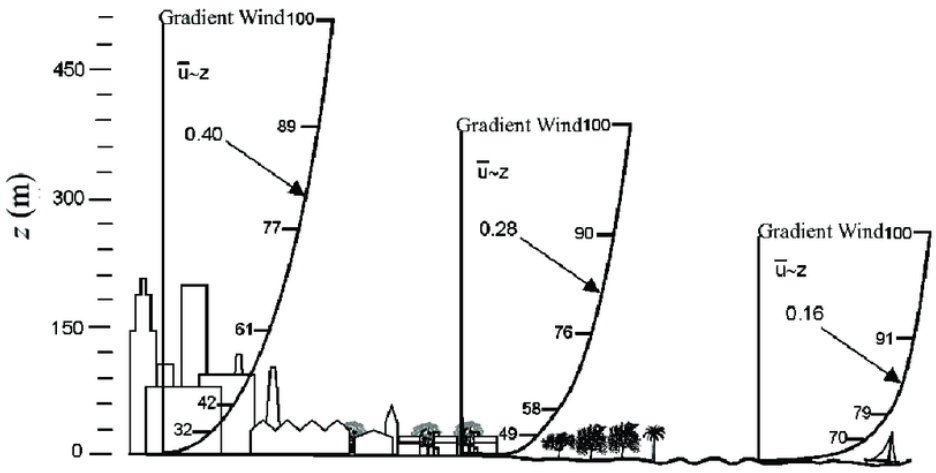

Figure 3.3: Wind Shear Profile [36]

Computational analysis reveals that a significant majority, exceeding 80% [37], of wind shear exponents (WSEs) exhibit values below 0.14. Additionally, the investigation unveils an upward trend in the mean WSE as wind speed increases, accompanied by a decreasing trend in the variance of WSE. The WSE also exhibits distinct temporal variations, peaking in April and reaching its lowest point during September and October. Furthermore, diurnal fluctuations in WSE become apparent, with higher values predominantly observed during nighttime hours, contrasting with daytime periods characterized by relatively lower and consistent values.

The presence of negative WSE values necessitates careful consideration during turbine blade installation. This phenomenon implies that wind speed increases at higher altitudes, highlighting the importance of establishing boundary conditions for turbine blade lift-off from the blade rack. The dynamics of the system change in relation to altitude compared to positive WSE.

Moreover, the analysis underscores the significant influence of atmospheric stability on WSE. Higher mean WSE values are observed during near-neutral and stable atmospheric conditions, indicating a strong interaction between wind shear and prevailing atmospheric stability patterns. This comprehensive investigation provides valuable insights into the complex dynamics of wind shear, contributing significantly to wind energy research and enhancing our understanding of wind behavior in offshore environments.

While a good understanding of the WSE is important, it is out of the out of the scope of this thesis. For the simulations is a WSE used which is set to the 1/7th power law.

3.2. Aerodynamic Loads

Multiple approaches exist for assessing the aerodynamic loads on a wind turbine rotor. These methods can be categorized based on various factors such as modeling fidelity, the extent to which loads can be resolved (integrated loads or spatially resolved), and computational resource requirements.

The blade element theory[38] offers a method to calculate the forces exerted on a rotor by considering the geometric and aerodynamic characteristics of individual span wise blade sections. This approach involves dividing the blade into discrete, radially distributed sections as be shown

in figure 3.4. The calculation of loads for each section is performed with the assumption that the airflow in each section behaves as if it were locally two-dimensional and confined to the plane of the airfoil section. This simplification enables the application of two-dimensional lift, drag, and moment coefficients in conjunction with the relative flow velocity to determine the aerodynamic forces acting on these sectional airfoil components.

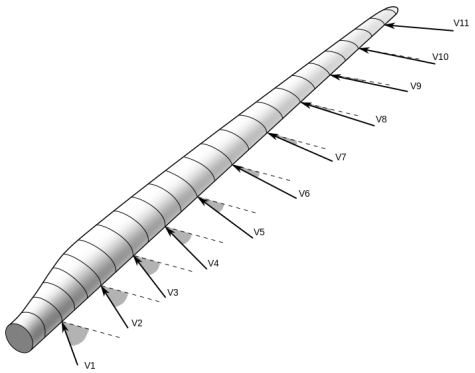

Figure 3.4: Sections of Airfoil [39]

In aerodynamics [40], the forces and moments acting on a body stem from two fundamental sources:

1. Pressure distribution across the body surface
2. Shear stress distribution across the body surface

Regardless of the complexity of the body's shape, all aerodynamic forces and moments originate solely from these two sources. These mechanisms represent nature's means of imparting force to a body moving through a fluid: pressure and shear stress distributions on the body surface. Both pressure (p) and shear stress (τ) are measured in terms of force per unit area. The combined impact of the pressure (p) and shear stress (τ) distributions, when integrated across the entire body surface, results in a resultant aerodynamic force and moment acting on the body. In this thesis, the consideration of moments acting on the body will be neglected.

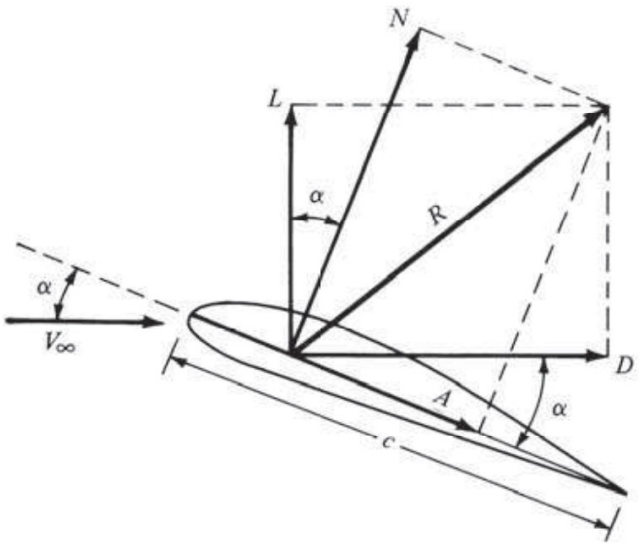

Figure 3.5: Resultant Aerodynamic Force and Components[41]

As can be seen in Figure 3.5 the resultant aerodynamic force can be split up in two sets. The Normal and axial force or the lift and drag force. The drag force is parallel to the incoming wind speed (V_∞), the lift force is perpendicular to the wind speed. This wind speed is called the freestream, which also is known as the undisturbed wind speed. The angle of attack (AOA) refers to the angle between an airfoil chordline and the direction of the freestream wind. The AOA can be calculated with following formula:

$$\alpha = \alpha_i + AOA_i + \mu \tag{3.3}$$

where:

$\alpha_i =$ incoming wind speed angle

$AOA_i =$ twist angle of blade section i

$\mu =$ rotation of blade around its longitudinal axis

Let ρ_∞ and V_∞ be the density and velocity in the undisturbed freestream. let's introduce a dimensional quantity termed the freestream dynamic pressure (with newtons per square meter as unit) as:

$$q_\infty = \frac{1}{2}\rho_\infty u_\infty^2 \tag{3.4}$$

With this the lift and drag forces on an airfoil can be computed. Therefor following formulas are stated:

$$F_l = q_\infty S_i C_{l,i} \tag{3.5}$$

$$F_d = q_\infty S_i C_{d,i} \tag{3.6}$$

where:

$S =$ area of the airfoil = width * chordline length

$C_l =$ lift coefficient

$C_d =$ drag coefficient

When equations 3.4, 3.5 and 3.6 are combined, it is possible to calculate the forces acting on a single blade element.

$$\mathbf{F_l} = \frac{1}{2}\rho_\infty S_i C_{l,i} \mathbf{u}_\infty |\mathbf{u}_\infty| \tag{3.7}$$

$$\mathbf{F_d} = \frac{1}{2}\rho_\infty S_i C_{d,i} \mathbf{u}_\infty |\mathbf{u}_\infty| \tag{3.8}$$

3.3. Number of Blade Elements

An imperative aspect is determining the requisite number of blade sections to ensure computational accuracy that closely mirrors reality. This section focuses on ascertaining the appropriate number of sections for our model.

To achieve this, our attention is drawn towards the drag force exerted on a turbine blade. When the turbine blade is treated as a singular entity, the computed force differs from that derived

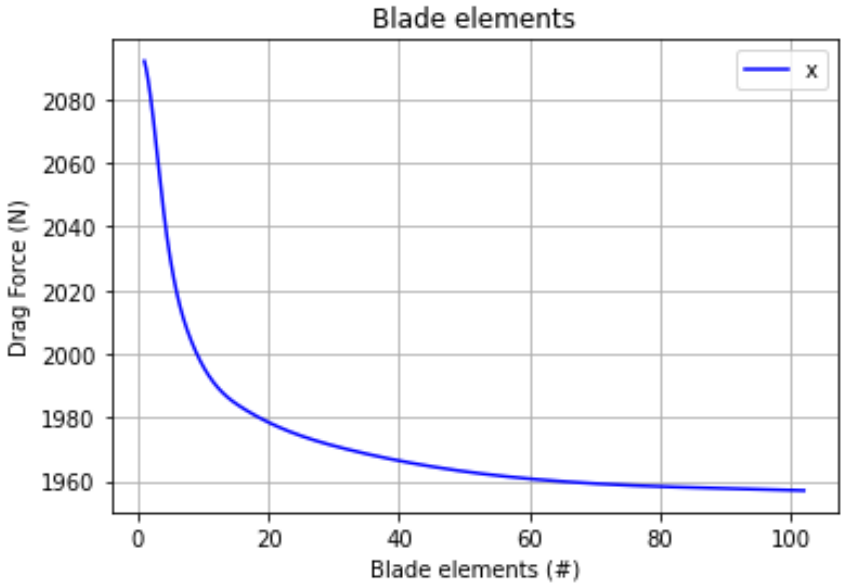

Figure 3.6: Force Sensibility to Number of Blade Elements

when it is divided into numerous elements, such as 100 sections. This variance arises due to differences in total area and the structural composition of individual airfoil sections. Table 3.6 presents the outcomes of a small case study conducted to explore this phenomenon, presuming uniform airfoil characteristics across the blade.

While the blade is simulated in different orientation also a study is done to the drag force when the blade is in vertical position. Results show same results as the study of Figure 3.6. These Results are shown in Appendix C, where the study to the moment of the blade with ascending numbers of blade elements are shown as well. All results show that when less blade elements are used, the forces and moment are higher compared to finer models.

As evidenced by the data in figure 3.6, employing a greater number of elements results in a reduction of the drag force. Notably, doubling the number of blade elements corresponds to a decrease in drag force. Moreover, as the number of elements increases, the disparity in drag forces diminishes, indicating convergence. Based on this analysis, seven blade sections in the simulation are simulated. The reference 15MW blade incorporates seven distinct airfoils positioned at specified locations along the blade span.

Moreover, employing fewer blade elements enhances computational efficiency. Although individual calculations of total drag force take less than a second, the cumulative effect of numerous intensive calculations within the overall model can lead to significant slowdowns. The drag force computed for this configuration amounts to 2013 Newtons, aligning closely with other computations. The margin of error is estimated to be less than 5% relative to the actual drag force exerted by the blade.

During the calculation of the center of gravity for the simplified blade, it was observed that this differed from that of the reference turbine blade. In the simulations, it is assumed that the center of gravity remains in the same position as stated for the reference blade.

3.3.1. Polar Extrapolation

Data of the 15MW Reference turbine[16] is available and lift and drag coefficients are widely available of the airfoils used. As can be seen in figure 3.7, the available data set is only in the

range of -20 to +20 degrees. While research is also needed for installation conditions in which the absolute value could be higher than 20 degrees, it need to be known what lift and drag coefficients should be considered during circumstances where the AOA is outside of the available range.

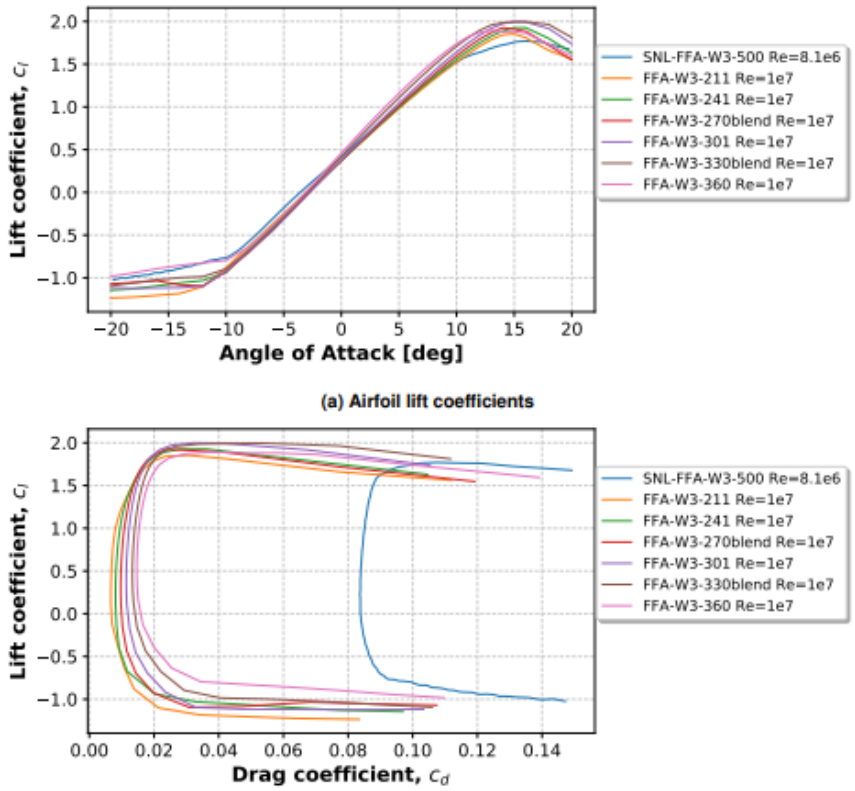

Figure 3.7: Airfoil Lift and Drag Coefficients[16]

To extend the values of the lift and drag coefficient, the Viterna method is used [42], also known as the Viterna-Corrigan method. This method is a data extrapolation method for AOA greater than stall angle, but less than or equal to 90 degrees. The approach was developed based on flat plate theory [43], necessitating an initial angle, along with its corresponding drag and lift coefficients, which must adhere to flat plate theory criteria. The Viterna method is designed to estimate the extrapolation of lift and drag coefficients using the following equation:

$$C_l = A_1 * sin(2\alpha) + A_2 \frac{cos^2(\alpha)}{sin(\alpha)} \tag{3.9}$$

$$C_d = B_1 sin^2(\alpha) + B_2 cos(\alpha) \tag{3.10}$$

where

$$C_{d_{max}} \approx 1,11 + 0,018AR \tag{3.11}$$

$$A_1 = \frac{C_{d_{max}}}{2} \tag{3.12}$$

$$B_1 = C_{d_{max}} \tag{3.13}$$

$$A_2 = (C_{l_{stall}} - C_{d_{max}} sin(\alpha_{stall}) cos(\alpha_{stall}) \frac{sin(\alpha_{stall})}{cos^2(\alpha_{stall})} \tag{3.14}$$

$$B_2 = \frac{C_{d_{stall}} - C_{d_{max}} * sin^2(\alpha_{stall})}{cos(\alpha_{stall})} \tag{3.15}$$

In equation 3.11, the symbol AR represents the aspect ratio, which is determined through the blade section length and area. A commonly recommended value for AR is 10 in most computational scenarios. Nevertheless, altering the value of AR is unlikely to significantly impact the final results. When extrapolating data for pitch angles greater than 90 degrees $(D > 90°)$ and smaller than a minimum value $(D < D_{min})$, the calculated values are taken into consideration.

The Viterna method, while not addressing the distribution of pressure or skin friction forces, can still provide a reasonable estimate by making a few basic assumptions. These assumptions can yield results that align with those predicted by the Viterna method. Although the method's computational results may not offer a precise representation of the underlying physics, they can furnish a reasonable estimate, particularly during the early stages of the design process.

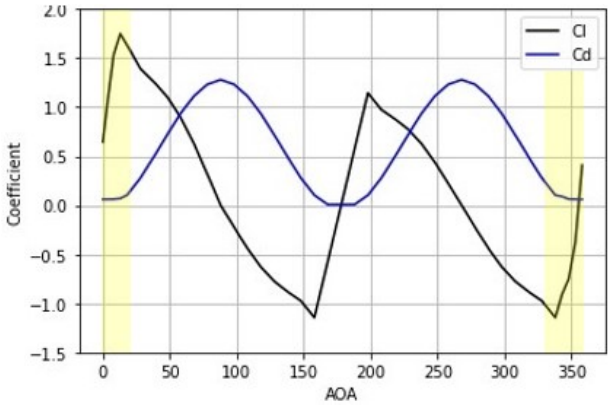

Figure 3.8: Airfoil Lift and Drag Coefficients of the SNL-FFA-W3-500 Airfoil

In Figure 3.8, an extrapolation of the SNL-FFA-W3-500 airfoil is shown, a critical piece of information that allows us to integrate these coefficients into the simplified turbine blade model discussed later in this thesis. As can be seen there are two coloured areas, these coloured areas are the lift and drag coefficients which are known from Figure 3.7. Everything outside the coloured area are values which are calculated with the Viterna extrapolation.

It's essential to recognize that while the lift and drag coefficients are influenced by the shape of the airfoil, they also depend significantly on the prevailing wind speed and other atmospheric conditions. While these coefficients may exhibit slight variations under different wind speeds, the simplifying assumption in this thesis of maintaining a consistent Reynolds number is made. However, it's worth noting that a comprehensive investigation into the influence of Reynolds numbers falls beyond the scope of this thesis. Nonetheless, for those interested, a brief exploration of this topic is available in Appendix F.

3.4. Beam Model

Beam deflection analysis is a fundamental aspect of structural engineering, providing crucial insights into how beams deform under various loads. The primary theoretical frameworks for this

analysis is the Euler-Bernoulli beam theory[44]. The Euler-Bernoulli simplifies the analysis for slender beams.

Blade deflection becomes increasingly significant with larger turbines, as the internal moment within the blade increases due to the greater distance to the center of gravity (COG). As blades increase in size, it becomes impractical to ignore blade deflection resulting from weight and wind loads. When zoomed in on the hub blade interface, it is important to know what the contribution of the blade deflection is to the set installation boundary conditions.

3.4.1. Euler Bernoulli beam

The Euler–Bernoulli beam theory, also referred to as classical beam theory, represents a simplified version of linear elasticity theory [45]. It serves as a method for evaluating the load-bearing capacity and deflection characteristics of beams, particularly when dealing with small deflections and lateral loads exclusively. By disregarding shear deformation and rotatory inertia effects, it can be regarded as a specific instance of the Timoshenko–Ehrenfest beam theory [46].

Despite the existence of more complex mathematical models, such as plate theory [47], the inherent simplicity of beam theory positions it as a valuable tool in various scientific disciplines, particularly in the realms of structural and mechanical engineering.

To use the Bernoulli-Euler beam theory three basic assumptions need to be made:

1. Plane sections that are initially perpendicular to the neutral axis will remain flat and perpendicular to the neutral axis even after deformation as shown in figure 3.9.
2. Deformations are small.
3. The beam exhibits linear elastic isotropic behavior, with no consideration given to the effects of Poisson's ratio.

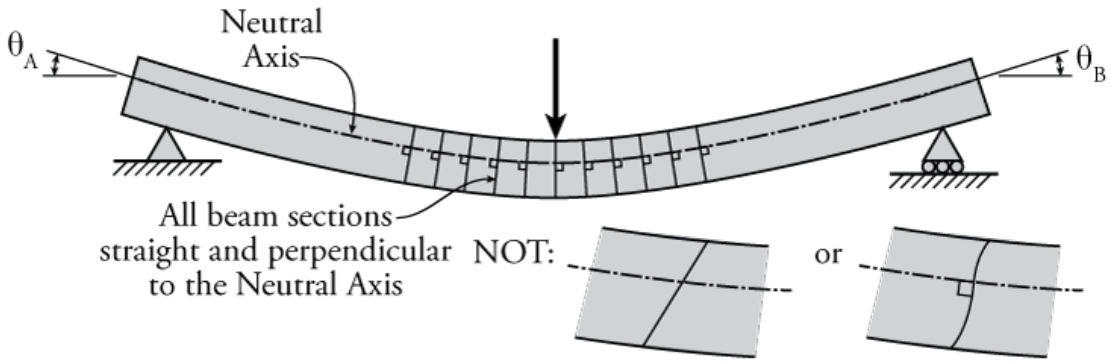

Figure 3.9: Euler-Bernoulli Beam [48]

To elaborate a bit on the Euler-Bernoulli beam a small example will be shown of a beam element. This beam element is shown in Figure 3.10. The beam is positioned in a manner where its primary axis aligns with X_1. The deformation is governed by a function $y(X_1)$ that characterizes the deformation of the neutral axis (as depicted in figure **??**). This initial condition enables the computation of the small strain matrix at any given location. The coordinates of a random point, denoted as p, prior to deformation are described as follows:

$$X = \begin{pmatrix} X_1^p \\ X_2^p \\ X_3^p \end{pmatrix} \tag{3.16}$$

Disregarding any influence from Poisson's ratio, the post-deformation coordinates of point p (as shown in figure 3.9 are provided as follows:

$$x = \begin{pmatrix} X_1^p - X_2^p * sin(\theta) \\ X_2^p + X_2^p * cos(\theta) \\ X_3^p \end{pmatrix} \tag{3.17}$$

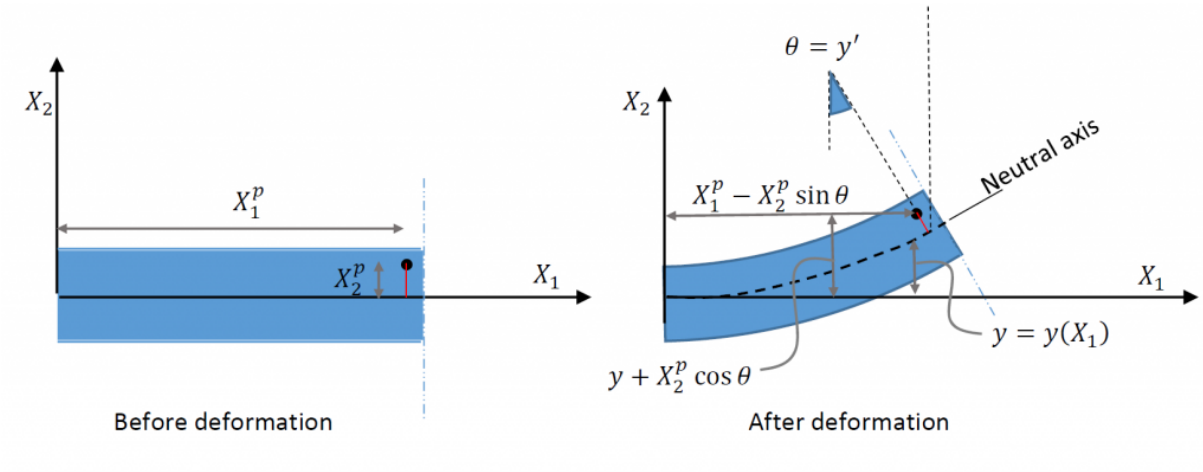

Figure 3.10: Euler-Bernoulli Beam Example [49]

The second assumption, which considers small deformations, permits the approximations $\theta \approx \sin\theta \approx \tan\theta$ and $\cos\theta \approx 1$. Consequently, the displacement function, when incorporating the assumption of small deformations, is expressed as follows:

$$u = x - X = \begin{pmatrix} -X_2^p * (\theta) \\ y \\ 0 \end{pmatrix} \tag{3.18}$$

The superscript p can be omitted since this is applicable to any arbitrary point. Additionally, it's worth noting that $y' = \tan\theta \approx \theta$. Consequently, the displacement function takes on the following structure:

$$u = x - X = \begin{pmatrix} -X_2 * \frac{d_y}{dX_1} \\ y \\ 0 \end{pmatrix} \tag{3.19}$$

Now is known how a blade section will deform it is important to know how forces will deform a simple beam. The following equations describes the relation between the applied load and the deflection:

$$\frac{d^2}{dx^2}(E * I * \frac{d^2w}{dx^2}) = Q \tag{3.20}$$

The function $w(x)$ represents the deflection of the beam in the z direction at a specific position x. It's important to remember that the beam is treated as a one-dimensional object in this model. The symbol Q signifies a distributed load, essentially a force per unit length (akin to pressure,

which is a force per unit area). This load can be a function of various variables, including x, w, or others. The parameters E and I denote the elastic modulus and the second moment of area of the beam's cross-section, respectively. It's crucial to compute I concerning the axis that is perpendicular to the applied loading. To clarify, for a beam aligned along the x axis with a load acting in the z direction, the beam's cross-section lies in the yz plane, and the pertinent second moment of area is determined as follows:

$$I = \int \int z^2 d_y d_x \tag{3.21}$$

In this context, assume is that the center of the cross-section is positioned at $y = z = 0$. Frequently, the product EI is considered constant, which results in:

$$E * I \frac{d^4 w}{dx^4} = Q(x) \tag{3.22}$$

This equation, which characterizes the deflection of a static, uniform beam, finds extensive use in engineering applications.

From equation 3.21 and 3.22 can be concluded what the deflection of the blade will be. But to do this their need to made a few assumptions. First of all some reference points need to be set, where the yoke will be attached to the blade. For the sake of simplicity is assumed that these are on the points where the blade elements end.

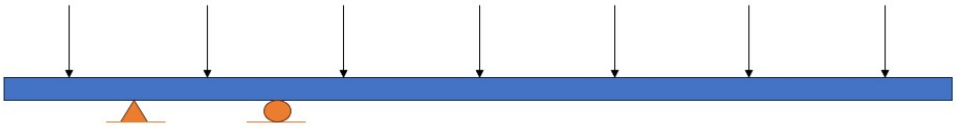

Figure 3.11: Blade Model

As can be seen in figure 3.11 the beam is supported at two points. With these points set it is able to calculate the deflection of this simple beam, while these points are set in space. So the left point is always at location (0,0) and the right point is always at point (x,0), but while small deformations is assumed, it can be said that the x-location of this point is equal to the distance of one blade element, which is 16,7 meter. The green section shows the wind load on the beam.

Now other boundary conditions can be added to solve the equation. While both ends of the blade are free in space at both ends following conditions should be considered for the model:

$$M = -(E * I * \frac{d^2 w}{dx^2}) = 0 \tag{3.23}$$

Which means that the bending moment should be zero. Next to this boundary condition, the shear force needs to be zero. Which is given in following equation:

$$Q = -\frac{d}{dx}(E * I * \frac{d^2 w}{dx^2}) = 0 \tag{3.24}$$

3.4.2. Conclusion

Now is known how the deflection of a simple beam can be calculated, a research to the deflection under static windspeeds is conducted. Figure 3.12 shows the deflection of the reference turbine blade under static windspeed. While force is quadratic to the incoming windspeed, the trend of the deflection which was found is also quadratic.

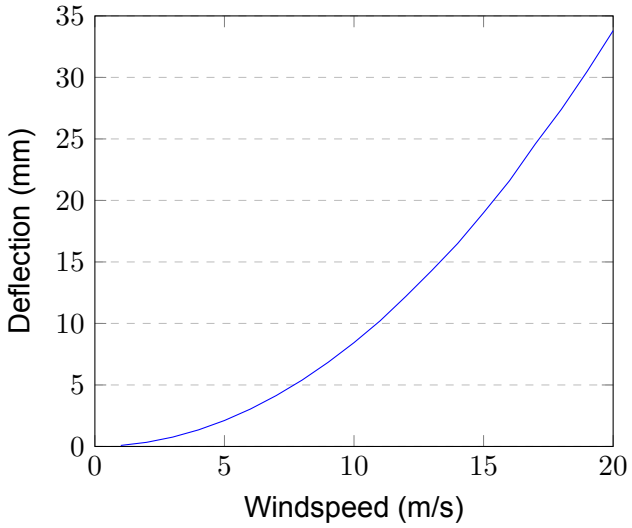

Figure 3.12: Turbine Blade Deflection

In the analysis presented in Figure 3.12, it is observed that the deflection of the turbine blade at the root is minimal. Specifically, when the blade is subjected to a wind speed of 12 m/s, the root deflection measures merely 12 mm. This finding is particularly relevant considering that the installation of turbine blades is typically constrained to environments where wind speeds do not exceed 10 to 12 m/s. Within this range of operational wind speeds, the variation in blade deflection is limited to a few millimeters. Despite its minimal contribution to the overall displacement at the blade root, this degree of deflection is not incorporated into the simulation model.

4

Dynamic Modelling of the Blade Installation

The methods we've set up for creating a computer model of the system let us analyze how the system acts under different situations. First off, we'll give a straightforward explanation on how to come up with the equation of motion.

4.1. Equation of Motion

During the lifting operation of the turbine blade, the system comprises a vessel with a load suspended from the crane, resulting in one body with 6 degrees of freedom, assuming rigid bodies. This leads to a total of 6 degrees of freedom, represented by the vector x:

$$x = [\eta_1, \eta_2, \eta_3, \eta_4, \eta_5, \eta_6]^T \tag{4.1}$$

In this context, the subscripts 1, 2, and 3 refer to rotations around the x, y, and z axes of the crane's body frame, respectively. Meanwhile, subscripts 4, 5, and 6 correspond to rotations around the x, y, and z axes of the blade. Figure 4.2 displays the axis systems used in the model. The subscript "c" indicates that it pertains to the crane's body frame, while the subscript "b" denotes the body axis of the blade.

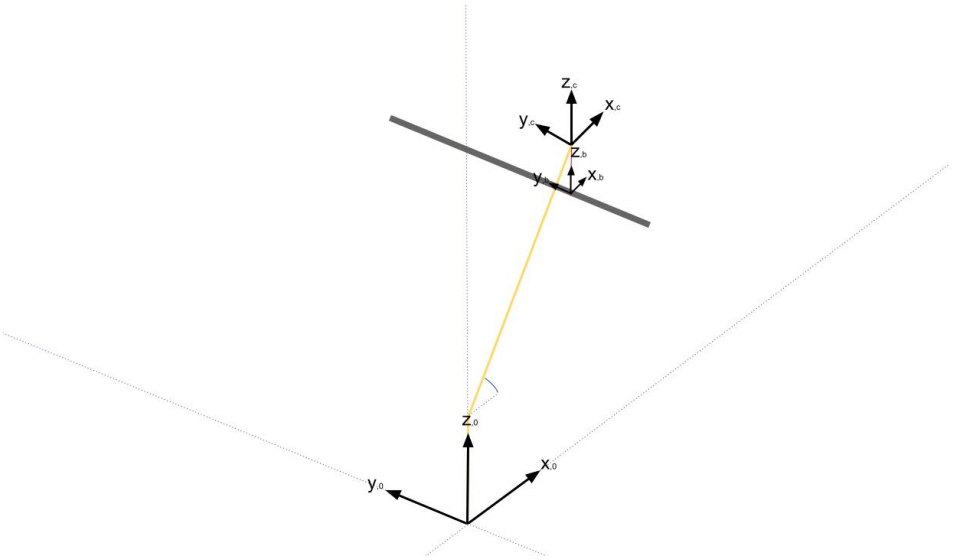

Figure 4.1: Simplified Blade Model

The equation of motion for the system is expressed as:

$$M\ddot{x} + B\dot{x} + Cx = F \tag{4.2}$$

The mass matrix M is derived based on the mass and inertia terms of the blade. The mass matrix contains the mass of the body on the diagonal entries for displacements in x, y, and z, with rotational inertia for rotations. The off-diagonal terms in the matrices are coupling terms, influencing motion in one degree of freedom by another. In the model these values are equal to zero.

The damping matrix B,is included in the dynamics of a system to account for the effects of resistance that oppose the motion of an object. It represents the forces that cause the gradual loss of energy in vibrating systems, such as friction in mechanical systems or electrical resistance in circuits. In the context of mechanical vibrations, damping is typically modeled in three main ways: viscous damping, frictional damping or structural damping. The inclusion of the damping term allows for the simulation of energy dissipation over time, providing a more accurate representation of the system's behavior under real-world conditions. In this thesis a damping of 0.5% is assumed.

The forcing vector F is obtained from the forces acting on the blade and yoke, representing wind forces on the blade. The sum of the wind forces (explained in section 3.2) account for the Force vector.

The Forward Euler method [50] is a simple yet powerful numerical technique used to approximate solutions to ordinary differential equations (ODEs). As a first-order numerical procedure, it belongs to the class of single-step methods for solving initial value problems. The method is named after the Swiss mathematician Leonard Euler, who is credited with its introduction.

The essence of the Forward Euler method lies in its approach to approximating the slope of the solution curve at a given point and then using this slope to predict the value of the solution at the next point. Given an ODE expressed as $\frac{dy}{dt} = f(t, y(t))$ with an initial condition $y(t_0) = y_0$, the Forward Euler method updates the solution from a current time step t_n to the next time step t_{n+1} using the formula:

$$y_{n+1} = y_n + \Delta t \cdot f(t_n, y_n)$$

where:

$$y_n = \text{the approximation of } y(t_n)$$

$$f(t_n, y_n) = \text{the rate of change (derivative) at } t_n$$

$$\Delta t = \text{the step size, a small increment in time moving from } t_n \text{ to } t_{n+1}$$

$$t_{n+1} = t_n + \Delta t$$

$$y_{n+1} = \text{the estimated value of } y(t) \text{ at time } t_{n+1}$$

The Forward Euler method's simplicity is one of its main advantages, making it straightforward to implement for solving a wide range of problems. However, this simplicity comes with limitations. The method's accuracy is highly dependent on the choice of the step size Δt; smaller step sizes can lead to more accurate solutions but at the cost of increased computational effort. Additionally, the Forward Euler method is an explicit method, which means it can be unstable for certain types of problems or for large step sizes. During the simulations, it was observed that a timestep value of 0.01 yielded clear results.

The Forward Euler method facilitates the calculation of the blade body's translational and rotational velocities and allows for the blade's position to be established. Utilizing the computed values, a rotational matrix and an angular velocity tensor can be constructed. These calculations enable the determination and analysis of the blade root's velocity and position.

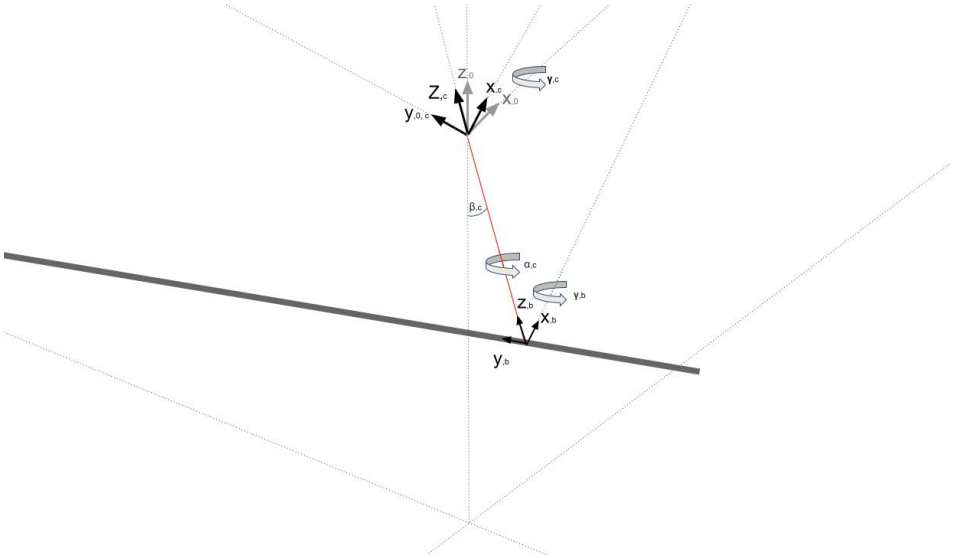

Figure 4.2: Rotated Blade Model

4.2. Model Set Up

This section systematically presents the progressive construction of the model. The process commences with the fixation of a blade, followed by its stabilization at the center of gravity. Shifting our focus, an alternative model is explored, centering on a pendulum-borne mass and predicting its ensuing motions. Building upon this, the study transitions to a more complex scenario involving a turbine blade affixed to a pendulum mechanism. Subsequent stages involve the incorporation of additional model components, culminating in the development of an overarching model. This ultimate configuration simulates a turbine blade suspended from a crane, creating a comprehensive framework for analysis.

4.2.1. Fixed Turbine Blade

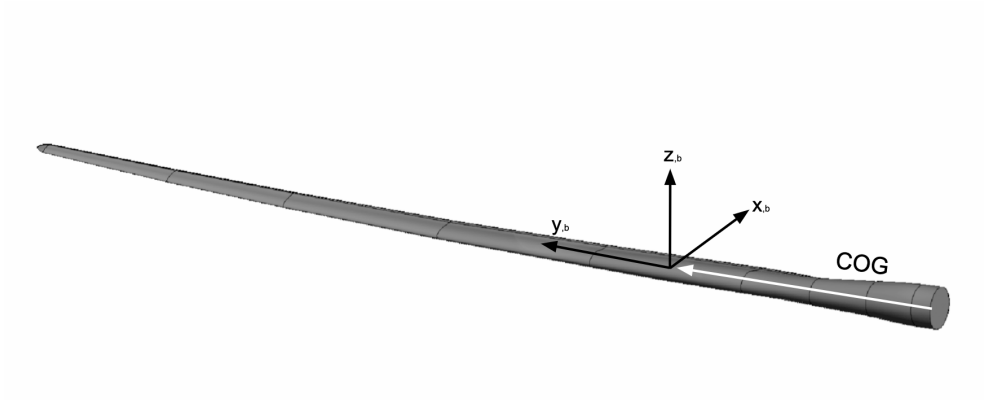

Figure 4.3: Body Axis of Turbine Blade

In Figure 4.6, the body-axis of the blade is depicted, which aligns precisely with the Center of Gravity (COG) of the turbine blade. At this point, the turbine blades are lifted using their yoke. Although the yoke is a significantly large piece of equipment, its center is meticulously designed to align with the blade's COG. Manufacturers typically specify the COG of the blade. For the 15MW reference blade, the COG is situated 26.8 meters from its root. During the modeling process, it was discovered that the COG of the simplified blade model was located 1.2 meters further from the root than originally stated in the specifications. However, the model assumes that the COG remains at its designated location.

Assuming rigid body dynamics to model the blade's dynamics, the simulation is divided into two distinct equations: one for the translation of the Center of Gravity (COG) and another for the rotation of the COG. The subsequent section of this chapter will detail the verification process for a simplified turbine blade model.

4.2.2. Anchored Blade

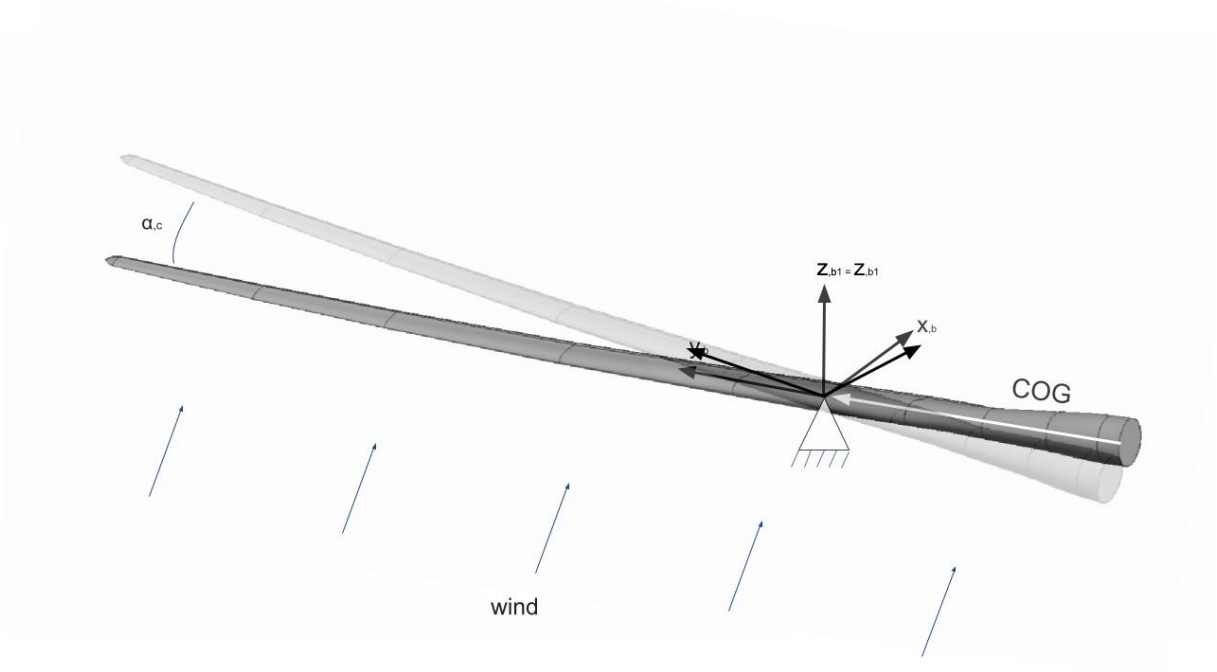

Figure 4.4: Rotation of Blade at Steady Wind

When the blade is anchored at its Center of Gravity (COG), as illustrated in Figure 4.6, it is capable of moving freely around this point. This movement can be conceptualized as if the blade were attached to the real world via a ball-and-socket joint (a connection the same as a human hip), allowing it to pivot around its COG. Modeling this scenario reveals that the blade's angle adjusts with the wind, settling into an equilibrium position where it aligns with the wind's direction, much like a weather vane.

Figure 4.5 demonstrates the angle the blade assumes in response to the incoming wind, starting from a 90-degree position. In this simulation the moment around the x- and y- body axis is restrained, so the blade is only able to spin around its own z- axis.

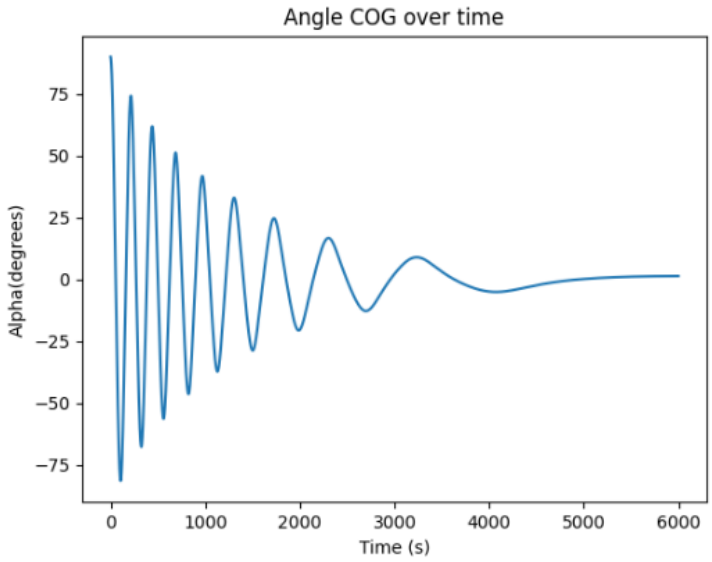

Figure 4.5: Angle Around z-Axis

As can be seen, the blade moves to its equilibrium point. In this point the blade is aligned with the wind direction. At this point there is no force acting on the blade while the airfoil is perpendicular to the wind. As stated before, only wind in the plane is contributing to the forces on the turbine blade.

The frequency of the turbine blade decreases, as illustrated in Figure 4.5. Initially, when the wind is parallel to the airfoil, the forces and consequently the moments exerted on the blade are at their maximum. This results in higher accelerations compared to subsequent cycles. As the turbine blade moves through the wind, it experiences damping due to its motion through wind. This damping causes the blade to lose energy, preventing it from returning to its exact original position before the cycle began. Consequently, in the following cycles, both the force and moment acting on the blade are reduced due to an angle between the wind and the equilibrium position of the blade, leading to lower frequencies.

Shifting the attachment point of the blade to its Center of Pressure (COP) results in the blade remaining stationary. This behavior is expected because the wind pressure is evenly distributed on both the left and right sides of the blade, effectively canceling out any potential movement. Identifying the COP is crucial for the design of wind turbine blade installation tools, as it helps in counteracting significant moments. Although this topic is highly relevant and warrants further investigation, it falls beyond the scope of this thesis.

4.2.3. Simple Pendulum

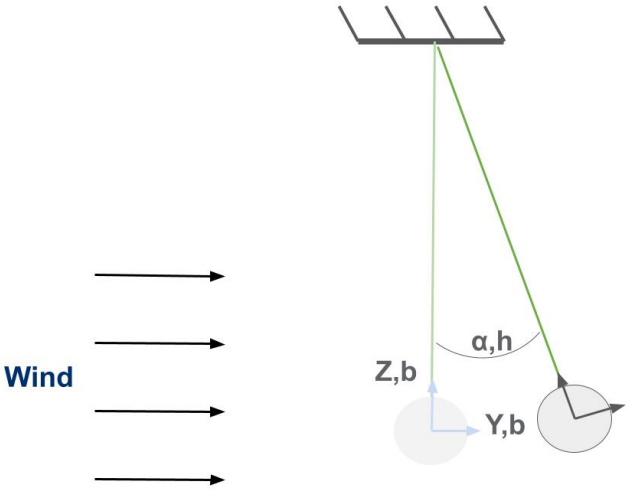

Figure 4.6: Simple Pendulum System

Now a simple mass pendulum system is modelled. The wind speed acting on the mass is the wind speed minus the speed of the mass itself. All forces acting on the mass are the local wind force, gravitational force and the force of the pendulum. As wind speeds get higher the equilibrium position of the mass gets higher, this is due to that the angle of the pendulum system should be higher to counteract for the wind force.

To understand the dynamic behavior of the rigid body in the system, an analysis of the natural periods is performed. This analysis primarily aims to identify the natural periods of the load hanging from the crane. Recognizing these natural periods is essential because if the load is excessively excited during these periods, it may start to oscillate similarly to a pendulum.

The equation used to calculate the natural period of pendulum-like motion, T_n, is based on the linearized pendulum model and is provided below:

$$T_n = \frac{2\pi}{\sqrt{\frac{L}{g}}} \tag{4.3}$$

Where

$$L = \text{length of pendulum}$$

$$g = \text{gravitational acceleration}$$

In Figure 4.7 two results are shown with different pendulum lengths. As can be seen the period is higher when the length of the pendulum is longer. With the simulation it was possible to calculate the period of the pendulum. These results were compared with equation 4.3 and results where very close to each other. With this result it is convenient that the pendulum model is simulating the motion in the right way.

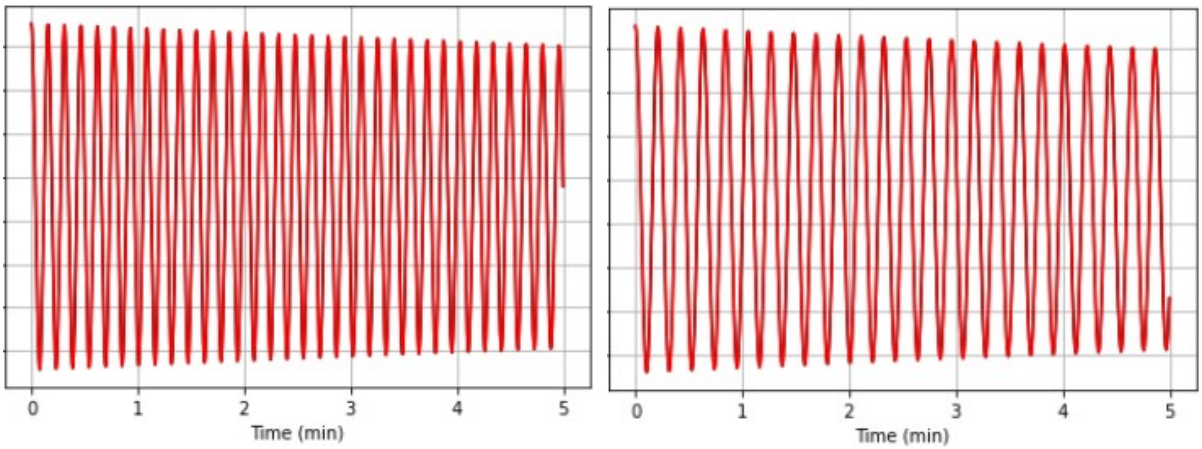

Figure 4.7: Crane Angle for a 21.5 (Left) and 40 (Right) Meter Long Pendulum System

As illustrated in the figure presented above, there is a gradual decrease in the maximum angle value observed. This phenomenon can be attributed to the effects of aerodynamic damping. Utilizing Python, it was possible to calculate a specific value that aligns perfectly with all the peaks observed in the graph. Through this process, the damping coefficient was successfully determined.

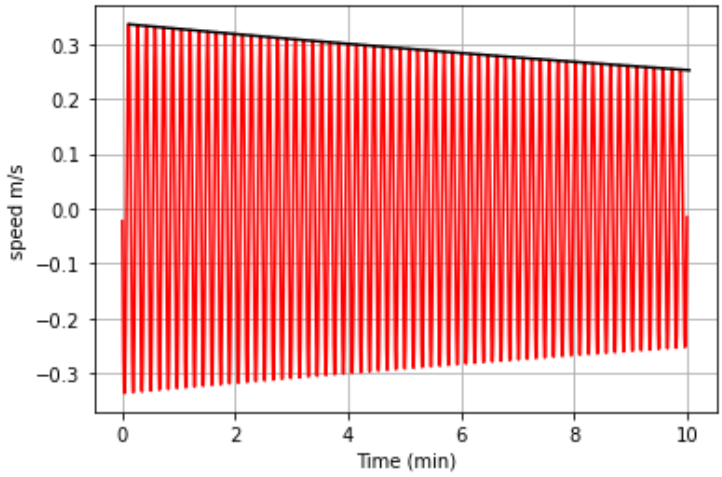

Figure 4.8: The Rate of Decaying of the Measured Signal which Corresponds to the Damping Coefficient of the Set-Up

The simulations conducted revealed that the damping experienced by the blade is influenced by the undisturbed wind speed, measured at a distance far from the turbine blade. For the purposes of this analysis, it has been assumed that the wind conditions are steady and devoid of turbulence. This assumption simplifies the modeling process and focuses the analysis on the direct effects of wind speed on blade damping. In Figure 4.9, the damping behavior of the system, modeled as a simple pendulum, is depicted. An examination of the data presented in the figure leads to the observation that there is a linear relationship between the wind speed and the damping effect. This relationship underscores the significance of wind speed as a determinant factor in the aerodynamic damping of turbine blades, suggesting that as wind speed increases, the damping effect on the blade also increases proportionally.

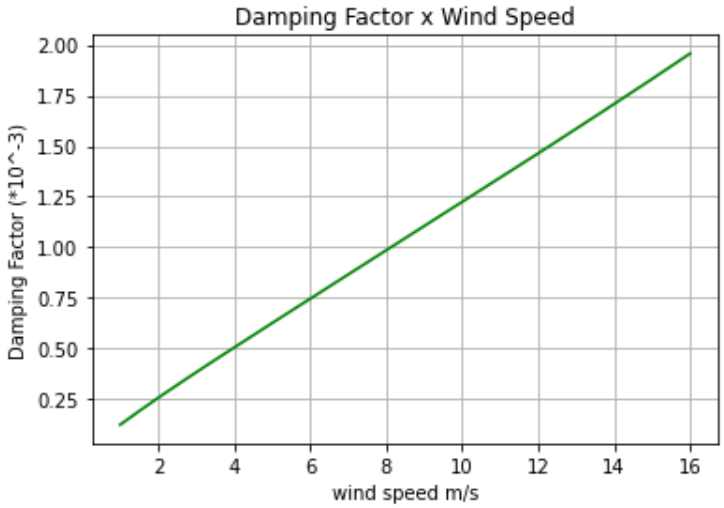

Figure 4.9: Damping of Turbine Blade

Force exerted on a turbine blade increases quadratically with wind speed, meaning that the force escalates more rapidly as wind speed rises. This quadratic relationship implies that the loads on the turbine blade also intensify significantly with an increase in wind speed. According to Newton's second law, there is a direct, linear correlation between force and acceleration, indicating that an increase in force proportionally increases acceleration.

Velocity, is derived from acceleration. Furthermore, the damping factor, acts against the velocity, effectively reducing the motion's energy. The observations presented in the figure verify these theoretical principles. The analysis confirms that the increase in force due to wind speed and the moderating effect of the damping factor are in line with established physical laws.

4.3. Wind Gusts

While wind is not steady a study to the sensitivity of a change in windspeed is conducted. A change of the height of a wind speed is also called a gust. A gust is when the wind suddenly gets faster for a short time. The definition of a wind gust tells that, a gust [51] is taking place when the fastest speed of the wind reaches at least 8 m/s, and there's a difference of at least 4.5 m/s between the fastest and slowest speeds [52].

As the height of windspeed is changing the forces and moments acting on the turbine crane and the lifting cables will change. This will ensure motions in the turbine blade. A study is done to the height of the amplitude of the direct distance of the hub to the bladeroot. Not only the height of the amplitude is tested, also the duration of recovery time for the blade root within the installation window can be found.

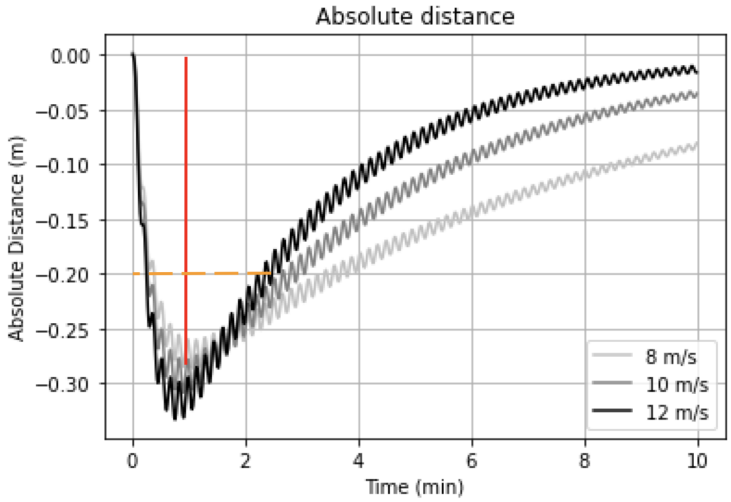

Figure 4.10: Motion Turbine Root due to Wind Gust with Same Length and Height of Wind Gust, HH-CB-CF-...-0

Figure 4.10 shows the result of simulations of wind gusts. At $t = 0s$ a wind gust is applied for 5 seconds with an increase of the windspeed of 4 m/s. The results show that the amplitude (line shown in red) is almost the same for all mean wind speeds. The orange line shows the recovery time which is needed for the blade to return within the installation bin. From the results can be observed that the recovery time of higher wind speeds is faster than that compared for lower wind speeds. This is related to the findings of section 4.2.3.

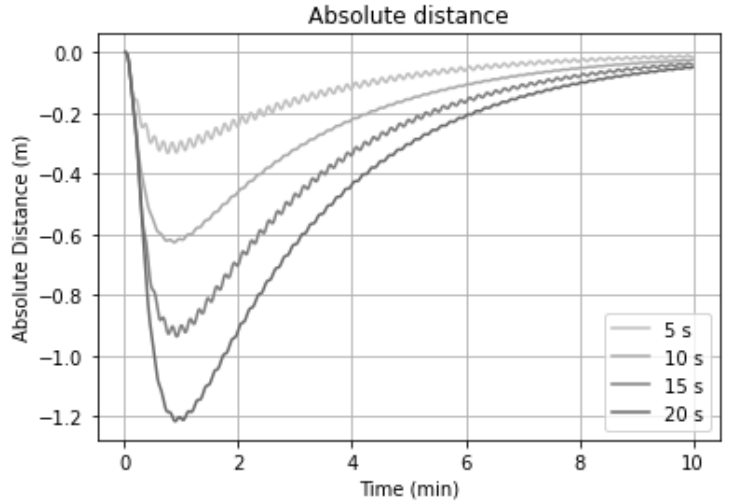

Figure 4.11: Motion Turbine Root due to Wind Gust with Various lengths, HH-CB-CF-8

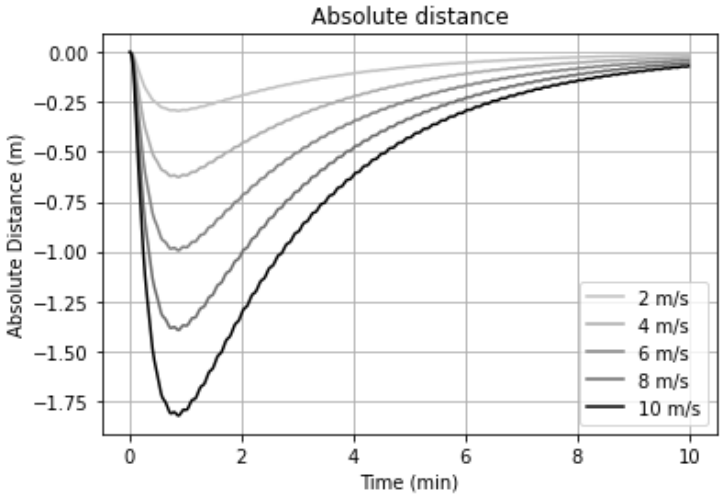

Figure 4.12: Motion Turbine Root due to Wind Gust with Various Wind Gust Heigths, HH-CB-CF-12

Figures 4.11 and 4.12 show the results of simulation of the turbine blade with different heights and lengths is the wind speed. In these simulations the mean wind speed before and after the wind gust is perfectly constant, which means the TI is zero.

Both results show that the height and length of the wind gust are of importance to the motion of the wind turbine blade. This is due to the higher wind loads acting on the turbine blade during the wind gust. The length of duration of the wind gust ensures that more energy is put in the system which results in higher displacement of the root. When the wind gust length is the same but the height of the wind gust is higher the force acting on the blade is higher for a certain time period, second law of newton tells us that higher forces results in higher accelerations. This results in a higher amplitude of the blade motion.

Figure 4.10 shows the amplitude of the motion of the turbine blade. As mentioned before this is dependent on both the time period and the height of the wind gust. 4.13 shows a 3D plot of the height of the amplitude of the root motions.

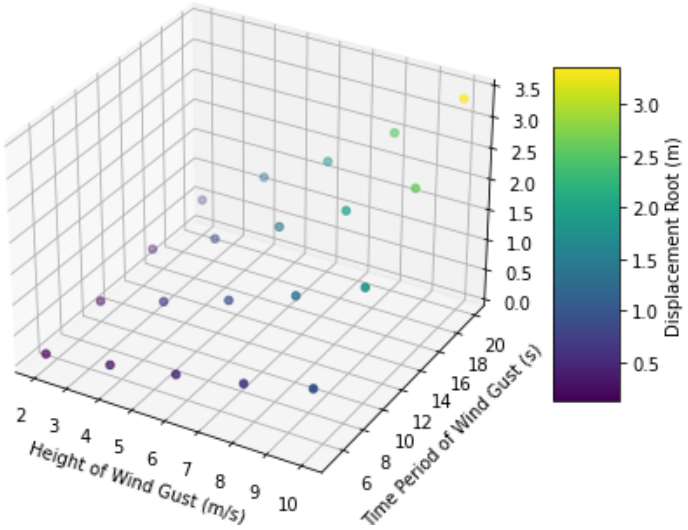

Figure 4.13: Height of Amplitude Root due to Wind Gust, HH-CB-CF-10-0

As mentioned before not only the amplitude is of importance but maybe even more important is the recovery time of the turbine blade. For turbine installation it is in the end most important to install a blade as fast as possible. Therefor it is of importance to understand what a wind gust does to installation time of the blade. Figures 4.14 and 4.15 show the results of this study. As can be seen ones again the length and height of the wind gust are of importance to the length of the recovery time. When both figures are compared to each other also can be seen that the mean wind speed is of importance as well, this is again related to the findings in section 4.2.3, which states that the damping factor is higher for higher wind speeds.

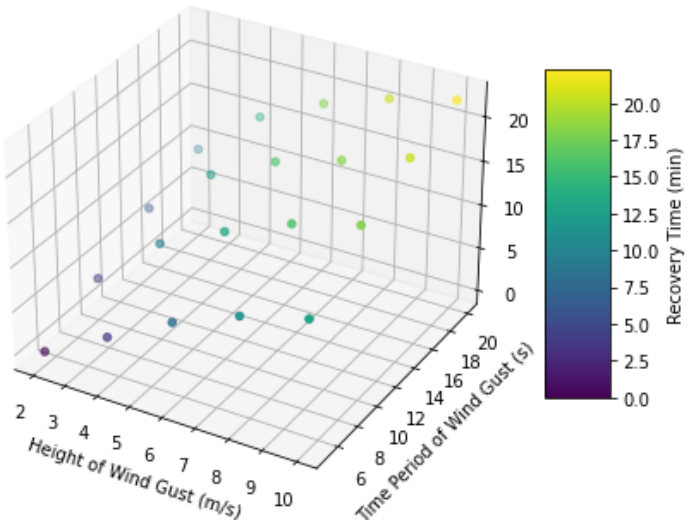

Figure 4.14: Recovery Time for Mean Wind Speed 8 m/s, HH-CB-CF-8-0

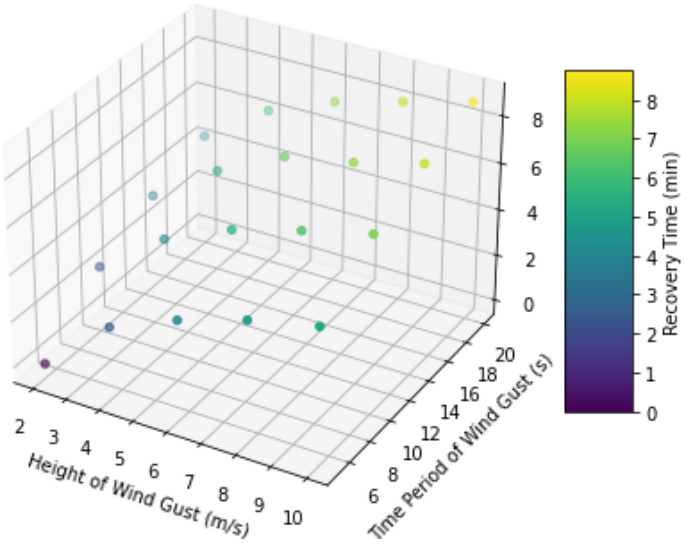

Figure 4.15: Recovery Time for Mean Wind Speed 12 m/s, HH-CB-CF-12-0

4.3.1. Wind Input

While simulating the motion of a turbine blade, as already mentioned before the wind is of big importance. In real life circumstances the wind is not steady, but there are fluctuations in its value and direction. This is also called turbulence. The turbulence intensity (TI) says something about these fluctuations. The TI can be calculated with following formula:

$$I_u = \frac{\sigma_u}{u_{mean}} \tag{4.4}$$

where:

$\sigma_u =$ standard deviation of wind

$u_{mean} =$ the mean wind speed

The IEC-6400-1 standard describes three different TI classes. These are categorized in three groups; high TI (class A), medium TI (class B) and low TI (class C).

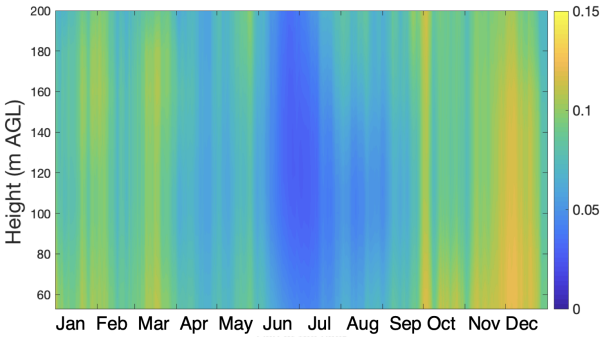

Figure 4.16: Turbulence Intensity [53]

Turbulence intensity is dependent on multiple factors, for example on the time of the year, as can be seen in Figure 4.16. In this thesis the TI is kept constant over the time period of the

simulation. The different TI values are dependent on the wind class and the wind speed [54]. Figure 4.17 shows the TI values for the 3 (IEC 61400-1 [55]) classes and the two offshore classes, offshore near-shore and offshore open sea (IEC 61400-3 [56]).

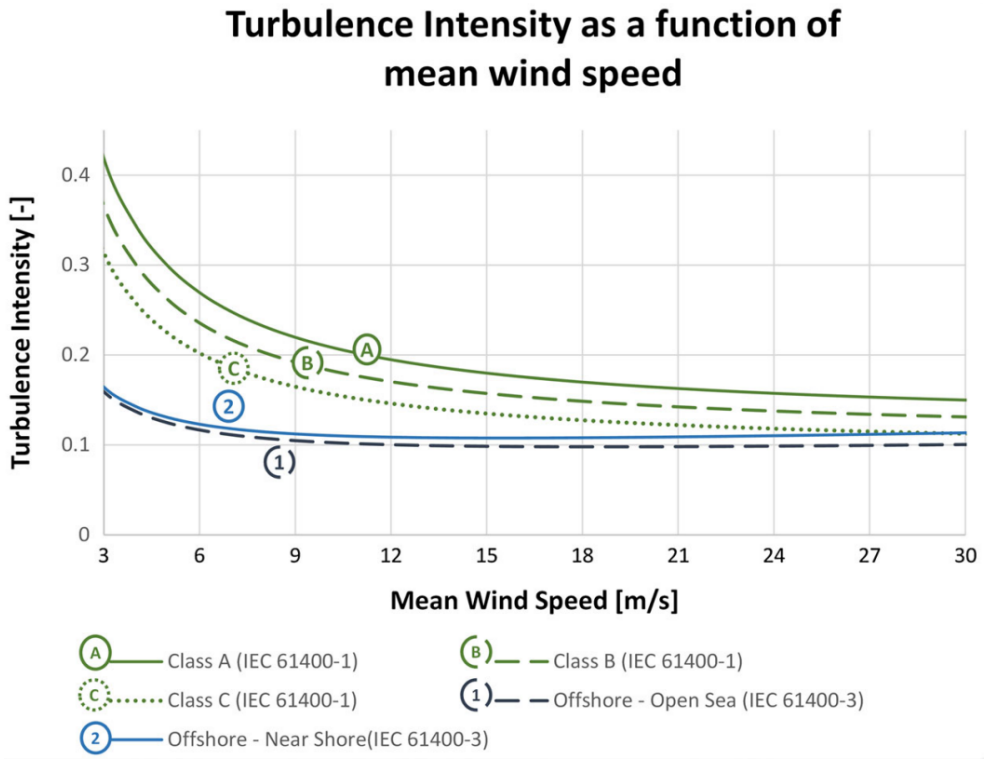

Figure 4.17: Turbulence for Three Wind Turbine Classes A, B and C and for Offshore Wind Turbines in Near-Shore (1) and Open-Sea (2) Locations as a Function of the 10 Min Mean Wind Speed [57]

The required windspeed series are created with the simulation tool PyConTurb [58]. This tool is able to construct 3D wind vectors in a 2D plane. With this tool it is so possible to have different wind speeds over the length of the turbine blade, in every direction, which is the same in real life circumstances. In Figure 4.18, a windseries shown which is simulated with the PyConTurb tool.

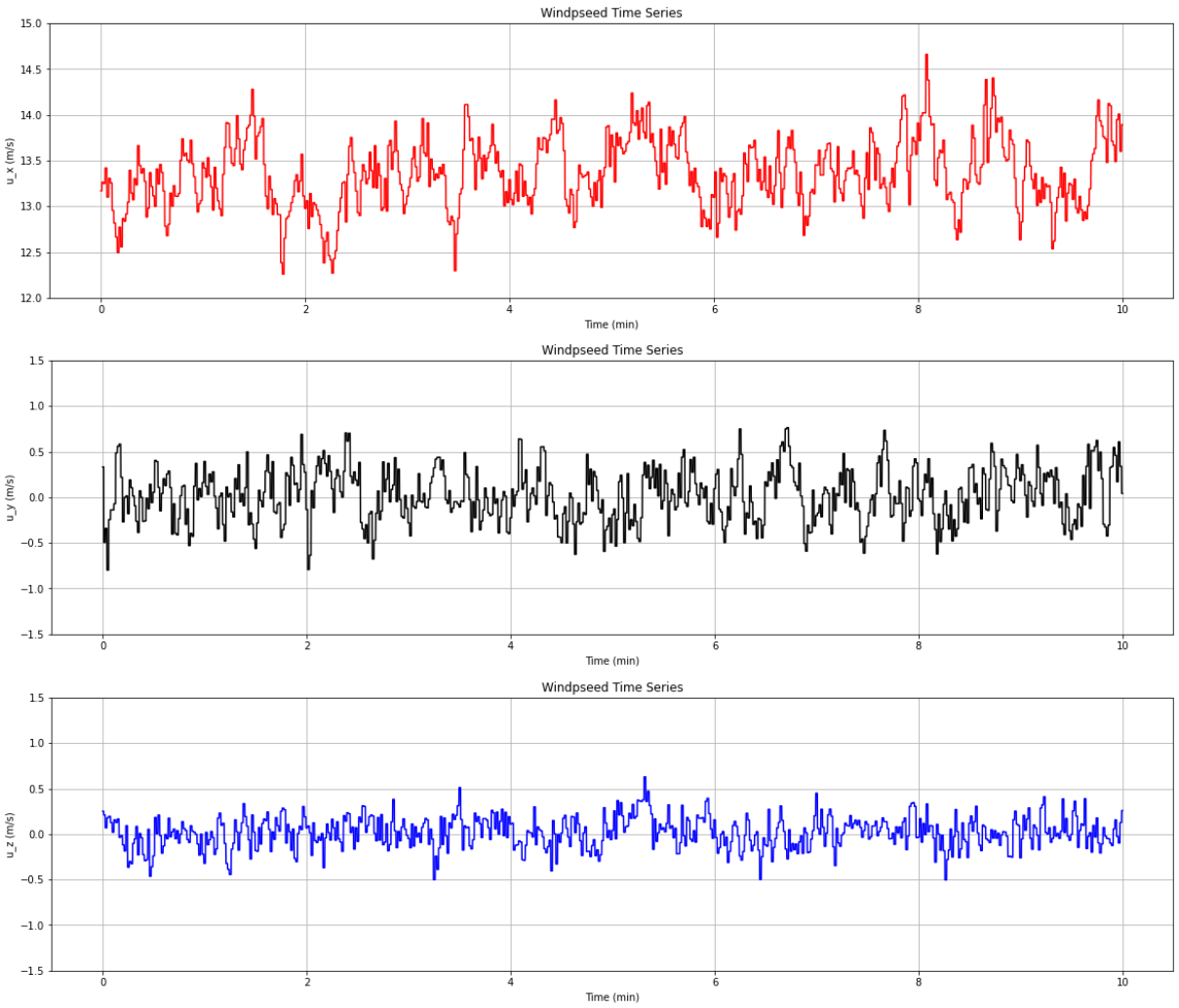

Figure 4.18: Wind Speed in x,y and z Direction (13.5 m/s, TI = 0.12)

As mentioned before there are various IEC defined wind classes. Each wind class and wind speed give a specific TI value which can be found in Figure 4.17. Figure 4.19 shows what this means in height of wind speed during a set time period.

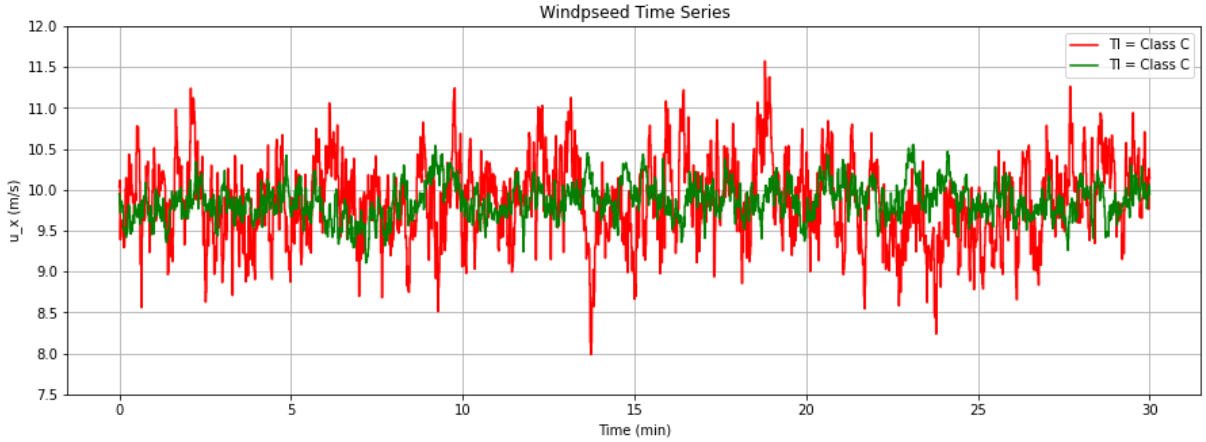

Figure 4.19: Wind Speed in x-Direction for Various TI, Mean = 10 m/s

4.4. Results Simulation

In the next section, findings will be derived from the results obtained. This analysis will focus on the HH-CB-DF-10-NS configuration. Initially, the simulation results will be presented, followed by the derivation of the findings. The simulation specifically modeled turbulence in the positive x-direction, which enhances the comparability of the outcomes.

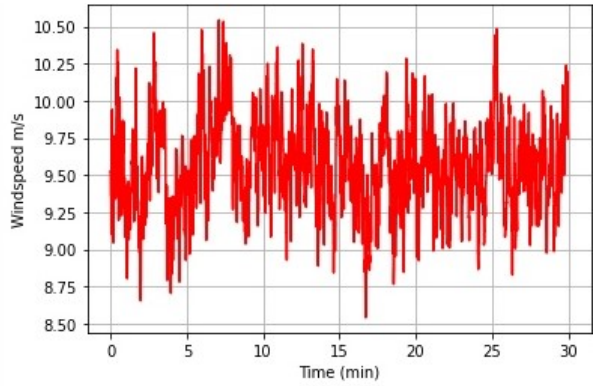

Figure 4.20: Simulated Wind Series (10 m/s Mean, TI = 0.12)

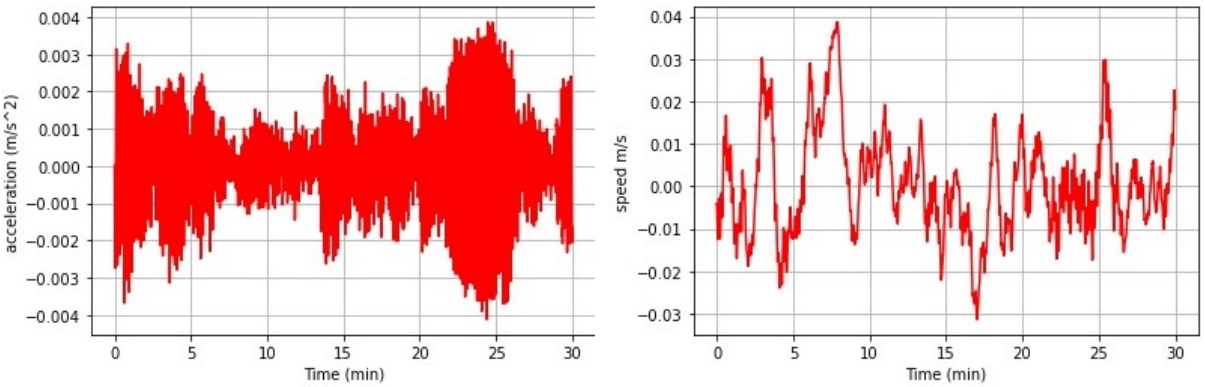

Figure 4.21: Blade Root Absolute Acceleration (Left) and Absolute Velocity (Right)

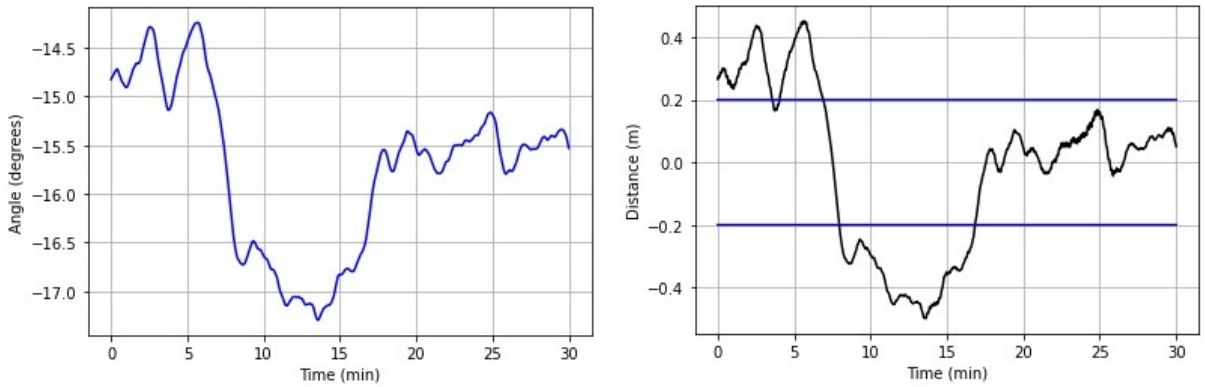

Figure 4.22: Blade Root Rotation (Left) and Absolute Distance (Right)

The results clearly demonstrate that the absolute distance of the blade primarily depends on its rotation around the z-axis. The trajectory of the absolute distance closely mirrors the path of

the angle, with only minor variations observed, which can be attributed to the blade's translation. Consequently, it can be concluded that the movements of the root are predominantly influenced by the blade's rotation.

Figure 4.23 shows a more specific region of the simulation with only a time series of 2 minutes. In this graph it can clearly be seen that location of the root is really dependent on the rotation of the blade. It clearly shows that next to the rotational motion another oscillation is responsible for the root motions. During simulations it was found that this oscillation is exactly the same as the pendulum motion of the COG. The period of these small oscillations are exactly the same as the outcome of the results shown in section 4.2.3.

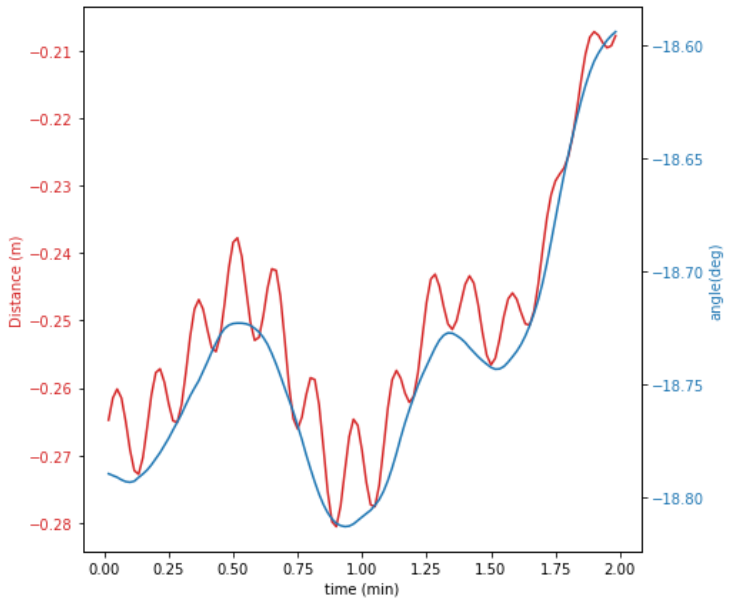

Figure 4.23: Blade Root Absolute Distance, Zoomed

An additional insight gained from the analysis is that the speed at the blade's root exhibits a pattern similar to that of the wind speed. Between 5 and 10 minutes, the average velocity initially trends towards higher speeds, peaking around the 7-minute mark before gradually declining. Observing the blade's movement reveals a similar pattern, indicating that the blade's motion is less affected by sudden changes in wind speed.

Comparing the wind speed with the blade's angle (and consequently, its absolute distance) reveals that in areas where the wind speed is higher, the rotation angle of the blade is smaller. This suggests that the blade rotates away from its initial position when exposed to stronger winds.

A further observation is that swift changes in wind velocity lead to greater accelerations. This is particularly evident when examining the period from minute 22 to 26, where accelerations are pronounced and the wind speed changes rapidly. A closer look at the absolute distance graph for this time interval shows that the graph line appears thicker, which, upon closer inspection, indicates a higher frequency and amplitude of displacement resulting from the blade's translation.

4.5. Future Turbine Blade Sizes

While the green energy transition is going on, turbine manufactures try to upscale the sizes of their wind turbines. With bigger size wind turbines it is possible to capture more energy out of the

wind. To calculate the power output of a wind turbine following formula is stated:

$$P = \frac{1}{2} C_p \rho \pi R^2 V^3 \tag{4.5}$$

This means that the sizes of wind turbines get bigger for higher power outputs [59]. The blades considered for this small study are scaled with a ratio of 10% and 20%.

The ”Definition of the IEA Wind 15-Megawatt Offshore Reference Wind Turbine” [16] provides a detailed explanation of the scaling process for the 15 MW reference turbine. It outlines how the ratios between length and weight, known as scaling factors, are employed to determine the weight of the scaled turbine blades.

Next to the scaling of the weight and dimensions it is of importance to have the data of the pre-twist for the model. In the report is stated that pre-twist is dependent on the place of the blade defined by the formula $r/R)$. Which tells us that the same pre-twist occurs for both blades at normalized locations.

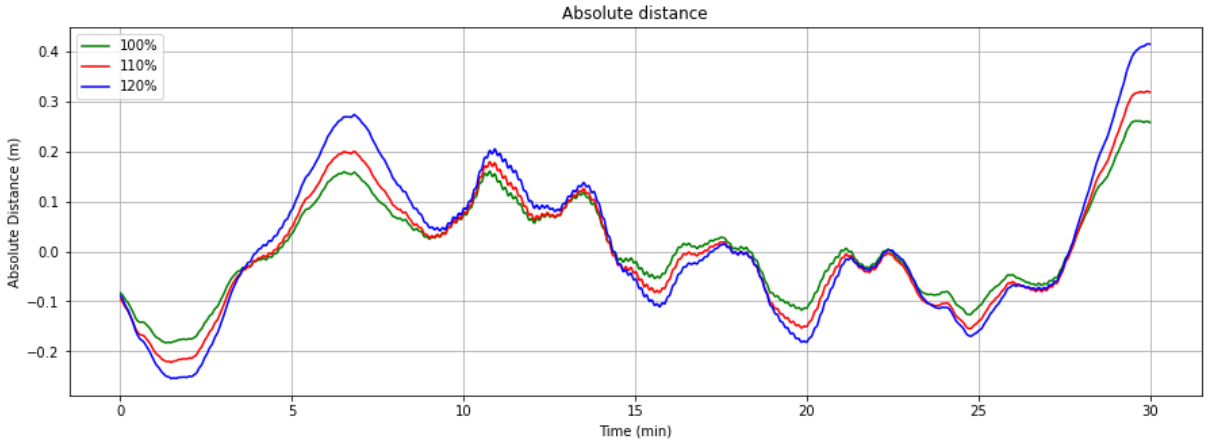

Figure 4.24: Blade Root Absolute Distance, Blade Sizes

Figure 4.24 shows the result of the case study to future size wind turbine blades. The results show that the future size wind turbine blades will be more sensitive to wind. Therefor it is important to do research in how those motions can be compensated. Whether this will be done with specific tagline systems or with specific lifting equipment such as vans or counterbalance weights/panels to overcome motions.

5

Results

In this section, the outcomes of various installation methods is presented. Initially, a comparison of the four different blade positions will be conducted. This will be followed by an evaluation of the tagline configuration and an examination of the control system. Towards the conclusion of this chapter, the operability of the most effective installation method will be explored.

The analysis will proceed in a systematic manner, focusing on determining the optimal operation. Each section will explain briefly the model under consideration and summarize the findings.

Blade Position	Tagline configuration	Tagline System	Wind speed
HH	Crane Boom (CB)	Constant Force (CF)	4 m/s
HV	Slewing Platform (SP)	Spring (SF)	8 m/s
VH	Crane + Slewing (C+S)	Damping Tuggers (DF)	10 m/s
VV			12 m/s
			14 m/s

Table 5.1: Considered Simulations

5.1. Blade Position

In conducting simulations to examine different blade positions, both the tagline configuration and system were kept unchanged. This method made it easier to compare results across the various simulations. To ensure a thorough examination, simulations included calculations for two wind speeds. During these simulations, the turbulence level was set to Class A.

Figures 5.1 and 5.2 show the results from simulations of vertical blade installations. It has to be noted that the COG is placed 19 metres under its lifting point. In these setups, the root experienced very high oscillations. The process involved measuring the straight-line distance to the center of the hub on the xy-plane at a height of 150 meters. The blade root's ability to move in the x and y directions is limited by the hoist cable and a single tagline at the blade's lower end. This setup causes the turbine blade to oscillate much like a flag. It allows the blade to circle around the central pole (crane) and to rotate around its own central axis (the z-axis of the blade body). These factors combined make the vertical installation method quite unstable.

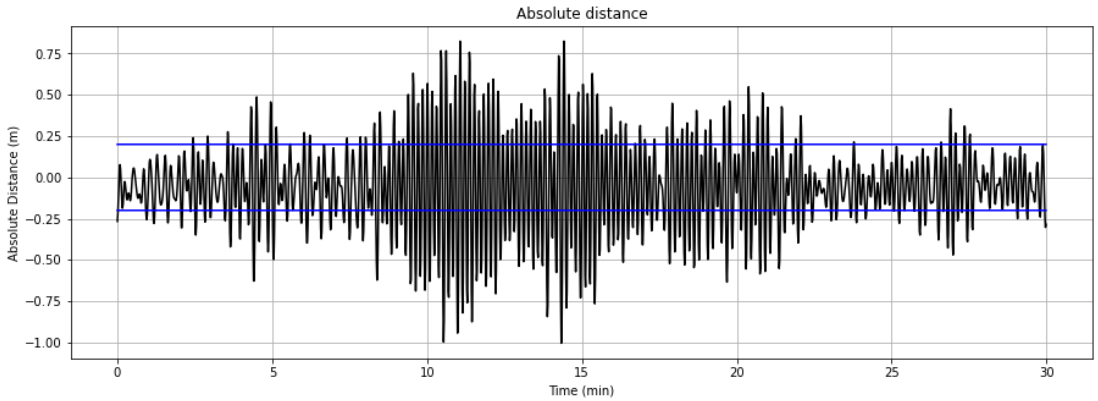

Figure 5.1: Vertical-Horizontal installation, VH-CB-CF-8-OS

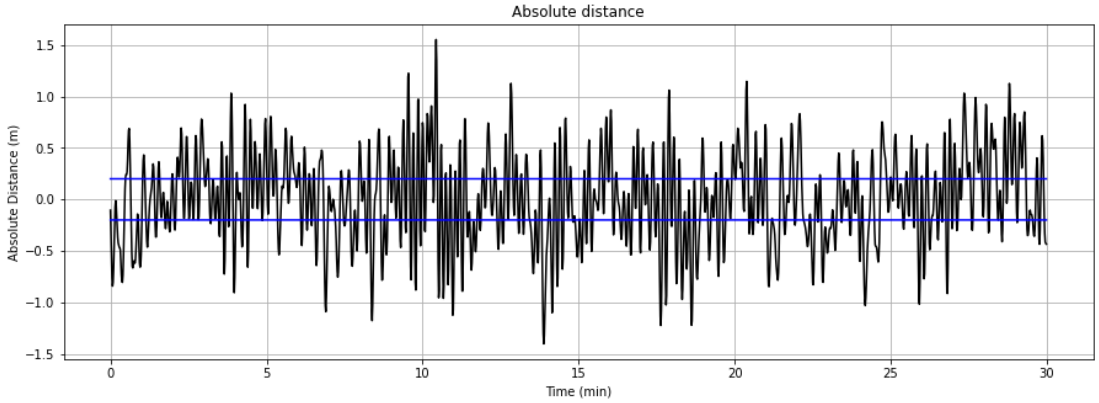

Figure 5.2: Vertical-Vertical installation, VV-CB-CF-8-OS

The results clearly show that vertically installing wind turbine blades is challenging, especially when using a hoist wire and a single tagline for guidance. As illustrated in Figure 5.2, the blade, once lifted at its center of gravity (COG) from the vessel, will rotate around its COG. While the tagline can mitigate the blade's pendulum motion, and rotation along its length can be controlled, controlling rotation around the blade's z-axis proves difficult. Consequently, managing motions at the blade root is challenging, complicating the blade's connection to the hub. This process involves significant movement in the x and y directions, with the crane also needing to lift the root upwards, resulting in motion in three dimensions. However, when a blade is attached to the hub from the side, z-direction motions are minimal, and only x-direction movements are crucial, with y-direction adjustments needed for hub connection.

Figure 5.3: Vertical-Vertical Installation

Despite these difficulties, it is not straightforward to deem this installation approach as less advantageous. When installation from the bottom is considered, the blade shouldn't be controlled solely with taglines connected to the blade lifting tool but also at the tail of the turbine blade. To do this engineering companies should work together with turbine manufacturers on how multiple tagline connection points can be attached to the blade. Next to a vertical blade installation where the blade is lifted in its COG other installation options should be considered. For instance, when the blade is directly connected to the vessel, it becomes directly linked to the crane, like how a roller coaster car is attached to its track. This comparison suggests that while challenging, vertical installation has its unique considerations. However, this study focuses exclusively on the horizontal blade installation positions, as the examination of direct blade-to-vessel connections falls outside the scope of this research.

The other installations options (where the longitudinal of the blade in parallel to the xy-plane), are a lot more stable as can be seen in 5.4. The Simulation where the blade is horizontal-vertical shows bigger oscillations. This is because the blade is more sensible to gusts of wind due to the higher drag forces. Both blade positions will be tested in later simulations.

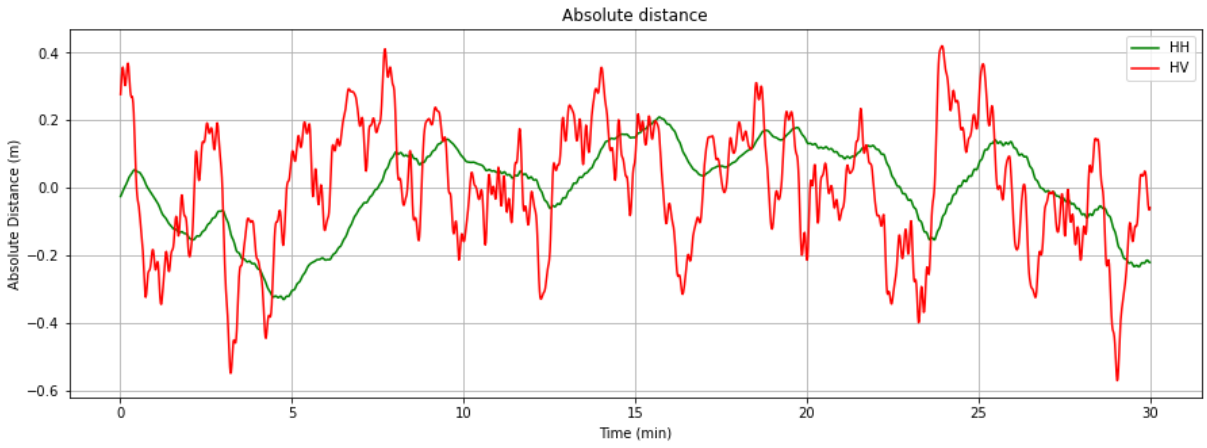

Figure 5.4: Comparison Between HH and HV Installation, ...-CB-DF-10-OS

Currently, turbine blades are installed using both methods depicted in Figure 5.4. This thesis overlooks the lift force, but real-world challenges stem from rotational forces caused by lifting. Thus, installing blades vertically can be advantageous since the lift force becomes minimal due to an approximately 90-degree angle of attack. Conversations with engineers from Cadeler [60] revealed that drag forces during installation are so significant that wind can easily affect the blades. Therefore, engineering solutions that allow the yoke to counteract rotations around its COG are crucial. This could be through precise tagline configurations , by adding vans or other devices to the yoke or a combination of these.

5.2. Tagline Configuration

In this section the different tagline connection positions are considered. The three considered positions are discussed in section 2.6. The taglines are connected to the crane boom, slewing platform or both. In the figure underneath the results of the tagline configuration of the tagline connected to the crane boom (CB,1), slewing platform (SP,2) and to both (CS,3) can be seen.

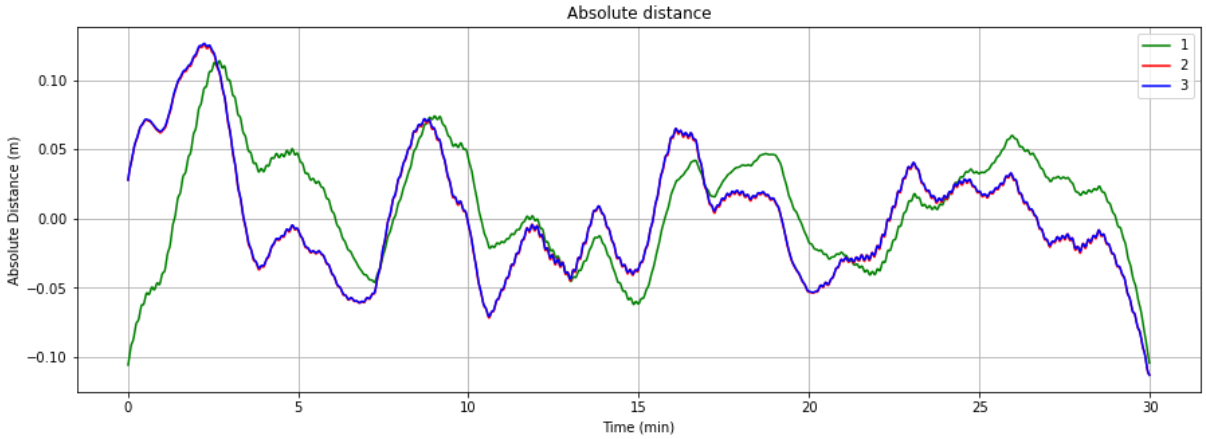

Figure 5.5: Comparison Between Tagline Configurations, HH-...-CF-4-Class C

The data presented in Figure 5.5 indicates that the specific position of the tagline connection points holds minimal significance. It should be noted that the moment around the body-frame x-axis is nearly zero while lift forces are disregarded, a scenario not covered in this thesis.

The positioning of taglines is critical when addressing the management of lift forces. The current focus of analysis is on the moment around the Z-axis, predominantly influenced by drag in the positive X-direction. In scenarios where lift becomes a factor for future research, the placement of taglines assumes increased significance. If taglines are connected solely to the crane boom, their effectiveness in mitigating lift forces is limited. Consequently, strategies to adjust the moment around the X-axis are necessary. These strategies could involve adding weight to the yoke, employing a gyroscope, or securing taglines to one side of the blade. However, such considerations fall outside the scope of this thesis.

Consequently, this analysis leads to the conclusion that the impact of the crane's connection point is almost negligible. Therefor for the future simulations a tagline only connected to the craneboom is considered.

5.3. Tagline System

In this section, a comparison is made between three distinct tagline systems: the constant force system, the brake mode system, and the damping system. The simulation of the motion control

system, modeled like a spring, yielded an unstable system. Stability was only achieved when the stiffness of the tagline was significantly reduced, resulting in values that could potentially be deemed acceptable. However, given that such a level of stiffness is unrealistic, further simulations of the brake mode motion control system were discontinued.

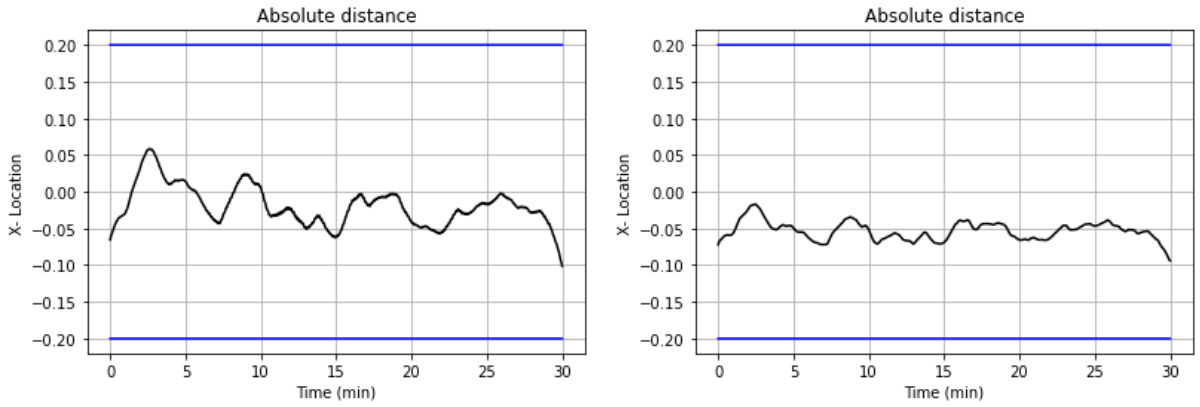

Figure 5.6: Horizontal Installation, Constant Force (left) vs Damping Force (right)

In Figure 5.6, the outcomes from simulating a constant force motion control system (shown on the left) and a damping tugger system (shown on the right) are displayed. The figure illustrates that the motions experienced by the damping taglines are significantly less pronounced than those of the blade when controlled by a constant force. It was discovered during simulations that the slope's steepness of a damping curve is a crucial determinant in the motion and rotational speed of the turbine blade. The steeper the slope the lower the motions are found.

These findings are supported by another study [61], which arrived at similar conclusions. This comparison clearly demonstrates the substantial benefits of damping tugger systems over brake force and constant force systems. Therefore, to enhance the operational efficiency of offshore turbine blade installations, incorporating a damping system could significantly reduce downtime.

It was found that the properties of the tagline system are of big importance. Therefor a small study to the steepness of the damping tugger (explained in Section 2.7.3) is done. In this the damping tugger is programmed in such a way that the force of the tagline at 0 m/s is equal to the force when constant force taglines are assumed. The maximum force was achieved for a speed of 2 m/s and the slope between these points were variable and tested, the outcomes of the simulations can be found in Table 5.2. The Root Mean Square (RMS) value is a statistical measure that calculates the magnitude of a varying quantity, typically used to assess the variation or fluctuation of a signal or set of values. It represents the square root of the average of the squares of the values, providing a way to quantify the overall level of variation or deviation from the mean.

Slope Steepness (N/m/s)	mean root square value
0	0.00615
500	0.00578
1000	0.00552
2500	0.00532

Table 5.2: Root Mean Square Value (HH-CB-DF-8-OS)

To evaluate the effectiveness of different damping tugger systems, a RMS calculation was performed on the absolute distance of the root to the hub. Initially, the slope was set to zero, effectively mimicking the behavior of the tagline system under constant tension conditions. Subsequently, the steepness of the slope was incrementally increased.

As illustrated in Table 5.2, a clear pattern emerged: the steeper the slope, the lower the RMS value, which means that the amplitude (direct distance) of the motion around the centre of the hub are less. This trend suggests that a steeper slope corresponds to reduced excitation at the turbine root. Consequently, by adjusting the slope steepness, it is feasible to modulate the blade movements, thereby maximizing the time to allign the blade.

5.4. Wind Speed

To evaluate the feasibility of installing single blade turbines, simulations were conducted across various wind speeds and turbulence classes. From these results and the set boundary conditions appointed in section 2.8 a workability assessment is set up. This assessment is shown and discussed in section.

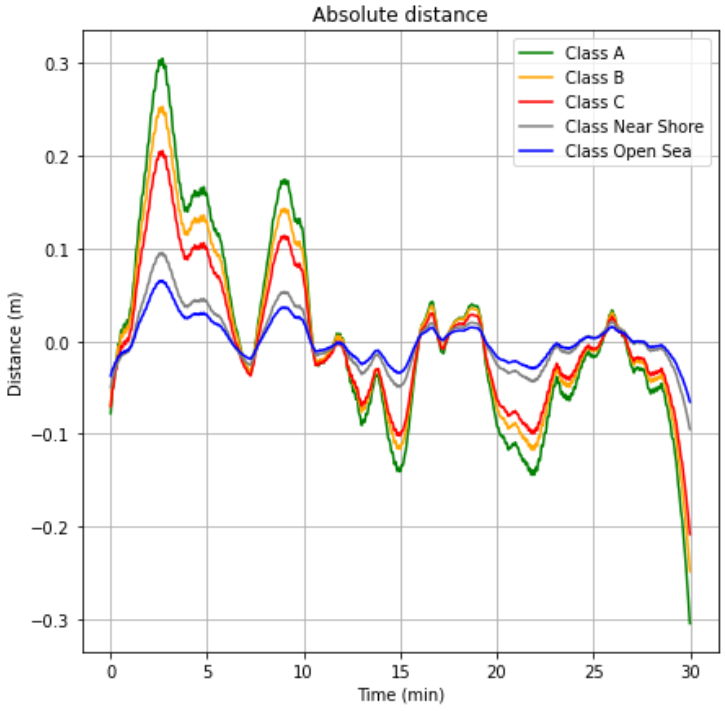

Figure 5.7: Comparison Installation under Various TI, HH-CB-DF-4-...

The installation which is simulated is the installation where the blade is in its horizontal-horizontal position. Taglines are connected to the craneboom and the exerting force of the taglines is dependent on the velocity of the attachment point of the turbine blade. Figure 5.7 shows that the influence of the turbulence intensity is of big importance. It can be seen that offshore conditions have way less motions compared to other turbulence intensities.

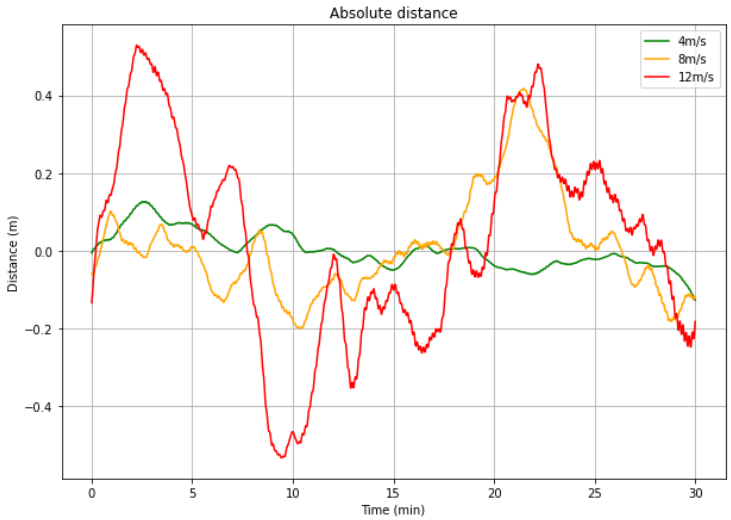

Figure 5.8: Comparison Installation under Various Wind Speeds, HH-CB-DF-...-OS

Figure 5.8 shows the results of simulations of various wind speeds under the same turbulence class (open-sea). As can be seen higher wind speeds results in higher blade motions. For higher wind speeds, not only is the maximum distance between the blade and hub is greater, but the changes in turbine blade position occur more swiftly compared to lower wind speeds.

For both the windspeed and TI simulations an histogram is created. In this histogram is the total number of outcrossings simulated. First the number of outcrossings are counted for a simulation period of 3 minutes, thereafter for each bin the simulation is extended by 3 minutes and the number of outcrossings is counted. As can be seen there is almost a linear trend in both higher TI and wind speed values. During simulation was so found that both can be responsible whether installation can go on.

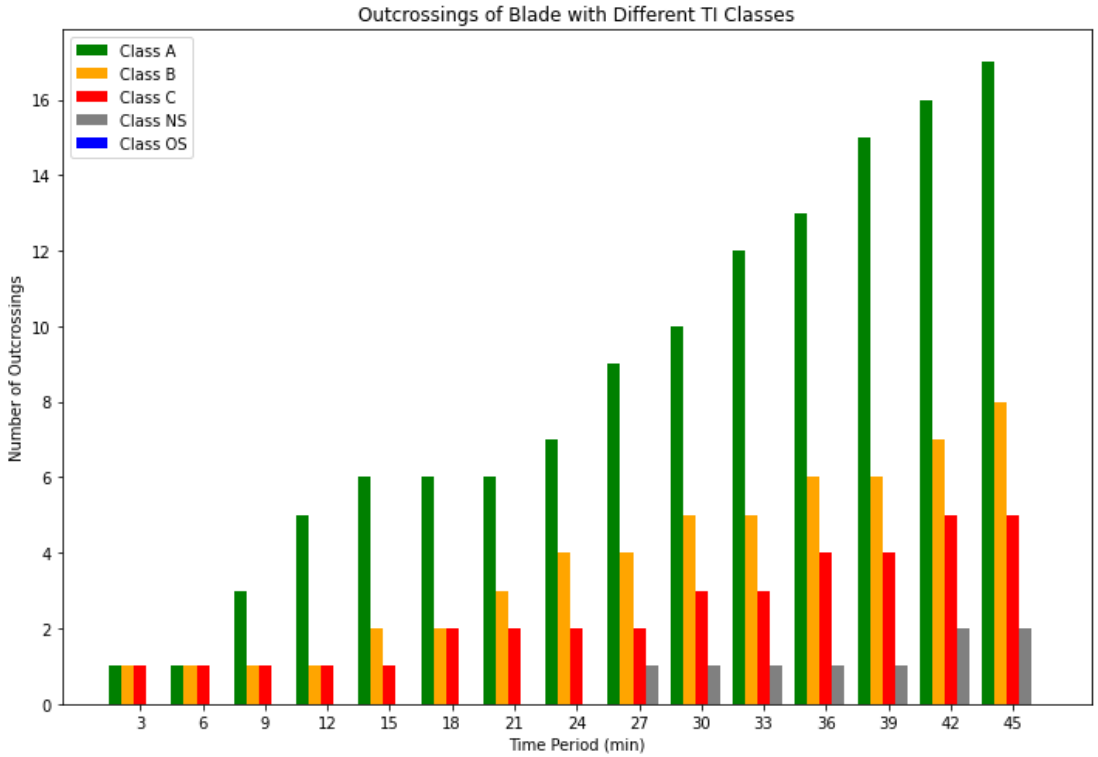

Figure 5.9: Number of Out-crossings for Various TI Classes, HH-CB-DF-4-...

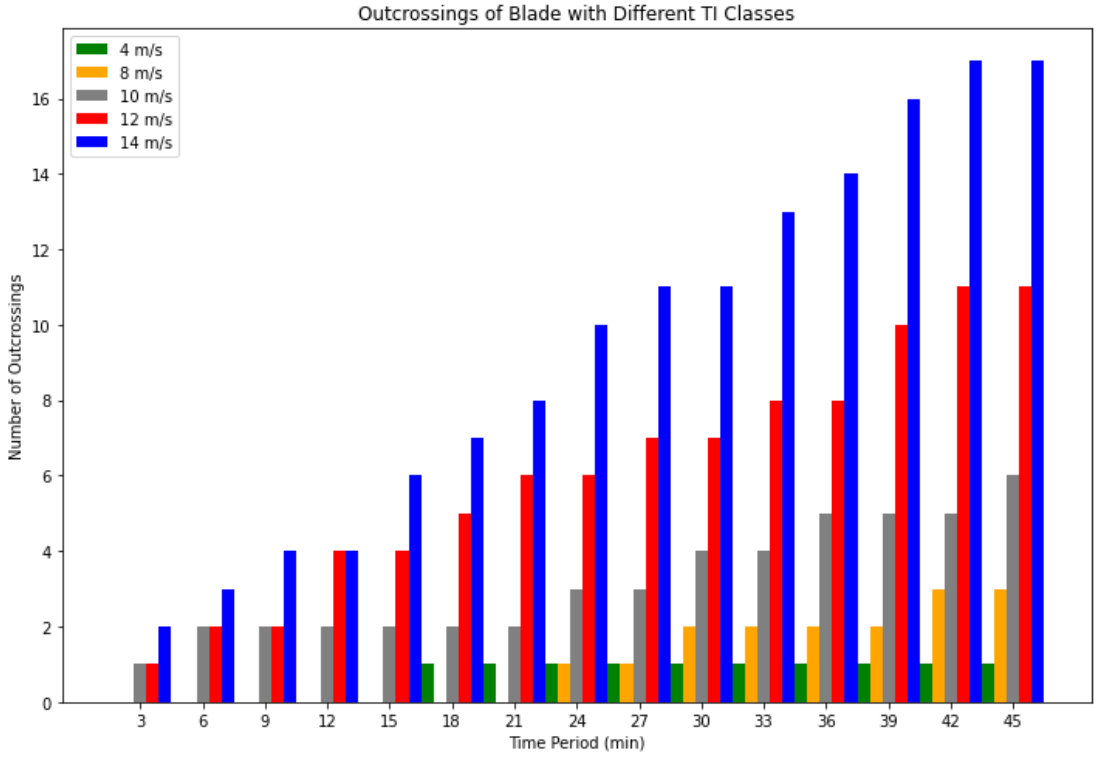

Figure 5.10: Number of Out-crossings for Various Wind Speeds, HH-CB-DF-...-OS

The tool is used to compute various wind and turbulence classes, to get a better understanding

of blade installations. During optimizing the tagline configuration was found that it is really dependent which values were chosen to operate the taglines. Therefor was chosen that the equilibrium angle of the turbine blade was -5 degrees around its z-axis. With this it is able to compare the outcomes of the simulations.

Wind Speed	# Out-crossings	% inside bin
4	0	100
8	1	94.47
10	3	72.25
12	8	57.25
14	11	48.14

Table 5.3: Result Blade Installation (HH-CB-DF-x)

With the boundary conditions assumed in section 2.8, a turbine blade can be installed for windspeeds till 12 m/s. This value is at the high side of blade installation. As already mentioned before turbine blade installation limits are in the region of 8-12 m/s. During simulations it was seen that the installation mean wind speed is heavily dependent on the turbulence intensity. It was found that installations can proceed when mean wind speeds has a value of 8 m/s. Thereafter the turbulence intensity was of importance as well. For mean windspeeds of 10 m/s was found that the maximum turbulence intensity cant exceed 0.14 which is equal to wind class C.

6

Conclusion and Recommendations

In this chapter, a deliberation on the results will be computed. These results will be used to give answer to the research questions which were appointed in section 1.6. Thereafter, based on the conclusion, several recommendations will be made.

6.1. Conclusion

For this thesis the following main research question was established:

How can various blade installation methods for wind turbines be modelled dynamically?

To address this question, it was necessary to investigate environmental factors. Previous studies identified wind as the predominant factor affecting blade alignment. By analyzing wind speed and direction, it became feasible to construct a force vector acting on blade elements with the use of the BEM-method. Simplifying the blade into elements revealed convergence towards 7 blade elements, leading to the conclusion that a turbine blade can be segmented for simulation purposes while the error was minimal. Additionally, research indicated the possibility of extrapolating lift and drag coefficients for angles of attack (AOA) beyond the typically available range. Given the scope of this research and the model developed, the deflection of the blade is not expected to significantly influence the results.

The correlation between the blade installation method and the blade's dynamic behavior is significant strong, but it has to be noted that the current research is a like-for-like comparison. The relative performance of the blade installation methods investigated shows that the horizontal-horizontal installation method is the most effective. From the simulations most likely can be concluded that installing a turbine blade in a vertical position (connecting the blade to the hub from the bottom) is not feasible with the installation method being researched. However from the simulations is expected that installation in horizontal positions is possible. Specifically, when the blade is installed in a flat position, it is less affected by wind. In the horizontal-vertical position the motions are bigger due to the larger forces involved. Consequently, the blade is more susceptible to turbulent wind, making flat installation preferable.

Analysis of blade motions revealed that the motions at the blade root are primarily influenced by the blade's angular velocity. To mitigate this, a damping tugger was identified as the most effective solution for stabilizing the blade. The effectiveness of the damping depends significantly on the steepness of the damping function, where force in the tuggerline is related to speed.

Unless results of this research need to be validated with field data the outcome of this research indicate that installation processes can proceed if wind speeds do not exceed 8 m/s. Beyond this threshold, not only the average wind speed but also the turbulence intensity becomes critical. At a wind speed of 10 m/s, the maximum allowable turbulence intensity should not be higher than 0.14, corresponding to class C conditions.

The developed tool could be used to simulate future scale wind turbines, highlighting the importance of thoroughly researching blade characteristics. If these characteristics closely match real values within an engineering tolerance, the resulting motions will align with those of a blade modeled with more elements. It is crucial to have access to comprehensive blade data, such as weight, prebend, and pre-twist, without this information, the tool cannot generate accurate enough results.

6.2. Recommendations

In this thesis, the approach to simulate the motions of the wind turbine blade involved a simplified model. This decision was made to focus on the core aspects of blade motion under specific conditions. However, this simplification also means that there are opportunities for future research to build upon the foundation laid here by incorporating additional complexities into the model. For future studies, the model could be expanded in several ways to enhance its accuracy and applicability to real-world scenarios.

In this thesis, the movements of vessels and cranes were not considered. However, it is crucial for future studies to take these factors into account, as they can significantly affect the dynamics of blade motions. While slow crane-tip motions wont effect the dynamics of the blade, a crane which is oscillating in the right frequencies can make blade root motions higher.

It is of importance to research the assumptions made about the lift and drag forces of the blade. Wind tunnel tests can give results if set assumptions are good enough for a turbine blade installation. Additionally, it is crucial to verify whether the available airfoil data yield results that closely match the airfoil sections designed by manufacturers.

This thesis did not explore bending effects on turbine blades, leaving unanswered questions about their significance as blade sizes increase. Future research is essential to determine if the negligible bending assumptions for smaller blades are still valid for larger ones. As turbine blades will be longer the bending moment will be higher, therefor if the stiffness of a turbine blade wont be engineered in such a way the blade is really stiff, the bending of the blade should be taken into account. Next to that the a research should be done to vortex-induced-vibrations while those can ensure problems during installation.

For future research, it is strongly recommended to conduct in-depth investigations into methods for stabilizing the root of turbine blades. Currently research only looks at the motions of the blade, while the root motions are of importance in the alignment phase. Especially investigation should be done on how the centre of pressure due to wind loads could be aligned with the centre of gravity.

Presently, tools are controlled mostly with tagline systems. Future research should be done on how a yoke can be used to counteract moments in every direction, with for example panels which acts as wings to counteract for rotation in any direction. Also the influence of gyroscopes and vans on top of a yoke should be researched.

Another recommendation to research is the possibility to install a blade like a slip joint. Currently it is hard to allign the guide pin exactly to the hole of the hub. If the blade already slips in the hub like a cap of a pen installation downtime can be improved.

References

[1] UNFCC. *The Paris agreement*. URL: https://unfccc.int/process-and-meetings/the-paris-agreement. (accessed: 11.09.2023).

[2] *Record High Global Temperatures in September 2023: So What Now?* URL: https://doctorclimatechange.com/blog/f/record-high-global-temperatures-in-september-2023-so-what-now.

[3] Government of the Netherlands. *Climate Policy*. URL: https://www.government.nl/topics/climate-change/climate-policy. (accessed: 11.09.2023).

[4] Ministerie van Economische Zaken en Klimaat. "Klimaatplan". In: (). URL: https://open.overheid.nl/documenten/ronl-c66c8a00-ac14-4797-a8ea-973a98c5bee0/pdf.

[5] Ministerie van Economische Zaken en Klimaat. *Integraal Nationaal Energie-en Klimaatplan*. 2021. URL: https://www.rijksoverheid.nl/documenten/rapporten/2019/11/01/integraal-nationaal-energie-en-klimaatplan.

[6] Ministerie van Economische Zaken en Klimaat. *National Climate Agreement - The Netherlands | Publicatie | Klimaatakkoord*. URL: https://www.klimaatakkoord.nl/documenten/publicaties/2019/06/28/national-climate-agreement-the-netherlands.

[7] Peter. *Dynamic Soil Structure of Offshore Wind Turbines and long term performance prediction: Linking scaled model test results to prototype prediction via element tests*. URL: https://www.vjtech.net/blog/dynamic-soil-structure-of-offshore-wind-turbines-and-long-term-performance-prediction-linking-scaled-model-test-results-to-prototype-prediction-via-element-tests.

[8] *Wind Project Development & EPC — Descriptive Information - Energy I-SPARK*. URL: https://ei-spark.lbl.gov/generation/onshore-wind/project/info/.

[9] Dang Ahn et al. "Comparative evaluation of different offshore wind turbine installation vessels for Korean west–south wind farm". In: *International Journal of Naval Architecture and Ocean Engineering* 9.1 (Jan. 2017), pp. 45–54. DOI: 10.1016/J.IJNAOE.2016.07.004. URL: https://www.researchgate.net/publication/306090368_Comparative_evaluation_of_different_offshore_wind_turbine_installation_vessels_for_Korean_west-south_wind_farm.

[10] Netherlands enterprise agency. *Plans 2030-2050*. URL: https://english.rvo.nl/information/offshore-wind-energy/offshore-wind-energy-plans-2030-2050#:~:text=In%202022%2C%20the%20Government%20raised,of%20our%20current%20electricity%20consumption.. (accessed: 11.09.2023).

[11] Netherlands enterprise agency. *Dutch ofshore wind market report 2023*. URL: https://english.rvo.nl/sites/default/files/2023/05/Offshore-Wind-Market-Report.pdf. (accessed: 11.09.2023).

[12] Hans Cleijne et al. *Rapport Noordzee energie outlook | Kamerstuk | Rijksoverheid.nl*. URL: https://www.rijksoverheid.nl/documenten/kamerstukken/2020/09/01/rapport-noordzee-energie-outlook.

[13] *Offshore jack-up installatieschepen | Jan De Nul*. URL: https://www.jandenul.com/nl/vloot/offshore-jack-up-installatieschepen.

[14] C. M. Wang et al. “Research on floating wind turbines: a literature survey”. In: *The IES Journal Part A: Civil & Structural Engineering* 3.4 (2010), pp. 267–277. DOI: 10.1080/19373260.2010.517395. URL: https://www.tandfonline.com/doi/abs/10.1080/19373260.2010.517395.

[15] Dimitris Al Katsaprakakis et al. “A comprehensive analysis of wind turbine blade damage”. In: *Energies* 14.18 (Sept. 2021). DOI: 10.3390/EN14185974.

[16] Evan Gaertner et al. “Definition of the IEA Wind 15-Megawatt Offshore Reference Wind Turbine Technical Report”. In: (2020). URL: www.nrel.gov/publications..

[17] *Offshore Blade Lifting Yokes | Offshore Installation Equipment | ENABL*. URL: https://enabl-wind.com/products/all-equipment/blade-lifting-yokes-offshore/.

[18] *LT5061 - Blade Eagle*. URL: https://liftra.com/products/lt5061-blade-eagle.html.

[19] Handelmaatschappij Vlierodam. “GEBRUIKSAANWIJZING STAALKABEL”. In: (). URL: www.vlierodam.nl.

[20] Volken-Jan Koelewijn. *Private conversation Volken-Jan Koelewijn*. 2024.

[21] *RHS Series Offshore Crane For Sale | Rainbow Heavy Industries Co.,Ltd.* URL: https://www.genmasolution.com/rhs-series-heavy-offshore-crane-16193157982824193.html.

[22] Piet Bastiaanse. *Private conversation Piet Bastiaanse*. 2024.

[23] *Steel Wire Rope | SWR Group*. URL: https://www.steelwirerope.com/index.html.

[24] *Winches - Huisman Equipment*. URL: https://www.huismanequipment.com/en/products/pipelay/pipelay_components/winches#photos.

[25] *Offshore winches | Royal IHC*. URL: https://www.royalihc.com/offshore-energy/offshore-equipment/tensioners-and-winches/offshore-winches.

[26] *Constant Tension Archives - Dromec Winches*. URL: https://www.dromecwinches.com/tag/constant-tension/.

[27] Zhengru Ren et al. “Active tugger line force control for single blade installation”. In: *Wind Energy* 21.12 (Dec. 2018), pp. 1344–1358. DOI: 10.1002/WE.2258.

[28] Geert Meskers et al. “A damping tugger system for offshore heavy lifts”. In: *Proceedings of the International Conference on Offshore Mechanics and Arctic Engineering - OMAE* 1 (2012), pp. 315–323. DOI: 10.1115/OMAE2012-83334. URL: https://www.researchgate.net/publication/267606730_A_Damping_Tugger_System_for_Offshore_Heavy_Lifts.

[29] Zhiyu Jiang. “The impact of a passive tuned mass damper on offshore single-blade installation”. In: *Journal of Wind Engineering and Industrial Aerodynamics* 176 (May 2018), pp. 65–77. DOI: 10.1016/J.JWEIA.2018.03.008.

[30] K. D. Leeuw. “Single lift blade alignment for large offshore wind turbines turbine blades”. In: (2019).

[31] Det Norkse Veritas. “DNVGL-ST-N001”. In: *Marine operations and marine warranty* (2018), p. 09.

[32] Koon Beng Ooi et al. “Verification of the performance of a vertical ground heat exchanger applied to a test house in Melbourne, Australia”. In: *Energies* 10.10 (Oct. 2017). DOI: 10.3390/EN10101558. URL: https://www.researchgate.net/publication/320314282_Verification_of_the_Performance_of_a_Vertical_Ground_Heat_Exchanger_Applied_to_a_Test_House_in_Melbourne_Australia.

[33] *Earth Global Circulation - en - Atmospheric circulation - Wikipedia*. URL: https://en.wikipedia.org/wiki/Atmospheric_circulation#/media/File:Earth_Global_Circulation_-_en.svg.

[34] Stefan Emeis et al. “Comparison of Logarithmic Wind Profiles and Power Law Wind Profiles and their Applicability for Offshore Wind Profiles”. In: *Wind Energy* (2007), pp. 61–64. DOI: 10.1007/978-3-540-33866-6{_}11. URL: https://www.researchgate.net/publication/225883255_Comparison_of_Logarithmic_Wind_Profiles_and_Power_Law_Wind_Profiles_and_their_Applicability_for_Offshore_Wind_Profiles.

[35] Daniel C. Bratton et al. “The wind shear exponent: Comparing measured against simulated values and analyzing the phenomena that affect the wind shear”. In: *ASME 2011 5th International Conference on Energy Sustainability, ES 2011* PARTS A, B, AND C (2011), pp. 2245–2251. DOI: 10.1115/ES2011-54823. URL: https://www.researchgate.net/publication/267492783_The_Wind_Shear_Exponent_Comparing_Measured_Against_Simulated_Values_and_Analyzing_the_Phenomena_That_Affect_the_Wind_Shear.

[36] Andrea Gasparella. “Preface”. In: *Building Simulation Applications* 2022-June (2022), p. IX. DOI: 10.13124/9788860461919. URL: https://www.researchgate.net/figure/The-power-law-profiles-for-the-velocity-distrubutions-in-boundary-layer-over-different_fig2_326967923.

[37] B. W. Yan et al. “Characterising wind shear exponents in the offshore area using Lidar measurements”. In: *Applied Ocean Research* 127 (Oct. 2022), p. 103293. DOI: 10.1016/J.APOR.2022.103293.

[38] S.L. Dixon et al. “Wind Turbines”. In: *Fluid Mechanics and Thermodynamics of Turbomachinery* (2014), pp. 419–485. DOI: 10.1016/B978-0-12-415954-9.00010-3. URL: https://linkinghub.elsevier.com/retrieve/pii/B9780124159549000103.

[39] G. Pechlivanoglou. “Passive and active flow control solutions for wind turbine blades”. In: (2013). DOI: 10.14279/DEPOSITONCE-3487.

[40] John Anderson. “Fundamentals of Aerodynamics”. In: ().

[41] *(PDF) Numerical analisys to evaluate NACA 0015 airfoil properties. Incompressible flow.* URL: https://www.researchgate.net/publication/327190063_Numerical_analisys_to_evaluate_NACA_0015_airfoil_properties_Incompressible_flow.

[42] Faisal Mahmuddin. “The Effect of Flat Plate Theory Assumption in Post-Stall Lift and Drag Coefficients Extrapolation with Viterna Method”. In: *Journal of Subsea and Offshore-Science and Engineering* 6 (2016).

[43] Snorri Gudmundsson. “Aircraft Drag Analysis”. In: *General Aviation Aircraft Design* (2022), pp. 657–752. DOI: 10.1016/B978-0-12-818465-3.00016-1.

[44] Erol Sancaktar. “Mechanics of solids and structures”. In: *ASME International Mechanical Engineering Congress and Exposition, Proceedings* 10 PART A (Jan. 2019), pp. 53–90. DOI: 10.1016/B978-0-12-818283-3.00002-6.

[45] Anton E. Bowden et al. “Computer Modeling and Simulation of UHMWPE”. In: *UHMWPE Biomaterials Handbook: Ultra High Molecular Weight Polyethylene in Total Joint Replacement and Medical Devices* (Jan. 2016), pp. 753–771. DOI: 10.1016/B978-0-323-35401-1.00039-9.

[46] David Thompson. “Track Vibration”. In: *Railway Noise and Vibration* (Jan. 2009), pp. 29–95. DOI: 10.1016/B978-0-08-045147-3.00003-7.

[47] Christian Mittelstedt. “Theory of Plates and Shells”. In: *Theory of Plates and Shells* (Jan. 2023), pp. 1–579. DOI: 10.1007/978-3-662-66805-4/COVER.

[48] *5.2 The Bernoulli-Euler Beam Theory | Learn About Structures*. URL: https://learnaboutstructures.com/Bernoulli-Euler-Beam-Theory.

[49] Osman Emre Celek et al. “A computer-aided design and analysis of a modular flexible fixturing system for aircraft fuselage panel assembly”. In: *International Journal on Interactive Design and Manufacturing* 17.4 (Aug. 2023), pp. 2005–2018. DOI: 10.1007/S12008-023-01330-8/TABLES/6. URL: https://link.springer.com/article/10.1007/s12008-023-01330-8.

[50] Riccardo Sacco et al. “Elements of Computational Methods”. In: *A Comprehensive Physically Based Approach to Modeling in Bioengineering and Life Sciences* (Jan. 2019), pp. 63–111. DOI: 10.1016/B978-0-12-812518-2.00011-1.

[51] *Wind Gust Definition*. URL: https://graphical.weather.gov/definitions/defineWindGust.html.

[52] *The Difference Between Wind Speed and Wind Gusts*. URL: https://ny1.com/nyc/all-boroughs/weather/2020/08/07/all-wind-is-not-created-equal.

[53] N Bodini et al. “Offshore Wind Turbines Will Encounter Very Low Atmospheric Turbulence”. In: *Journal of Physics: Conference Series* 1452 (2023), p. 12023. DOI: 10.1088/1742-6596/1452/1/012023.

[54] Matthew Huaiquan Zhang. “Wind Resource Assessment and Micro-siting: Science and Engineering”. In: *Wind Resource Assessment and Micro-siting: Science and Engineering* (July 2015), pp. 1–293. DOI: 10.1002/9781118900116. URL: https://onlinelibrary.wiley.com/doi/book/10.1002/9781118900116.

[55] *NEN-EN-IEC 61400-1:2019 en*. URL: https://www.nen.nl/nen-en-iec-61400-1-2019-en-257967.

[56] *NEN-EN-IEC 61400-3-1:2019 en*. URL: https://www.nen.nl/nen-en-iec-61400-3-1-2019-en-263714.

[57] Lászlõ Arany et al. “Simplified critical mudline bending moment spectra of offshore wind turbine support structures”. In: *Wind Energy* 18.12 (Dec. 2015), pp. 2171–2197. DOI: 10.1002/WE.1812.

[58] Jennifer M Rinker. “PyConTurb: an open-source constrained turbulence generator”. In: (2018), p. 62032. DOI: 10.1088/1742-6596/1037/6/062032. URL: https://gitlab.windenergy.dtu.dk/rink/pyconturb..

[59] Abdollah Malekjafarian et al. “Foundation damping for monopile supported offshore wind turbines: A review”. In: *Marine Structures* 77 (May 2021), p. 102937. DOI: 10.1016/J.MARSTRUC.2021.102937.

[60] Marijn Dijk et al. *Private conversation with Marijn Dijk and Quentin Meissonnier*. 2023.

[61] *Our Capabilities - Robert Allan Ltd.* URL: https://ral.ca/our-capabilities/.

[62] Burak Urazel et al. “A new solution approach for non-convex combined heat and power economic dispatch problem considering power loss”. In: *Energy* 278 (Sept. 2023), p. 128031. DOI: 10.1016/J.ENERGY.2023.128031.

[63] *Manchester Sling Company - Offshore Technology*. URL: https://www.offshore-technology.com/contractors/installation/manchester-sling-company/.

[64] Ty Bugdin et al. *Design of a Fixed Wing Micro Aerial Vehicle A Major Qualifying Project Report Submitted to the Faculty of the WORCESTER POLYTECHNIC INSTITUTE in Partial Fulfillment of the Requirements for the Degree of Bachelor of Science in Aerospace Engineering*. Tech. rep. 2021.

[65] David Plant. *Investigation of indentations versus surface roughness for fluid induced motion of an elastically attached circular cylinder at velocities relevant to the marine environment using CFD*. 2019. URL: https://researchportal.murdoch.edu.au/esploro/outputs/graduate/Investigation-of-indentations-versus-surface-roughness/991005545160907891.

A

Operation of Blade Installation

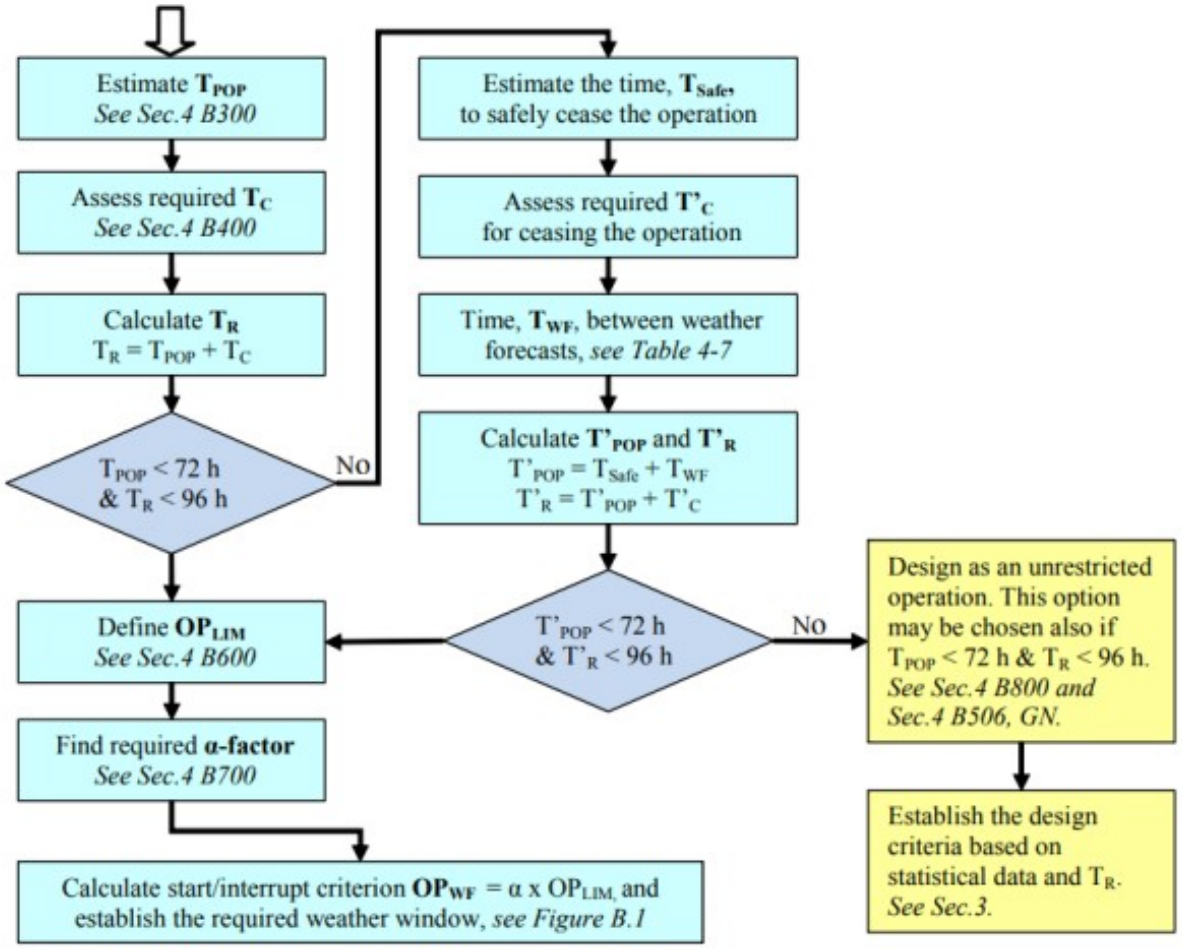

Figure A.1: Restricted or Unrestricted Operation of Blade Installation [62]

B

Appendix Reference Blade

Parameter	Units	Value
Power rating	MW	15
Turbine class	-	IEC Class 1B
Specific rating	W/m^2	332
Rotor orientation	-	Upwind
Number of blades	-	3
Control	-	Variable speed Collective pitch
Cut-in wind speed	m/s	3
Rated wind speed	m/s	10.59
Cut-out wind speed	m/s	25
Design tip-speed ratio	-	90
Minimum rotor speed	rpm	5.0
Maximum rotor speed	rpm	7.56
Maximum tip speed	m/s	95
Rotor diameter	m	240
Airfoil series	-	FFA-W3
Hub height	m	150
Hub diameter	m	7.94
Hub overhang	m	11.35
Rotor precone angle	deg	-4.0
Blade prebend	m	4
Blade mass	t	65
Drivetrain	-	Direct drive
Shaft tilt angle	deg	6
Rotor nacelle assembly mass	t	1,017
Transition piece height	m	15
Monopile embedment depth	m	45
Monopile base diameter	m	10
Tower mass	t	860
Monopile mass	t	1,318

Figure B.1: Key Parameters for the IEA Wind 15-MW Turbine [16]

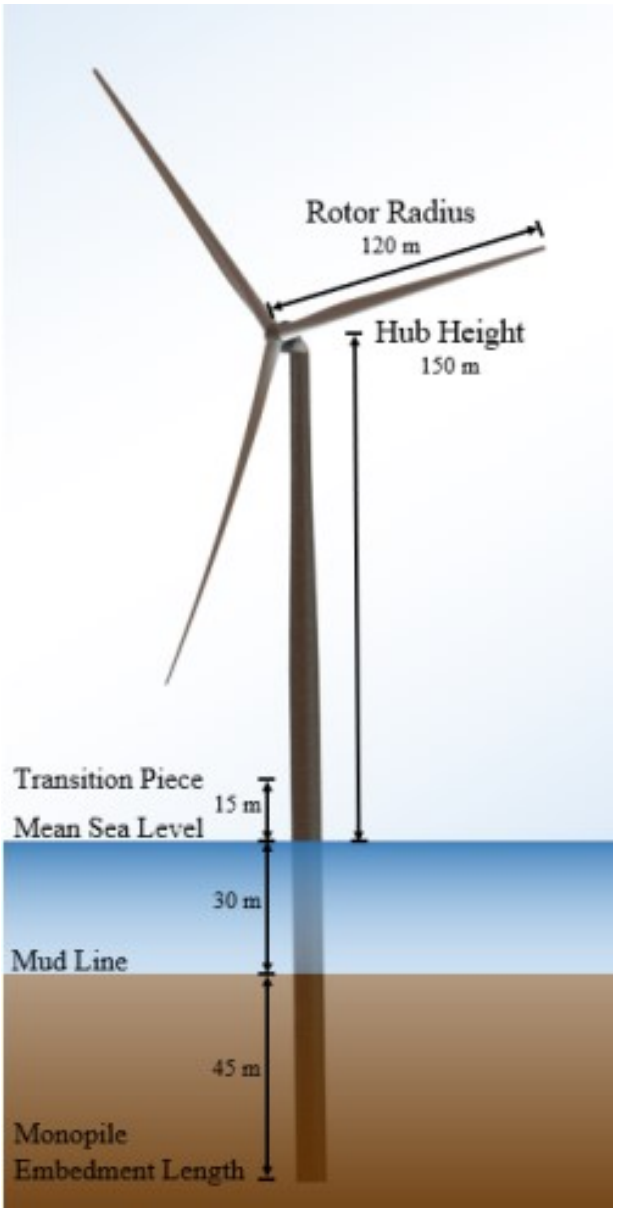

Figure B.2: The IEA 15MW Reference Wind Turbine [16]

Figure B.3: View from the Suction Side (Top) and Trailing Edge (Bottom) of the Offshore Wind Turbine Blade [16]

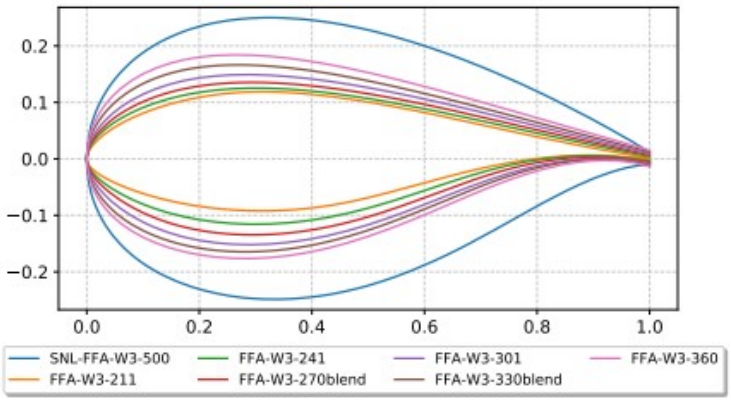

Figure B.4: DTU FFA-W3 Airfoil Family Used in the IEA Wind 15-MW Blade Design [16]

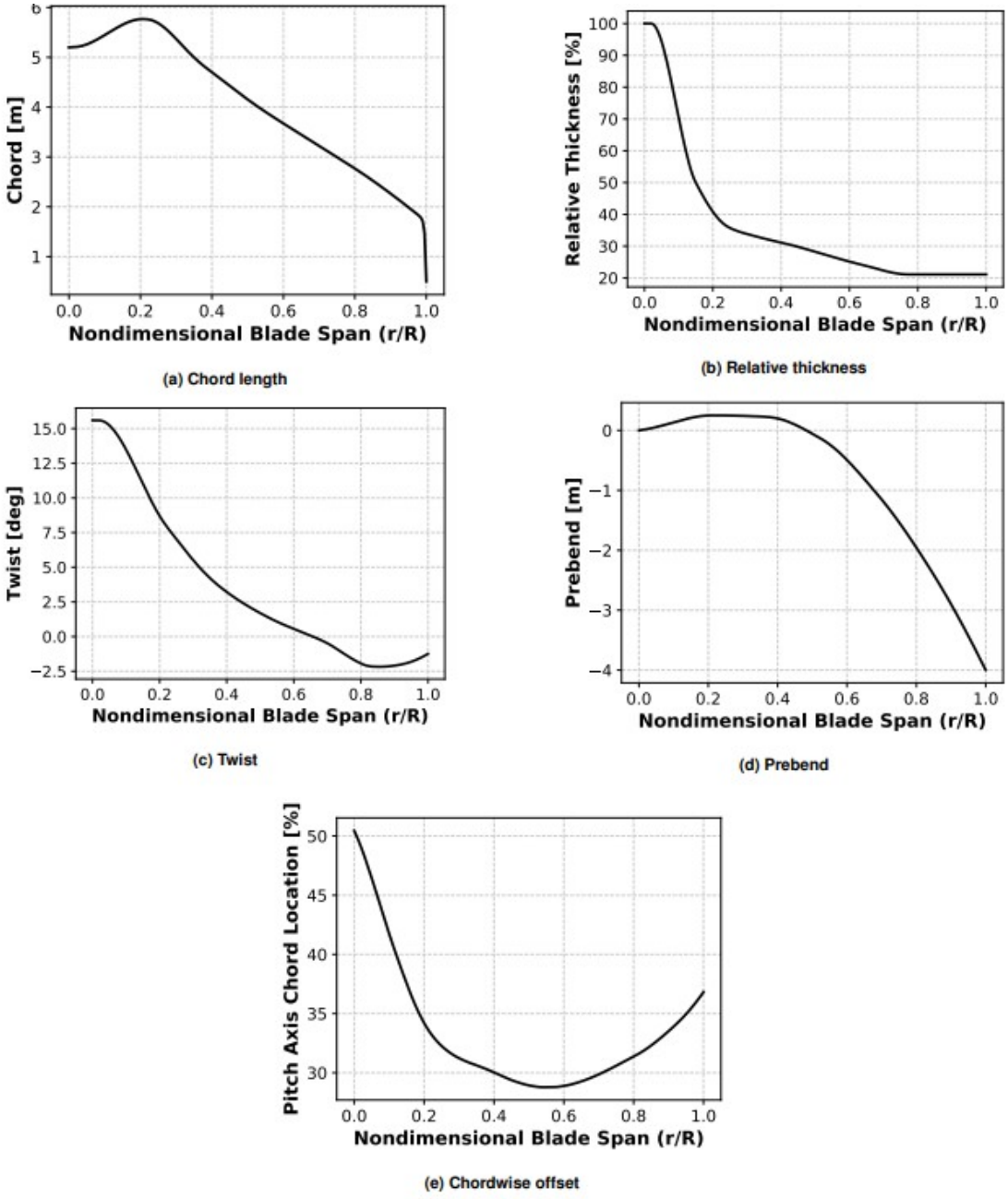

Figure B.5: Blade Planform Spanwise Quanties [16]

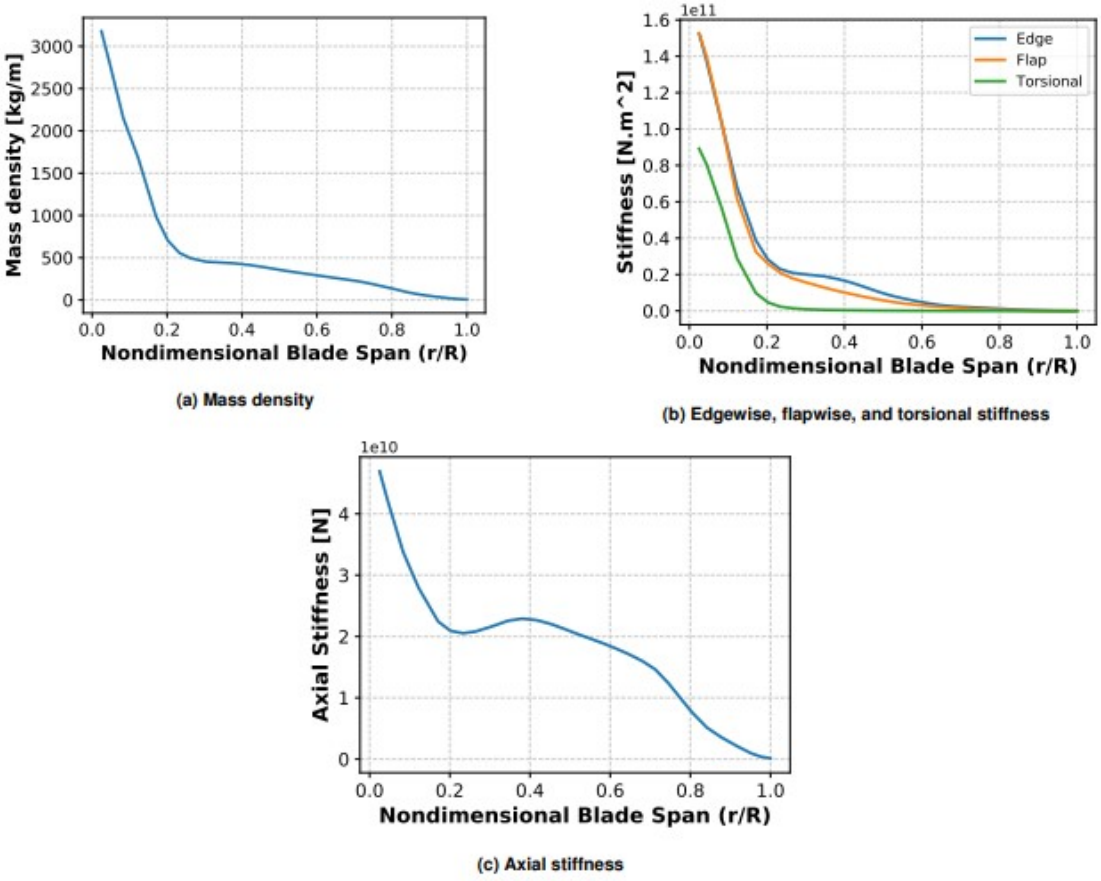

Figure B.6: Blade Beam Structural Properties [16]

C

Turbine Blade Simplification

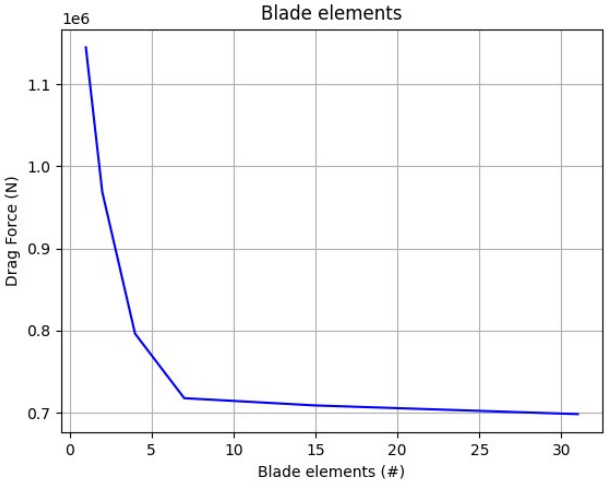

Figure C.1: Force Sensibility to Number of Blade Elements, Moment

Figure C.2: Force Sensibility to Number of Blade Elements, Horizontal- Vertical Installation

D

Appendix Main Hook Terminology

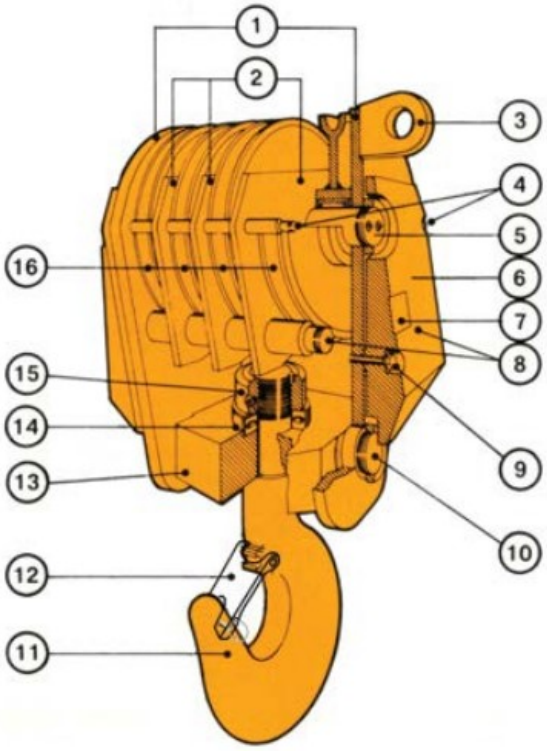

1. Side Plates
2. Center Plates
3. "Mouse Ear" Deadend
4. Upper Tie Bolts
5. Center Pin
6. Cheek Weight
7. Safety Precautions Plate: Tonnage Rating Nameplate (Opposite sides)
8. Lower Tie Bolts
9. Cheek Weight Cap Screw(s) (1 or 2)
10. Trunnion Pin, or Hook Housing Trunnion
11. Hook
12. Hook Latch
13. Hook Housing
14. Thrust Bearing
15. Hook Nut
16. Wire Rope Sheaves

Figure D.1: Terminology of a Crane Main Hook [63]

E

Viterna Extrapolation

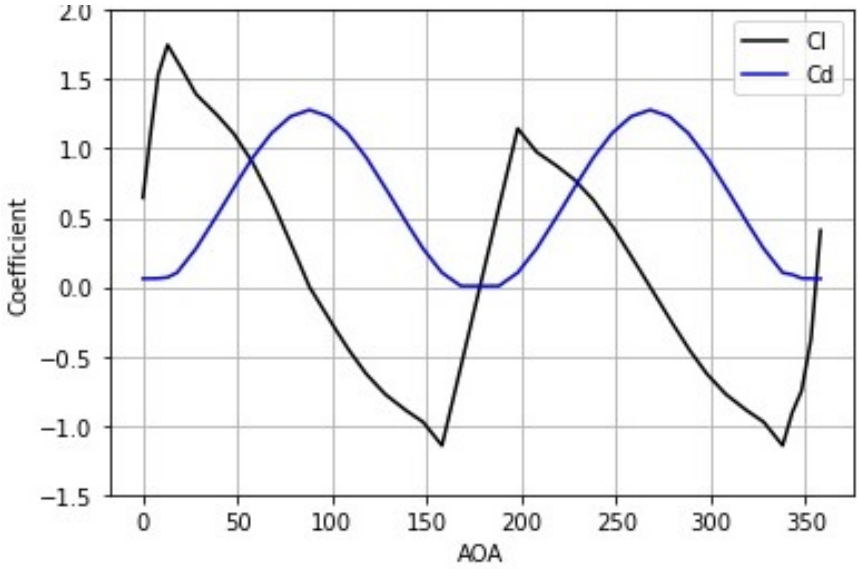

Figure E.1: FFA-W3-500 Airfoil Lift and Drag Coefficients

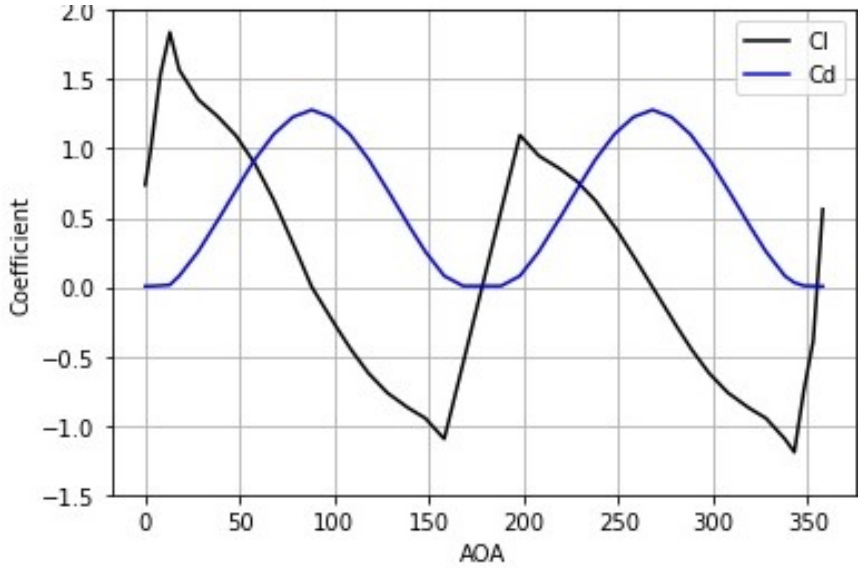

Figure E.2: FFA-W3-211 Lift and Drag Coefficients

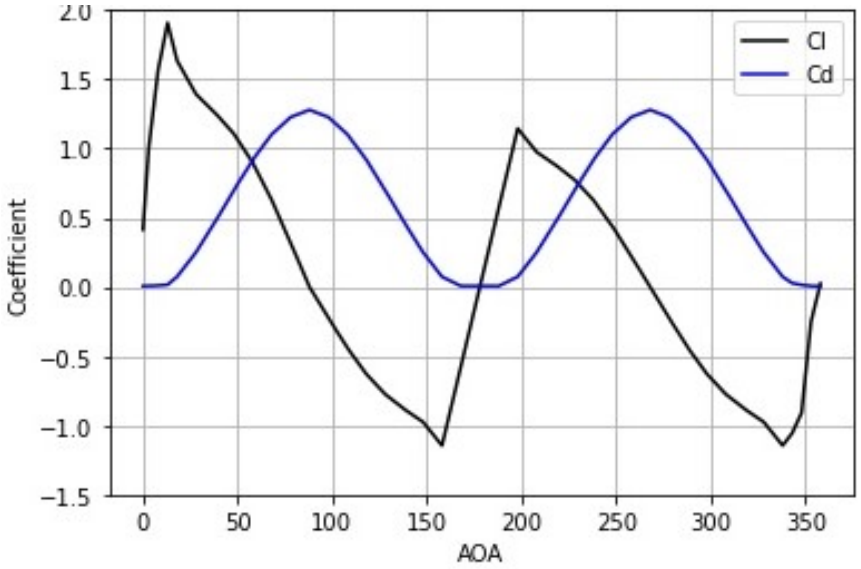

Figure E.3: FFA-W3-241 Airfoil Lift and Drag Coefficients

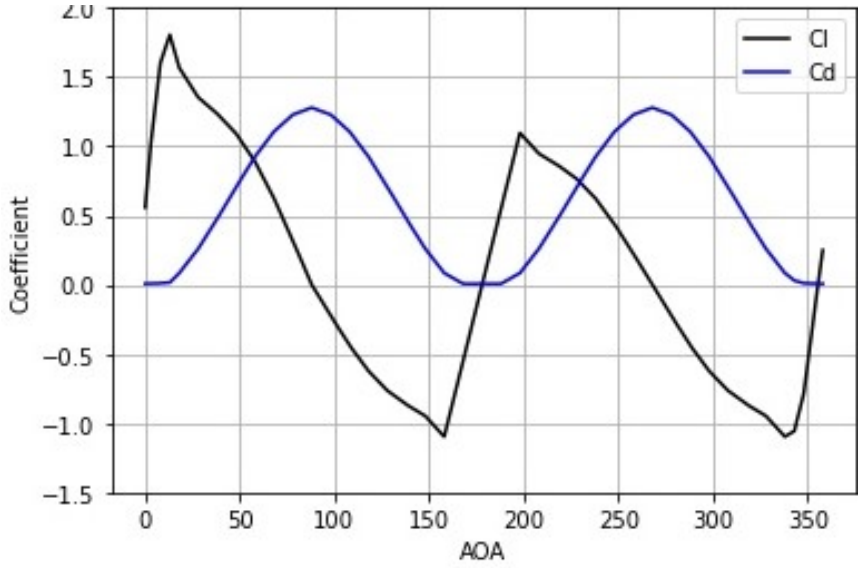

Figure E.4: FFA-W3-270blend Airfoil Lift and Drag Coefficients

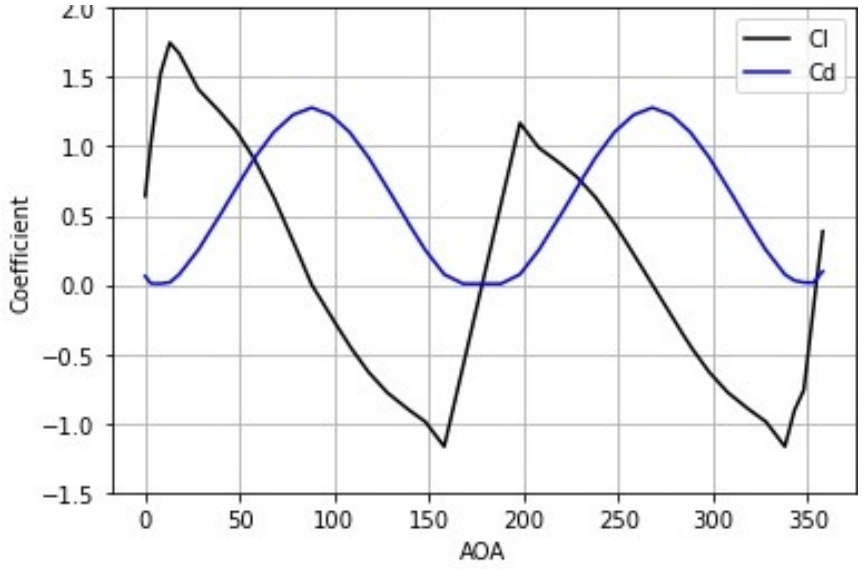

Figure E.5: FFA-W3-301 Airfoil Lift and Drag Coefficients

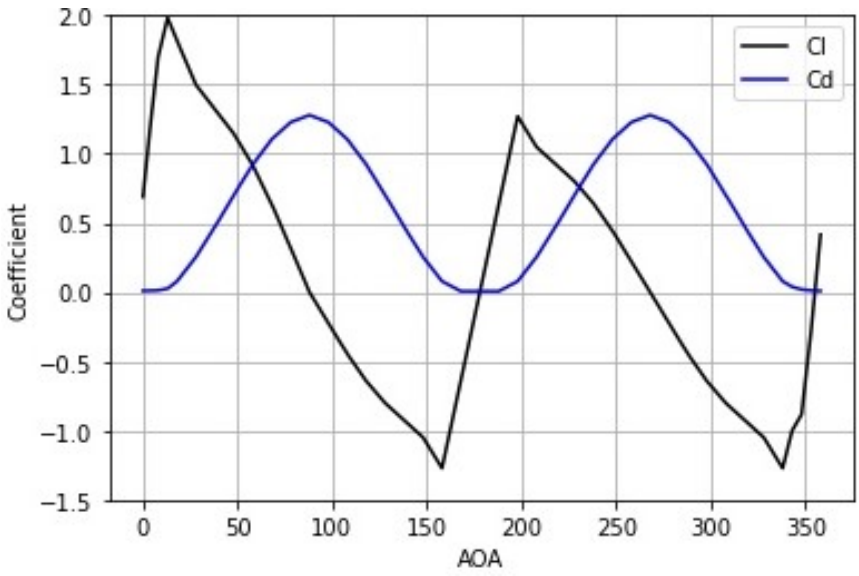

Figure E.6: FFA-W3-330blend Airfoil Lift and Drag Coefficients

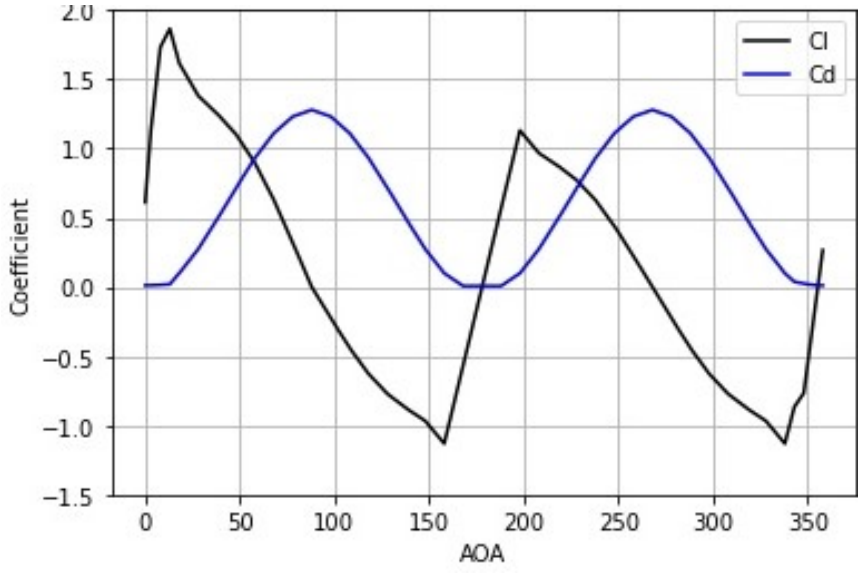

Figure E.7: FFA-W3-360 Airfoil Lift and Drag Coefficients

F

Reynolds number

F.1. Understanding Reynolds Number

The Reynolds number (Re) is a dimensionless parameter used in fluid dynamics to characterize the relative importance of inertial forces to viscous forces within a fluid flow. It is defined as the ratio of inertial forces ($\rho \cdot V \cdot L$) to viscous forces ($\mu \cdot L$), where ρ is the fluid density, V is the velocity of the flow, L is a characteristic length (such as chord length for airfoils), and μ is the dynamic viscosity of the fluid. Mathematically, it is expressed as:

$$Re = \frac{\rho \cdot V \cdot L}{\mu} \tag{F.1}$$

F.2. Calculation of Reynolds Number

To calculate the Reynolds number, one needs to determine the relevant parameters of the gas flow. These include the fluid density, velocity of the flow, characteristic length, and dynamic viscosity of the fluid. These values can be obtained experimentally or through computational simulations. The Reynolds number provides critical insights into the flow regime, aiding in the prediction of flow behavior and its effects on aerodynamic performance.

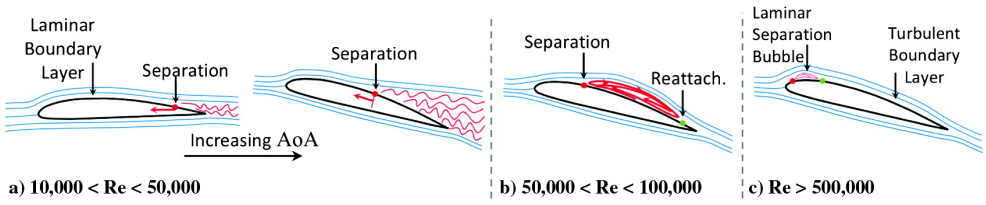

Figure F.1: Streamline with Increasing Reynolds Number [64]

F.3. Relationship with Lift and Drag Forces

The Reynolds number plays a significant role in determining the lift and drag coefficients of airfoils. At lower Reynolds numbers, typically associated with laminar flow regimes, airfoils tend to exhibit smoother airflow patterns. This can result in delayed stall and higher lift coefficients (C_L) due to reduced drag (C_D). Conversely, at higher Reynolds numbers, turbulent flow dominates, leading to increased drag and potential early stall occurrences, thereby affecting both lift and drag coefficients. As can be seen in figure F.1, with increasing Reynolds number the separation point moves forward on the airfoil. Because of this the separation changes and reattaches to the airfoil.

In essence, the Reynolds number serves as a crucial parameter influencing the aerodynamic characteristics of airfoils and other structures. By understanding its impact on lift and drag

coefficients, engineers can optimize airfoil designs for various operating conditions, thereby enhancing aerodynamic efficiency and performance across a range of applications. In figure F.2 the drag coefficient of different 2D structures is shown for different Reynolds numbers.

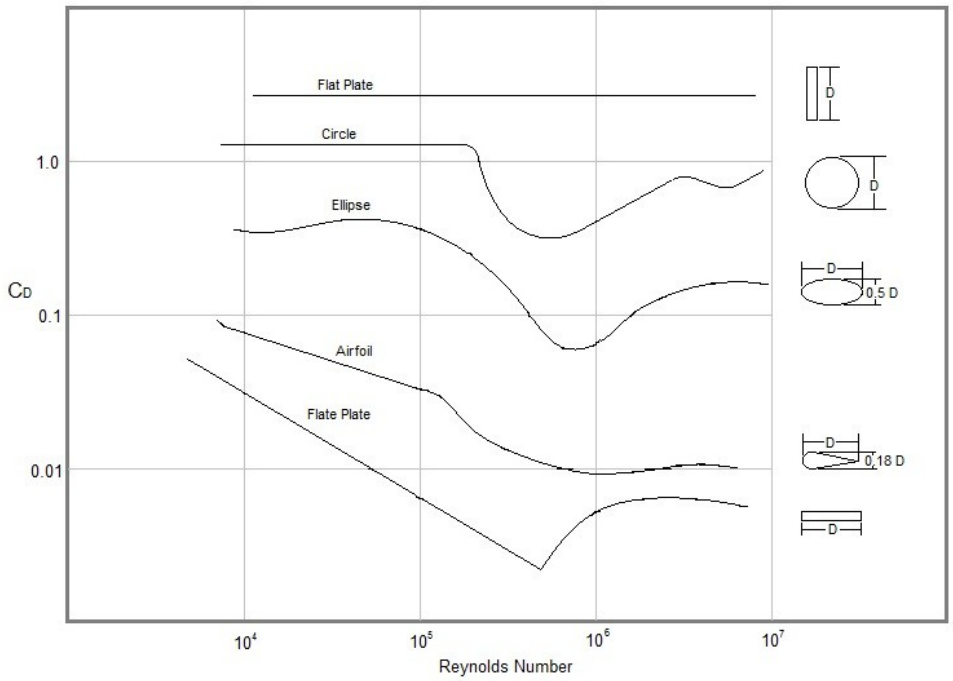

Figure F.2: Drag Coefficient of 2D Structures [65]

G

Flowchart Numerical Model

next page

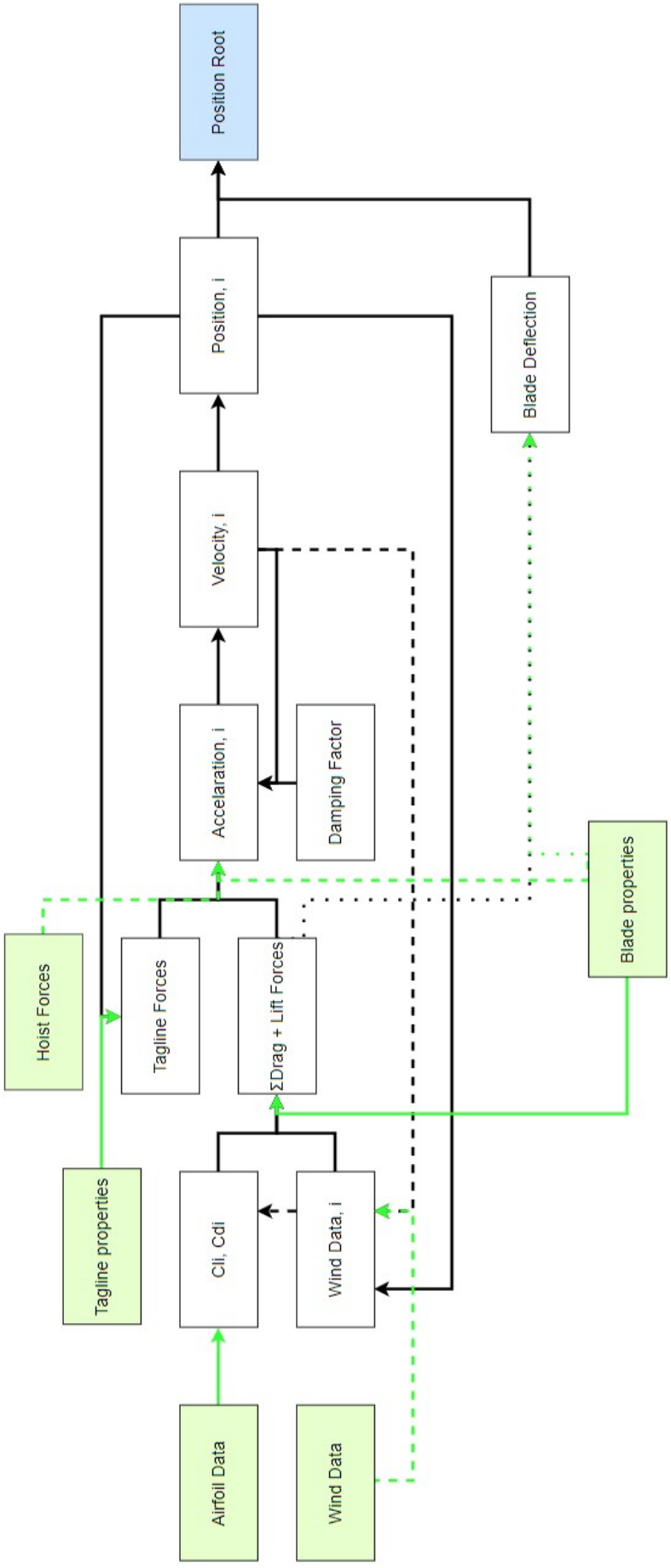

Figure G.1: Flowchart of the Numerical Model

H

Python Code

In this section the python code is shown.

```
# this document can be used to calculate the dynamics of an airfoil, please make sure you read everything carefully
# this document is so written that everything related to a specific section starts with a capital letter of that
# section, for example for things related to the blade they start with B
# First all parameters of the airfoil are added, the height of the number of airfoils is something you can choose
# yourself
# keep in mind that blade section has equal length
import pandas as pd
import matplotlib.pyplot as plt
from numpy import sqrt, cos, arctan, pi, sin, radians, degrees, arccos, tan, exp, log
import time
import numpy as np
from numpy.linalg import norm
from collections import defaultdict
from matplotlib.animation import FuncAnimation
from numpy import polyfit
import statistics

# add all vectors which should be created, this is something we try now

LocationsCOG = []
LocationTIP = []
LocationROOT = []
Speeds = []
Accelerations = []
Forces = []
Moments = []
NORMVEG = []
TAGFORCESL = []
TAGFORCESR = []
ANGLECOG = []
SPEEDCOG = []
SPEEDROOT = []
MTOTListx = []
MTOTListy = []
MTOTListz = []
DRAGSTART = []
FINDDRAG = []
TIME = []
PLOTFIX = []
FTOTx = []
FTOTy = []
FTOTz = []

#########################################################################################################################
# BLADE DATA #
#########################################################################################################################
# all data related to the blade starts with the letter B
# create number of sections otherwise add like stated
# blade length and airfoil length, in meters!
BLe = 117  # blade length in meters
BSe = 7  # number of airfoil sections
BALe = BLe / BSe  # airfoil length
```

```
BALe = BLe / BSe  # airfoil length
BLCOG = 26.8  # place of COG in meters from root
# change the hanging point if not same as COG here, positive is to the tip, negative to the root
BPP = 0 # in meters
# (1.93175) COMBINED point of zero rotation around x-axis of blade
# (2.06549055 is the addition to cog for this model to compensate mass)
# (-8.525)  is the addition to overcome pitch around z axis @ 4 m/s, by drag
# (234.265) for no spin around x axis to compensate lift
TL = 41.8  # position  of the left tagline connection from root
TR = 11.8  # position  of the right tagline connection from root
# here we create the arms of the blade in 3D dimension
# First all centres of the blade elements are calculated
BY1 = -BLCOG + (BALe / 2) + BPP
BY2 = -BLCOG + ((BALe / 2) + BALe) + BPP
BY3 = -BLCOG + ((BALe / 2) + (2 * BALe)) + BPP
BY4 = -BLCOG + ((BALe / 2) + (3 * BALe)) + BPP
BY5 = -BLCOG + ((BALe / 2) + (4 * BALe)) + BPP
BY6 = -BLCOG + ((BALe / 2) + (5 * BALe)) + BPP
BY7 = -BLCOG + ((BALe / 2) + (6 * BALe)) + BPP
BE1A = np.array([[0], [BY1], [0]])
BE2A = np.array([[0], [BY2], [0]])
BE3A = np.array([[0], [BY3], [0]])
BE4A = np.array([[0], [BY4], [0]])
BE5A = np.array([[0], [BY5], [0]])
BE6A = np.array([[0], [BY6], [0]])
BE7A = np.array([[0], [BY7], [0]])
# Here the locations of the connection to the tagline is calculated.
BETL = np.array([[0], [-BLCOG + TL], [0]])
BETR = np.array([[0], [-BLCOG + TR], [0]])
# pitch of airfoil section, in degrees!
BPi1 = 14.5
BPi2 = 9.25
BPi3 = 4.5
BPi4 = 1.75
BPi5 = 0
BPi6 = -1.5
BPi7 = -1
# PI# = # add if blade is split up in more sections
# add the length of cord line of each section, make sure the cord line correspond to the right blade angle, in meters!
BCL1 = 5.35
BCL2 = 5.6
BCL3 = 4.9
BCL4 = 4.2
BCL5 = 3.5
BCL6 = 2.8
BCL7 = 1.65
# CL# = #  add if blade is split up in more sections
# add weight of each blade section, make sure the weight correspond to the right blade section, in kg!
BWe1 = 39268
BWe2 = 10500
BWe3 = 6219
BWe4 = 4836
```

```
BWe4 = 4836
BWe5 = 3450
BWe6 = 2069
BWe7 = 680
# BWE# = # add if blade is split up in more sections
BWeT = BWe1 + BWe2 + BWe3 + BWe4 + BWe5 + BWe6 + BWe7  # total weight of blade, add sections if there are more blade sections
# calculate the moment of inertia of the blade
BI = BWe1 * (BY1 ** 2) + BWe2 * (BY2 ** 2) + BWe3 * (BY3 ** 2) + BWe4 * (BY4 ** 2) + BWe5 * (BY5 ** 2) + BWe6 * (BY6 ** 2) + BWe7 * (BY7 ** 2)

# airfoil data of each airfoil will be different, please add blade data to your computer and store it at an
# easy-to-access place, you can use the viterna extrapolation tool from NREL (search on Google to airfoilprep). It is
# important to know if you interpolate the data in steps of 1/5/10 degrees,how smaller the step how more accurate the
# load calculations, please make sure that the first row corresponds to the first lift coefficient, the second row
# corresponds to the first drag coefficient, the third row to the second airfoil lift coefficient, the fourth row to the
# second drag coefficient and so on.
# make sure that the name between brackets corresponds to the name of the blade coefficient file

# starting angle of the blade in relation to the O,everything is put the zero when the blade lies in the direction of
# the y,axis
B_alpha = 0  # around x axis in degrees
B_beta = 0  # around y axis in degrees, if blade is rotated around its length during installation, zero if aoa is 0
B_gamma = 0  # around z axis in degrees
Balpha = radians(B_alpha)
Bbeta = radians(B_beta)
Bgamma = radians(B_gamma)
# starting velocity of turbine blade COG and angular velocity
BCOGV = np.array([[0], [0], [0]])
BWx = 0  # rad/s
BWy = 0  # rad/s
BWz = 0  # rad/s

#  Getting the blade data from the file added
blade_data = pd.read_csv('blade_data.csv')

########################################################################################################################
# CRANE DATA #
########################################################################################################################
# maximum lifting height of a crane (voltaire) is about 162,5m
# jack up height above sea level, in meters
CJH = 10
# level difference  of boom above decklevel, height of z direction crane minus jack up height
CDB = 30
# boomlength, in meters
CBL = 140
# boom angle in meters from horizon, in degrees, voltaire max is about 70 degrees
CBA_h = 70  # in degrees
CBAh = radians(CBA_h)
# beem angle around its central axis, in degrees
CBA_z = 0  # in degrees
CBAz = radians(CBA_z)
# length of hoist cable
CHL = 21.5
```

```
CHL = 21.5
# with this info set, the  position of the crane tip can be calculated, after that the blade cog rotation
CHPx = CBL * cos(CBAz) * cos(CBAh)
CHPy = CBL * sin(CBAz) * cos(CBAh)
CHPz = CJH + CDB + CBL * sin(CBAh)
CHP = np.array([[CHPx], [CHPy], [CHPz]])

# with this info set, the starting position of the blade can be calculated
BCOGx = CHPx - 0.5
BCOGy = CHPy
BCOGz = CHPz - CHL
BCOGP = np.array([[BCOGx], [BCOGy], [BCOGz]])

########################################################################################################################
# TOWER DATA #
########################################################################################################################
# position from the projected origin at sea level of the bottomside of the craneboom, in meters!
# for now is assumed the tower is standing still, later on we will change this section
# the position of the monopile penetrating the water is called M
Hx = 50
Hy = -28
Hz = 150

########################################################################################################################
# air data
########################################################################################################################
AD = 1.2225  # air density, in kg/m^3!
windspeedvector2 = np.array([[12], [0], [0]])
wind_data = pd.read_csv('wind,12000,12.csv')  #4, 8, 10, 12, 14, zelfde nummer als hierboven

########################################################################################################################
# Tagline Configurations
########################################################################################################################
TAGLINE = 1
# 1 = constant force, 2 =  springforce, 3 = pull out speed -> pull force
# Change values of the tagline values
# Tagline configuration 1
TSLH1 = 8595 # Newton
TSRH1 = 7800
TSLB1 = 500
TSRB1 = 500
# Tagline configuration 2
Td = 0.108
TSLH2 = (4.04 * (10 ** 10)) * (Td * 2)  # Newton per meters, tagline stiffness, data from orcina orcaflex
TSRH2 = (4.04 * (10 ** 10)) * (Td * 2)
TSLB2 = (4.04 * (10 ** 10)) * (Td * 2)  # Newton per meters
TSRB2 = (4.04 * (10 ** 10)) * (Td * 2)
TLLH2 = (CHL/tan(CBAh)) - 0.1  # tagline L0 in meters
TLRH2 = (CHL/tan(CBAh)) - 0.1
TLLB2 = 10
TLRB2 = 10
```

```
# Tagline configuration 3
TSL3XA = 0  # Point A (left side) of tug out speed m/s or x
TSL3YA = 120.66173167  # Point A (left side) of pull force according to  speed in Newton
TSL3XB = 5  # Point B (right side) of tug out speed m/s or x
TSL3YB = 500  # Point B (right side) of pull force according to  speed in Newton
TSR3XA = 0
TSR3YA = 3.77044502
TSR3XB = 5
TSR3YB = 500

# How taglines are connected to the tower
# 1 = horizontal, 2 = to crane legpoint, 3 = horizontal  Crane legpoint
TAGSETTING = 1

########################################################################################################################
#  Run Data
########################################################################################################################
# make the loop work, change here the total run time of the model and the time step
start_time = time.time()
calculationtime = 200  # in minutes
timelength = calculationtime * 60  # in seconds
timestep = 0.1  # in seconds
time = 0

MINMIN = 100
MINMAX = 130
xMINplot = round((MINMIN*60)/timestep)
yMINplot = round((MINMAX*60)/timestep)
AVERAGE  = 39

########################################################################################################################
########################################################################################################################
# DON'T CHANGE ANYTHING FROM HERE; ONLY ADD MORE LINES FOR BLADE ELEMENTS
########################################################################################################################
########################################################################################################################

###### Enter calculations of what the minimum tagline length should be #######

while time < timelength:
    print(round((time / timelength) * 100), "% completed")
    timeround = round(time)

    if timeround > 11990:
        timeround = timeround - 11990
    if timeround > 23980:
        timeround = timeround - 23980
    if timeround > 35970:
        timeround = timeround - 35970

    windx = wind_data.iloc[timeround+1][0]
    windy = wind_data.iloc[timeround+1][1]
```

```
windz = wind_data.iloc[timeround+1][2]

windspeedvector1 = np.array([[windx], [windy], [windz]])

if time < 100 / timelength:
    windspeedvector = windspeedvector2

if time >= 100 / timelength:
    windspeedvector = windspeedvector1


WV1 = windspeedvector
WV2 = windspeedvector
WV3 = windspeedvector
WV4 = windspeedvector
WV5 = windspeedvector
WV6 = windspeedvector
WV7 = windspeedvector


# In this section for every blade section their local windspeed will be calculated, this is done by the speed of the
# COG and the rotational speed of the blade, the blade deflection is neglected. Following calculations are needed
# First we calculate the Blade COG Rotation Matrix, this to calculate the positions of the blade elements
BCOGRM = np.array([[cos(Bbeta) * cos(Bgamma), sin(Balpha) * sin(Bbeta) * cos(Bgamma) - cos(Balpha) * sin(Bgamma),
                    cos(Balpha) * sin(Bbeta) * cos(Bgamma) + sin(Balpha) * sin(Bgamma)],
                   [cos(Bbeta) * sin(Bgamma), sin(Balpha) * sin(Bbeta) * sin(Bgamma) + cos(Balpha) * cos(Bgamma),
                    cos(Balpha) * sin(Bbeta) * sin(Bgamma) - sin(Balpha) * cos(Bgamma)],
                   [-sin(Bbeta), sin(Balpha) * cos(Bbeta), cos(Balpha) * cos(Bbeta)]])


BCOGAVT = np.array([[0, -BWz, BWy], [BWz, 0, -BWx], [-BWy, BWx, 0]])

# calculating all places in xyz
x = np.array([[1], [0], [0]])
y = np.array([[0], [1], [0]])
z = np.array([[0], [0], [1]])
BCOGx = norm(x * BCOGP)
BCOGy = norm(y * BCOGP)
BCOGz = norm(z * BCOGP)

# Here we calculate the position of each blade element
B1PA = np.dot(BCOGRM, BE1A)
B2PA = np.dot(BCOGRM, BE2A)
B3PA = np.dot(BCOGRM, BE3A)
B4PA = np.dot(BCOGRM, BE4A)
B5PA = np.dot(BCOGRM, BE5A)
B6PA = np.dot(BCOGRM, BE6A)
B7PA = np.dot(BCOGRM, BE7A)
BE1P = BCOGP + B1PA
BE2P = BCOGP + B2PA
BE3P = BCOGP + B3PA
BE4P = BCOGP + B4PA
```

```
BE4P = BCOGP + B4PA
BE5P = BCOGP + B5PA
BE6P = BCOGP + B6PA
BE7P = BCOGP + B7PA

# Here the place of the taglines is calculated.
BTLPA = np.dot(BCOGRM, BETL)
BTRPA = np.dot(BCOGRM, BETR)
BTCLP = BCOGP + BTLPA
BTCRP = BCOGP + BTRPA

# Here the velocity of each blade segment is calculated
BE1V = BCOGV + (np.dot(BCOGAVT, BE1A))
BE2V = BCOGV + (np.dot(BCOGAVT, BE2A))
BE3V = BCOGV + (np.dot(BCOGAVT, BE3A))
BE4V = BCOGV + (np.dot(BCOGAVT, BE4A))
BE5V = BCOGV + (np.dot(BCOGAVT, BE5A))
BE6V = BCOGV + (np.dot(BCOGAVT, BE6A))
BE7V = BCOGV + (np.dot(BCOGAVT, BE7A))

# Here the speed of the taglines connection point is calculated.
TCLVV = (BCOGV + np.dot(BCOGAVT, BETL)) * x
TCLV = TCLVV[[0], [0]]
TCRVV = (BCOGV + np.dot(BCOGAVT, BETR)) * x
TCRV = TCRVV[[0], [0]]

# Here the cumulative wind speed of each blade section is calculated
BE1VC = WV1 - BE1V
BE2VC = WV2 - BE2V
BE3VC = WV3 - BE3V
BE4VC = WV4 - BE4V
BE5VC = WV5 - BE5V
BE6VC = WV6 - BE6V
BE7VC = WV7 - BE7V

# to calculate the lift and drag coefficient the projected windspeed of the velocity vector perpendicular to the
# blade needs to be known, while we know what the normal of that plane is we can calculate this
BPN = (BE7P - BE6P)  # Blade plane normal vector,
# the cumulative wind speed is the vector which will be projected on the plane BPN
BPNT = BPN.transpose()
BPNNorm = np.sqrt(sum(BPN ** 2))
BE1PC = (np.dot(BPNT, BE1VC) / BPNNorm ** 2) * BPN
BE2PC = (np.dot(BPNT, BE2VC) / BPNNorm ** 2) * BPN
BE3PC = (np.dot(BPNT, BE3VC) / BPNNorm ** 2) * BPN
BE4PC = (np.dot(BPNT, BE4VC) / BPNNorm ** 2) * BPN
BE5PC = (np.dot(BPNT, BE5VC) / BPNNorm ** 2) * BPN
BE6PC = (np.dot(BPNT, BE6VC) / BPNNorm ** 2) * BPN
BE7PC = (np.dot(BPNT, BE7VC) / BPNNorm ** 2) * BPN

# now we need to substract this from the velocity vector, and we have the projection
BE1Proj = BE1VC - BE1PC
BE2Proj = BE2VC - BE2PC
```

```
BE2Proj = BE2VC - BE2PC
BE3Proj = BE3VC - BE3PC
BE4Proj = BE4VC - BE4PC
BE5Proj = BE5VC - BE5PC
BE6Proj = BE6VC - BE6PC
BE7Proj = BE7VC - BE7PC

# we need to define the vector on the plane which is equal to the blade its zero degree aoa, this can be done by
# taking the dot product of the vector from the cog to the crane tip and the vector in the length of the blade
BCOGtoCV = CHP - BCOGP
B0AOA = (-1 * (np.cross(BCOGtoCV.transpose(), BPN.transpose()))).T
BEA0A11 = (np.degrees(np.arctan2(np.cross(B0AOA.T, BE1Proj.T), np.dot(B0AOA.T, BE1Proj))))
BEA0111 = round(-1 * (BEA0A11[0][1]) - B_beta + (BPi1-BPi2))
BEA0A1 = BEA0111
BEA0A22 = (np.degrees(np.arctan2(np.cross(B0AOA.T, BE2Proj.T), np.dot(B0AOA.T, BE2Proj))))
BEA0222 = round(-1 * (BEA0A22[0][1]) - B_beta + (BPi2-BPi2))
BEA0A2 = BEA0222
BEA0A33 = (np.degrees(np.arctan2(np.cross(B0AOA.T, BE3Proj.T), np.dot(B0AOA.T, BE3Proj))))
BEA0333 = round(-1 * (BEA0A33[0][1]) - B_beta + (BPi3-BPi2))
BEA0A3 = BEA0333
BEA0A44 = (np.degrees(np.arctan2(np.cross(B0AOA.T, BE4Proj.T), np.dot(B0AOA.T, BE4Proj))))
BEA0A444 = round(-1 * (BEA0A44[0][1]) - B_beta + (BPi4-BPi2))
BEA0A4 = BEA0A444
BEA0A55 = (np.degrees(np.arctan2(np.cross(B0AOA.T, BE5Proj.T), np.dot(B0AOA.T, BE5Proj))))
BEA0555 = round(-1 * (BEA0A55[0][1]) - B_beta + (BPi5-BPi2))
BEA0A5 = BEA0555
BEA0A66 = (np.degrees(np.arctan2(np.cross(B0AOA.T, BE6Proj.T), np.dot(B0AOA.T, BE6Proj))))
BEA0666 = round(-1 * (BEA0A66[0][1]) - B_beta + (BPi6-BPi2))
BEA0A6 = BEA0666
BEA0A77 = (np.degrees(np.arctan2(np.cross(B0AOA.T, BE7Proj.T), np.dot(B0AOA.T, BE7Proj))))
BEA0A777 = round(-1 * (BEA0A77[0][1]) - B_beta + (BPi7-BPi2))
BEA0A7 = BEA0A777

# Now we can look for the blade lift and drag coefficients
BLC1 = blade_data.iloc[BEA0A1, 0]
BLC2 = blade_data.iloc[BEA0A2, 2]
BLC3 = blade_data.iloc[BEA0A3, 4]
BLC4 = blade_data.iloc[BEA0A4, 6]
BLC5 = blade_data.iloc[BEA0A5, 8]
BLC6 = blade_data.iloc[BEA0A6, 10]
BLC7 = blade_data.iloc[BEA0A7, 12]
BDC1 = blade_data.iloc[BEA0A1, 1]
BDC2 = blade_data.iloc[BEA0A2, 3]
BDC3 = blade_data.iloc[BEA0A3, 5]
BDC4 = blade_data.iloc[BEA0A4, 7]
BDC5 = blade_data.iloc[BEA0A5, 9]
BDC6 = blade_data.iloc[BEA0A6, 11]
BDC7 = blade_data.iloc[BEA0A7, 13]

#  calculating the magnitude of the velocity in the plane
VM1 = norm(np.sqrt(sum(BE1Proj ** 2)))
VM2 = norm(np.sqrt(sum(BE2Proj ** 2)))
```

```
VM2 = norm(np.sqrt(sum(BE2Proj ** 2)))
VM3 = norm(np.sqrt(sum(BE3Proj ** 2)))
VM4 = norm(np.sqrt(sum(BE4Proj ** 2)))
VM5 = norm(np.sqrt(sum(BE5Proj ** 2)))
VM6 = norm(np.sqrt(sum(BE6Proj ** 2)))
VM7 = norm(np.sqrt(sum(BE7Proj ** 2)))

# With this info known we can calculate the lift and drag forces acting on a blade
BLF1 = 0.5 * AD * (VM1 ** 2) * BLC1 * BCL1 * BALe
BLF2 = 0.5 * AD * (VM2 ** 2) * BLC2 * BCL2 * BALe
BLF3 = 0.5 * AD * (VM3 ** 2) * BLC3 * BCL3 * BALe
BLF4 = 0.5 * AD * (VM4 ** 2) * BLC4 * BCL4 * BALe
BLF5 = 0.5 * AD * (VM5 ** 2) * BLC5 * BCL5 * BALe
BLF6 = 0.5 * AD * (VM6 ** 2) * BLC6 * BCL6 * BALe
BLF7 = 0.5 * AD * (VM7 ** 2) * BLC7 * BCL7 * BALe
BDF1 = 0.5 * AD * (VM1 ** 2) * BDC1 * BCL1 * BALe
BDF2 = 0.5 * AD * (VM2 ** 2) * BDC2 * BCL2 * BALe
BDF3 = 0.5 * AD * (VM3 ** 2) * BDC3 * BCL3 * BALe
BDF4 = 0.5 * AD * (VM4 ** 2) * BDC4 * BCL4 * BALe
BDF5 = 0.5 * AD * (VM5 ** 2) * BDC5 * BCL5 * BALe
BDF6 = 0.5 * AD * (VM6 ** 2) * BDC6 * BCL6 * BALe
BDF7 = 0.5 * AD * (VM7 ** 2) * BDC7 * BCL7 * BALe

# With BEM Theory Known we know that the drag force is in line with the projected vector so first we make a unit
# vector of that vector thereafter we multiply it with the drag force
BDV1 = BE1Proj / sqrt(sum(BE1Proj ** 2))
BDV2 = BE2Proj / sqrt(sum(BE2Proj ** 2))
BDV3 = BE3Proj / sqrt(sum(BE3Proj ** 2))
BDV4 = BE4Proj / sqrt(sum(BE4Proj ** 2))
BDV5 = BE5Proj / sqrt(sum(BE5Proj ** 2))
BDV6 = BE6Proj / sqrt(sum(BE6Proj ** 2))
BDV7 = BE7Proj / sqrt(sum(BE7Proj ** 2))
BDFV1 = BDV1 * BDF1
BDFV2 = BDV2 * BDF2
BDFV3 = BDV3 * BDF3
BDFV4 = BDV4 * BDF4
BDFV5 = BDV5 * BDF5
BDFV6 = BDV6 * BDF6
BDFV7 = BDV7 * BDF7
# lift forces are perpendicular to the drag force in the airfoil plane
BPNN = BPN / sqrt(sum(BPN ** 2))
BLV1 = np.cross(BDV1.transpose(), BPNN.transpose())
BLV2 = np.cross(BDV2.transpose(), BPNN.transpose())
BLV3 = np.cross(BDV3.transpose(), BPNN.transpose())
BLV4 = np.cross(BDV4.transpose(), BPNN.transpose())
BLV5 = np.cross(BDV5.transpose(), BPNN.transpose())
BLV6 = np.cross(BDV6.transpose(), BPNN.transpose())
BLV7 = np.cross(BDV7.transpose(), BPNN.transpose())
BLFV1 = (BLV1 * BLF1).transpose()
BLFV2 = (BLV2 * BLF2).transpose()
BLFV3 = (BLV3 * BLF3).transpose()
BLFV4 = (BLV4 * BLF4).transpose()
```

```
    BLFV4 = (BLV4 * BLF4).transpose()
    BLFV5 = (BLV5 * BLF5).transpose()
    BLFV6 = (BLV6 * BLF6).transpose()
    BLFV7 = (BLV7 * BLF7).transpose()
    # Lift and drag force vector together
    BFV1 = BDFV1 + BLFV1
    BFV2 = BDFV2 + BLFV2
    BFV3 = BDFV3 + BLFV3
    BFV4 = BDFV4 + BLFV4
    BFV5 = BDFV5 + BLFV5
    BFV6 = BDFV6 + BLFV6
    BFV7 = BDFV7 + BLFV7

    # Calculate the Moment around the blade caused by lift + drag
    MBF1 = np.cross(B1PA.transpose(), BFV1.transpose())
    MBF2 = np.cross(B2PA.transpose(), BFV2.transpose())
    MBF3 = np.cross(B3PA.transpose(), BFV3.transpose())
    MBF4 = np.cross(B4PA.transpose(), BFV4.transpose())
    MBF5 = np.cross(B5PA.transpose(), BFV5.transpose())
    MBF6 = np.cross(B6PA.transpose(), BFV6.transpose())
    MBF7 = np.cross(B7PA.transpose(), BFV7.transpose())
    MBW = MBF1 + MBF2 + MBF3 + MBF4 + MBF5 + MBF6 + MBF7

    # Now all drag and lift forces are known and put in a vector for the COG
    BDTV = BDFV1 + BDFV2 + BDFV3 + BDFV4 + BDFV5 + BDFV6 + BDFV7  # in vector
    BLTV = BLFV1 + BLFV2 + BLFV3 + BLFV4 + BLFV5 + BLFV6 + BLFV7
    BDT = BDF1 + BDF2 + BDF3 + BDF4 + BDF5 + BDF6 + BDF7  # In total
    BLT = BLF1 + BLF2 + BLF3 + BLF4 + BLF5 + BLF6 + BLF7

    # In this section the blade normalvector of the gravitational force is calculated
    BCOGMV = np.array([[0], [0], [-9.81]])
    BMFV = BWeT * BCOGMV
    BMFV1 = BWe1 * BCOGMV
    BMFV2 = BWe2 * BCOGMV
    BMFV3 = BWe3 * BCOGMV
    BMFV4 = BWe4 * BCOGMV
    BMFV5 = BWe5 * BCOGMV
    BMFV6 = BWe6 * BCOGMV
    BMFV7 = BWe7 * BCOGMV

    # Calculate the Moment around the blade caused by mass
    MBM1 = np.cross(B1PA.transpose(), BMFV1.transpose())
    MBM2 = np.cross(B2PA.transpose(), BMFV2.transpose())
    MBM3 = np.cross(B3PA.transpose(), BMFV3.transpose())
    MBM4 = np.cross(B4PA.transpose(), BMFV4.transpose())
    MBM5 = np.cross(B5PA.transpose(), BMFV5.transpose())
    MBM6 = np.cross(B6PA.transpose(), BMFV6.transpose())
    MBM7 = np.cross(B7PA.transpose(), BMFV7.transpose())
    MBM = (MBM1 + MBM2 + MBM3 + MBM4 + MBM5 + MBM6 + MBM7).transpose()

    # Here the points of the taglines connected to the crane are calculated
    TBL = np.array([[0], [-BLCOG + TL], [CJH + CDB]])  # if tag connected to bottom of crane
```

```
    TBL = np.array([[0], [-BLCOG + TL], [CJH + CDB]])  # if tag connected to bottom of crane
    TBR = np.array([[0], [-BLCOG + TR], [CJH + CDB]])
    THH = np.array([[0], [0], [1]]) * BCOGP
    THHV = norm(np.sqrt(sum(THH ** 2)))
    THL = np.array([[0], [-BLCOG + TL], [BTCLP[2][0]]])
    THR = np.array([[0], [-BLCOG + TR], [BTCRP[2][0]]])

    # In this section the normal vector of the taglines will be calculated, the forcevector is created and the total
    # forces and moments are calculated
    if TAGSETTING == 1:
        TLtoTCLH = BTCLP - THL
        TRtoTCRH = BTCRP - THR
        TLHN = TLtoTCLH / norm(np.sqrt(sum(TLtoTCLH ** 2)))
        TRHN = TRtoTCRH / norm(np.sqrt(sum(TRtoTCRH ** 2)))
        TLHL = norm(np.sqrt(sum(TLtoTCLH ** 2)))
        TRHL = norm(np.sqrt(sum(TRtoTCRH ** 2)))
        if TAGLINE == 1:
            TFLH = TSLH1
            TFRH = TSRH1
            TFLFV = TFLH * -TLHN
            TFRFV = TFRH * -TRHN
        elif TAGLINE == 2:
            TFLH = (TLHL - TLLH2) * TSLH2
            TFRH = (TRHL - TLRH2) * TSRH2
            if TFLH < 0:
                print("the tagline is not under tension")
                TFLH = 0
                # break
            if TFRH < 0:
                print("the tagline is not under tension")
                TFRH = 0
                # break
            TFLFV = TFLH * -TLHN
            TFRFV = TFRH * -TRHN
        elif TAGLINE == 3:
            if TCLV <= TSL3XA:
                TFLH = TSL3YA
            elif TSL3XA < TCLV < TSL3XB:
                THelL = ((TSL3YB - TSL3YA) / (TSL3XB - TSL3XA))
                TX0YL = TSL3YA - (THelL * TSL3XA)
                TFLH = TX0YL + (TCLV * THelL)
            elif TCLV >= TSL3XB:
                TFLH = TSL3YB
            TFLFV = TFLH * -TLHN
            if TCRV <= TSR3XA:
                TFRH = TSR3YA
            elif TSR3XA < TCRV < TSR3XB:
                THelR = ((TSR3YB - TSR3YA) / (TSR3XB - TSR3XA))
                TX0YR = TSR3YA - (THelR * TSR3XA)
                TFRH = TX0YR + (TCRV * THelR)
            elif TCRV >= TSR3XB:
                TFRH = TSR3YB
```

```
            TFRH = TSR3YB
        TFRFV = TFRH * -TRHN

elif TAGSETTING == 2:
    TLtoTCLB = BTCLP - TBL
    TRtoTCRB = BTCRP - TBR
    TLBN = TLtoTCLB / norm(np.sqrt(sum(TLtoTCLB ** 2)))
    TRBN = TRtoTCRB / norm(np.sqrt(sum(TRtoTCRB ** 2)))
    TLBL = norm(np.sqrt(sum(TLtoTCLB ** 2)))
    TRBL = norm(np.sqrt(sum(TRtoTCRB ** 2)))
    if TAGLINE == 1:
        TFLB = TSLB1
        TFRB = TSRB1
        TFLFV = TFLB * -TLBN
        TFRFV = TFRB * -TRBN
    elif TAGLINE == 2:
        TFLB = (TLBL - TLLB2) * TSLB2
        TFRB = (TRBL - TLRB2) * TSRB2
        if TFLB < 0:
            print("the tagline is not under tension")
            break
        if TFRB < 0:
            print("the tagline is not under tension")
            break
        TFLFV = TFLB * -TLBN
        TFRFV = TFRB * -TRBN
    elif TAGLINE == 3:
        if TCLV <= TSL3XA:
            TFLB = TSL3YA
        elif TSL3XA < TCLV < TSL3XB:
            THelL = ((TSL3YB - TSL3YA) / (TSL3XB - TSL3XA))
            TX0YL = TSL3YA - (THelL * TSL3XA)
            TFLB = TX0YL + (TCLV * THelL)
        elif TCLV >= TSL3XB:
            TFLB = TSL3YB
        TFLFV = TFLB * -TLBN
        if TCRV <= TSR3XA:
            TFRB = TSR3YA
        elif TSR3XA < TCRV < TSR3XB:
            THelR = ((TSR3YB - TSR3YA) / (TSR3XB - TSR3XA))
            TX0YR = TSR3YA - (THelR * TSR3XA)
            TFRB = TX0YR + (TCRV * THelR)
        elif TCRV >= TSR3XB:
            TFRB = TSR3YB
        TFRFV = TFRB * -TRBN

elif TAGSETTING == 3:
    TLtoTCLH = BTCLP - THL
    TRtoTCRH = BTCRP - THR
    TLtoTCLB = BTCLP - TBL
    TRtoTCRB = BTCRP - TBR
    TLHN = TLtoTCLH / norm(np.sqrt(sum(TLtoTCLH ** 2)))
```

```
    TLHN = TLtoTCLH / norm(np.sqrt(sum(TLtoTCLH ** 2)))
    TRHN = TRtoTCRH / norm(np.sqrt(sum(TRtoTCRH ** 2)))
    TLBN = TLtoTCLB / norm(np.sqrt(sum(TLtoTCLB ** 2)))
    TRBN = TRtoTCRB / norm(np.sqrt(sum(TRtoTCRB ** 2)))
    TLHL = norm(np.sqrt(sum(TLtoTCLH ** 2)))
    TRHL = norm(np.sqrt(sum(TRtoTCRH ** 2)))
    TLBL = norm(np.sqrt(sum(TLtoTCLB ** 2)))
    TRBL = norm(np.sqrt(sum(TRtoTCRB ** 2)))
    if TAGLINE == 1:
        TFLH = TSLH1
        TFRH = TSRH1
        TFLB = TSLB1
        TFRB = TSRB1
        TFLFV = TFLB * -TLBN + TFLH * -TLHN
        TFRFV = TFRB * -TRBN + TFRH * -TRHN
    elif TAGLINE == 2:
        TFLH = (TLHL - TLLH2) * TSLH2
        TFRH = (TRHL - TLRH2) * TSRH2
        TFLB = (TLBL - TLLB2) * TSLB2
        TFRB = (TRBL - TLRB2) * TSRB2
        if TFLH < 0:
            print("the tagline is not under tension")
            break
        if TFRH < 0:
            print("the tagline is not under tension")
            break
        if TFLB < 0:
            print("the tagline is not under tension")
            break
        if TFRB < 0:
            print("the tagline is not under tension")
            break
        TFLFV = TFLB * -TLBN + TFLH * -TLHN
        TFRFV = TFRB * -TRBN + TFRH * -TRHN
    elif TAGLINE == 3:
        if TCLV <= TSL3XA:
            TFLH = TSL3YA
            TFLB = TSL3YA
        elif TSL3XA < TCLV < TSL3XB:
            THelL = ((TSL3YB - TSL3YA) / (TSL3XB - TSL3XA))
            TX0YL = TSL3YA - (THelL * TSL3XA)
            TFLH = TX0YL + (TCLV * THelL)
            TFLB = TX0YL + (TCLV * THelL)
        elif TCLV > TSL3XB:
            TFLH = TSL3YB
            TFLB = TSL3YB
        TFLFV = TFLB * -TLBN + TFLH * -TLHN
        if TCRV <= TSR3XA:
            TFRH = TSR3YA
            TFRB = TSR3YA
        elif TSR3XA < TCRV < TSR3XB:
            THelR = ((TSR3YB - TSR3YA) / (TSR3XB - TSR3XA))
```

```
                THelR = ((TSR3YB - TSR3YA) / (TSR3XB - TSR3XA))
                TX0YR = TSR3YA - (THelR * TSR3XA)
                TFRH = TX0YR + (TCRV * THelR)
                TFRB = TX0YR + (TCRV * THelR)
            elif TCRV > TSR3XB:
                TFRH = TSR3YB
                TFRB = TSR3YB
            TFRFV = TFRB * -TRBN + TFRH * -TRHN

    # Calculate moment caused by tagline forces
    MBTL = np.cross(BETL.transpose(), TFLFV.transpose())
    MBTR = np.cross(BETR.transpose(), TFRFV.transpose())
    MBT = MBTL + MBTR

    # Now all forces are known the hoist force needs to be calculated
    FTOT_h = BDTV + BLTV + BMFV + TFLFV + TFRFV
    FHZ = -FTOT_h[2, 0]
    if FHZ < 0:
        print("The lift force is higher than the gravitational force")
        FHZ = 0
    BHVN = BCOGtoCV / BCOGtoCV[2]
    BHFV = FHZ * BHVN

    #  Now all forces are known
    FTOT = FTOT_h + BHFV

    # With this we can calculate the new acceleration, speed en location of the BCOG
    BCOGA = FTOT / BWeT - 0.005 * BCOGV
    BCOGV = BCOGV + BCOGA * timestep
    BCOGP = BCOGP + BCOGV * timestep

    # Also the total moment is known
    MTOT = MBM + MBW.T + MBT.T

    # With this we can calculate the new angular acceleration, angular speed and angle of the BCOG
    BCOGV_angular = MTOT / BI  # - 0.005*BWz
    BWx = BWx + (BCOGV_angular[0][0] * timestep)
    BWy = 0  #BWy + (BCOGV_angular[1][0] * timestep)
    BWz = BWz + (BCOGV_angular[2][0] * timestep)

    Bgamma = Bgamma + BWx * timestep
    Bbeta = Bbeta + BWy * timestep
    Balpha = Balpha + BWz * timestep


    time = time + timestep

#########################################################################################################
# Simulations ended
#########################################################################################################

#########################################################################################################
```

```
#########################################################################################################
# Calculate which moments an forces are needed to stablize the blade
#########################################################################################################

print('Mx:', MTOTListx[0])
print('My:', MTOTListy[0])
print('Mz:', MTOTListz[0])
print('Fx:', FTOTx[0])
print('Fy:', FTOTy[0])
print('Fz:', FTOTz[0])

T1 = (-MTOTListz[0]-15*FTOTx[0])/30
T2 = -FTOTx[0] - T1

print(T1, T2)

#########################################################################################################
# Find the damping factor
#########################################################################################################

def find_peaks(TIME, FINDDRAG):

peak_x = []
peak_vals = []
for i in range(len(FINDDRAG)):
    if i == 0:
        continue
    if i == len(FINDDRAG) - 1:
        continue
    if (FINDDRAG[i-1] < FINDDRAG[i]) and (FINDDRAG[i+1] < FINDDRAG[i]):
        peak_x.append(TIME[i])
        peak_vals.append(FINDDRAG[i])


plt.plot(peak_x, peak_vals, color='red', label='x')
plt.plot(TIME, PLOTFIX, color='blue', label='exp')
plt.title("Drag coefficient")
plt.xlabel("Time (min)")
plt.ylabel("Force peaks")
plt.grid(True)  # Add grid lines for better visualization
plt.show()

m,b = polyfit(peak_x, log(peak_vals), 1)
print(m,b)

#########################################################################################################
# In this section all plots are generated
#########################################################################################################
```